Enabling wearable soft tactile displays with dielectric elastomer actuators

Gabriele Frediani

Submitted in partial fulfilment of the requirements of the degree of Doctor of Philosophy

School of Engineering and Materials Science

Queen Mary University of London

February 2017

Acknowledgments

First of all, I would like to express my deep and sincere gratitude to Prof. Federico Carpi who has been my supervisor for most of my PhD project. With his patience, and motivation, he guided me in all the time of research and writing of this thesis. I could not have imagined having a better supervisor and mentor for my Ph.D study. Working with him has been an invaluable experience that really helped me to grow not only as an engineer, but also as a man.

I'm also extremely grateful to Professor James Busfield who is become my first supervisor during the last year. I've always really appreciated his constant and strong support, even when he was my second supervisor. I couldn't have written these lines if he had not have taken me under his wing.

A very special thanks goes to Hugh Boys, a talented engineer that with his experience and knowledge contributed in so many ways to this thesis. I will never thank him enough.

I would also like to thank all the people that I met during these years, regardless the large or small contribution they gave to my work.

I also need to thank Queen Mary University of London for this amazing opportunity. During this journey the college and London have become my second home, I met people from all around the world and travelled to many places.

I would finally like to dedicate this thesis to the ones that love me, without their support I would have never been able to overcome the difficulties I encountered during my PhD.

Abstract

Touch is one of the less exploited sensory channels in human machine interactions. While the introduction of the tactile feedback would improve the user experience in several fields, such as training for medical operators, teleoperation, computer aided design and 3D model exploration, no interfaces able to mimic accurately and realistically the tactile feeling produced by the contact with a real soft object are currently available. Devices able to simulate the contact with soft bodies, such as the human organs, might improve the experience.

The existing commercially available tactile displays consist of complex mechanisms that limit their portability. Moreover, no devices are able to provide tactile stimuli via a soft interface that can also modulate the contact area with the finger pad, which is required to realistically mimic the contact with soft bodies, as needed for example in systems aimed at simulating interactions with virtual biological tissues or in robot-assisted minimally invasive surgery.

The aim of this thesis is to develop such a wearable tactile display based on the dielectric elastomer actuators (DEAs). DEAs are a class of materials that respond to an electric field producing a deformation.

In particular, in this thesis, the tactile element consists of a so-called hydrostatically coupled dielectric elastomer actuator (HC-DEAs). HC-DEAs rely on an incompressible fluid that hydrostatically couples a DEA-based active part to a passive part interfaced to the user.

The display was also tested within a closed-loop configuration consisting of a hand tracking system and a custom made virtual environment. This proof of concept system allowed for a validation of the abilities of the display. Mechanical and psychophysical tests were performed in order to assess the ability of the system to provide tactile stimuli that can be distinguished by the users.

Also, the miniaturisation of the HC-DEA was investigated for applications in refreshable Braille displays or arrays of tactile elements for tactile maps.

Contents

List of figures

List of tables

List of symbols and abbreviations

2D	Two dimensional
3D	Three dimensional
a	Psychometric curve fitting parameter
A	Electrode area or unstretched membrane radius
b	Psychometric curve fitting parameter or radius of contact in the reference and stretched state
B	Radius of contact in the reference and unstretched state
C	Capacitance
CE	Constant error
cm	Centimetres
CNT	Carbon nanotubes
CP	Conjugated or conducting polymers
CT	Computed tomography
d	*Thickness of the dielectric elastomer layer*
$D\tilde{}$	Nominal electric displacement.
d_a	Active membrane thickness
$d_{a,0}$	Active membrane thickness after the pre-stretch
DEA	Dielectric elastomer actuator
ΔI	Intensity variation needed for a stimulus to be perceived as different
DOF	Degree-of-freedom
d_p	Passive membrane thickness
$d_{p,0}$	Passive membrane thickness after the pre-stretch
DSA	Dynamic scanning actuation
dU	Variation of the energy of the system
dz	Change in thickness
E	Electric field.
$E\tilde{}$	Nominal electric field
$\varepsilon 0$	Dielectric permittivity of vacuum
EAP	Electroactive polymer
EP	Electrostrictive polymer

$\varepsilon\rho$	Relative dielectric constant of the elastomer,
F_0-F_{11}	Force values used in the psychophysical tests
FA I	Fast adapting type I afferents
FA II	Fast adapting type II afferents
F_c	Psychometric curve fitting parameter
F_{JND}	Force values obtained as a result of the JND tests
F_N	Generic reference stimulus used in the JND tests
GPa	Gigapascal
h	Actuated membrane height
H	Unstretched membrane thickness
h_0	Membrane height at rest (no voltage applied)
h_a	Active cap height
HC-DEA	Hydrostatically coupled dielectric elastomer actuator
h_p	Passive cap height
Hz	Hertz
I	Stimulus intensity
IDE	Integrated development environment
I_{max}	EMCO maximum output current
IPMC	Ionic polymer–metal composites
IR	Infra-red
JND	Just noticeable difference
k	Weber's constant
kPa	Kilopascal
kV	Kilovolt
$\lambda 1$	Longitudinal stretch
$\lambda 2$	Latitudinal stretch
LC	Liquid crystalline
LCE	Liquid crystal elastomers
LED	Light-emitting diode
λr	Radial pre-stretch
μ	Small shear stress
mA	Milliampere
min	Minutes
ML	Maximum-likelihood procedure

ml	Millilitre
mm	Millimetre
μm	Micrometre
mN	Millinewton
MR	Magnetorheological
MRI	Magnetic resonance imaging
MΩ	Megaohm
N	Newton
P	Probability in the psychometric curve
p	Pressure
PEST	Parameter estimation by sequential testing
PG	Polymer gel
PMMA	Poly(methyl methacrylate)
POE	Point of Objective Equality
PP	Piezoelectric polymer
PSE	Point of subjective equivalence
PWM	Pulse width modulated
R	Discharge resistor
R	Radial coordinate
$r(R)$	Coordinate of the material particle
r_0	Initial base radius of the elastomer cylinder
r_p	Base radius of the elastomer cylinder after the pre-stretch
S_0	Cap initial surface
s_1	Latitudinal stress
s_2	Longitudinal stress
S_a	Active cap surface
SA I	Slowly adapting type I afferents
SA I	Slowly adapting type I afferents
SA II	Slowly adapting type II afferents
SMA	Shape memory alloys
S_p	Passive cap surface
SS	Sensory substitution
SSU	Self-sensing unit
t_0	Initial thickness of the elastomer cylinder

t_p	Thickness of the elastomer cylinder after the pre-stretch
USB	Universal serial bus
V	Volt
V_0-V_{11}	Voltage values used in the psychophysical tests
V_{JND}	Voltage values collected during the JND tests
V_{Max}	EMCO maximum output voltage
Vol_0	Initial volume of the elastomer cylinder
Vol_a	Active membrane final volume
$Vol_{a,0}$	Active membrane initial volume
Vol_p	Volume of the elastomer cylinder after the pre-stretch
Vol_p	Final volume of the passive membrane
$Vol_{p,0}$	Initial volume of the passive membrane
W	Watt
W	Helmholtz free energy
Wel	Helmholtz free energy associated to the electric field
$Wstretch$	Helmholtz free energy associated with the stretching
x_f	Fingertip distance from the virtual plane
x_s	Position of the virtual plane
$z(R)$	Coordinate of the material particle
δQ	Variation of heat added to the system
δW	Variation of work done by the system
ε	Permittivity of the elastomer
$\theta(R)$	Slope of a membrane at the coordinate R
λ	Prestretch
Φ	Voltage
$\Phi(\lambda)$	Voltage-stretch curve
$\Phi B(\lambda)$	Breakdown voltage-stretch curve

Chapter 1 Introduction

1.1. Background and motivation

Virtual reality has been successfully employed into a variety of fields, such as simulators for computer aided design and 3D modelling (Seth et al. 2011), or training of medical operators (Friedl 2002). An example of this is when three dimensional (3D) models of computer-generated organs or anatomical regions are used to help train surgeons, reducing the need for learning and practicing with patients or animals (Seymour et al. 2002).

Data from diagnostic techniques such as, computed tomography (CT), magnetic resonance imaging (MRI) and angiography, can be used to create 3D reconstructions and can create visualisation of complex biological structures, such as the skull, the hip and the coronary arteries. This serves to increase the speed and accuracy of the diagnosis and the additional information provided by the 3D reconstruction of organs and body parts is starting to help inform clinicians and improve clinical practice. This is because the medical team can plan a surgical procedure more reliably and they can use the models to help build surgical practice and improve their operating skills (Sakas 2002).

Systems able to use data from body scans to generate an accurate virtual rendering of a surgical environment have already been developed. Systems such as True 3D viewer (EchoPixel, Inc., USA) allows the user to visualize 3D MRI and CT data scans from a patient. True 3D is a platform that presents image data in an open space; using a special stylus, users can interact with the objects that appear to float in the air (Massat 2014). The Realview holographic display (RealView Imaging Ltd, Israel) projects 3D colour images that appear within touching distance from the observer, who can manipulate them using a proprietary hand-held tool (Bruckheimer et al. 2016, RealView medical holography 2016).

Despite the quality of such systems, the level of interaction between the user and the virtual images is purely visual (and possibly also acoustic). This kind of interaction is not sufficient to generate a truly realistic virtual experience, as it completely lacks any sense of touch and feel.

Indeed, among all the senses, touch is the most significant for creating a feeling of real presence in a virtual or remote environment (Krueger 1970). Furthermore, the softness of an object (as well as its texture and thermal conductivity) provides perceptual information much more readily than geometrical properties such as size and shape alone would permit. So, the exploration on the compliance of an object is used after the initial contact to rapidly assess the properties of that object (Klatzky et al. 1989).

Therefore, the integration of tactile feedback in virtual reality systems would enable users to manipulate virtual objects in a more natural fashion. In the biomedical field, for instance this might enable a realistic experience to be achieved by allowing 3D models to accurately mimic the physio-pathological compliance of tissues. As another example, tactile feedback systems might improve the performance and the dexterity of operators in telemanipulation and teleoperation (Sarakoglou et al. 2012).

Several commercial interfaces, capable of providing users with tactile feedback, are currently available. For example, Geomagic Touch (Geomagic, Inc., USA) can produce considerable forces, even though it is far from being wearable (Prattichizzo et al. 2013). The CyberGrasp system can provide force feedback to the five fingers (Aiple and Schiele 2013); however, its complex mechanics, made of tendons routed via an exoskeleton, and the need for an external actuator module, limit its portability (Prattichizzo et al. 2013). CyberTouch is designed to add tactile feedback to the CyberGrasp device and whilst it can individually stimulate each finger and the palm of the hand with 6 vibrotactile actuators, it can generate only vibratory patterns; so, the sensations that can be produced are limited to vibrations rather than a real contact with an object (CyberGlove Systems LLC 2016b).

In order to overcome these limitations, several devices have been proposed with the aim of displaying a variable compliance (Minamizawa et al. 2007, Prattichizzo et al. 2012, Scilingo et al. 2010), as presented in the next chapters of this thesis.

Despite the advances achieved with such approaches, to the best of our knowledge no tactile device is currently available to mimic virtual contact with soft bodies, delivered via soft controllable interfaces. Indeed, an interface that is soft and mechanically controllable is needed in order to ensure that the compliance of the display conforms to the deformable finger pulp, so as to allow for a tuneable contact area, which is expected to improve the tactile perception of the rendered soft bodies.

Furthermore, a device conceived for virtual environment exploration should be wearable, compact, lightweight and have a simple structure that does not limit the mobility of the fingers, the hand and the arm. Moreover, it should also be acoustically silent and generate low heat, so as to favour the user's comfort.
Aimed at addressing all these requirements, this thesis describes an approach to develop radically new types of tactile interfaces based on electromechanically tuneable smart materials.

1.2. Objectives of the work

According to the state of the art briefly outlined above (which will be detailed in the following section), the objectives of this work are:

- Design soft wearable tactile displays based on DEAs able to mimic physical contact with soft bodies.
- Prototyping of the system, including the development of a custom manufacturing process and the associated driving electronics.
- Validation of the prototype device including both bench testing and psychophysical evaluation.

1.3. Thesis outline

The main objective at the outset of this programme of study was to develop a tactile feedback system based on dielectric elastomer actuators (DEAs). DEAs are a promising technology for soft, lightweight and compact actuators (Carpi et al. 2008). The actuator configuration that was used and developed in this thesis to generate the tactile stimulus consists of the hydrostatically coupled DEA (HC-DEA) (Carpi et al. 2010b).
The thesis presents the design of the tactile display, its fabrication and its characterisation from the mechanical and psychophysical standpoints.
The thesis is organized as follows. Chapter 2 and Chapter 3 present a literature review on the human tactile system and methods used for the assessment of their characteristics. Chapter 4 and Chapter 5 describe state-of-the-art wearable tactile devices and the current need for soft tactile display technologies.

Chapter 6 and Chapter 7 report the fundamentals of soft actuation technologies, with a particular emphasis on DEAs.
In Chapter 8 the details of the tactile devices that have been developed together with their fabrication processes and the experimental procedures used to assess their performance are presented, while the related results are shown and discussed in Chapter 9 . Chapter 10 and Chapter 11 report the achievements in the miniaturization of the HC-DEA with the aim of enabling refreshable Braille and tactile maps. Chapter 12 discusses the future work that is still required to optimize the performance of the device.

1.4. Novel contributions

The novel contributions of this thesis are the following:

- A new fabrication method for the actuator has been conceived. In particular, it facilitates the encapsulation of the filling fluid within the actuator.
- A novel design for a fingertip mounted tactile display which integrates a HC-DEA stimulator and the high voltage driving electronics.
- The tactile display has been demonstrated able provide electrically tuneable tactile stimuli.
- A first system, in which the actuator worked in closed loop with a motion tracking system and a virtual environment, has been demonstrated.
- The downward scalability of the HC-DEA technology has been shown, with the aim of enabling refreshable Braille dots.

Chapter 2 Human tactile system

2.1. Finger pad skin physiology and sense of touch

The human glabrous skin consists of epidermis, dermis and subcutaneous fat tissue. In particular, in the finger pad, the dermal papillae, small extensions (or interdigitations) at the interface of the dermis and epidermis, form the epidermal ridges, also, known as the fingerprints.

The glabrous skin of the human hand is innervated by several classes of afferent fibres comprising pain afferents (Raja et al. 1988), thermoreceptive afferents (Darian–Smith 1984), proprioceptive afferents (Clark and Horch 1986), and four types of mechanoreceptive afferents responsive to mechanical deformation.

The tactile information is acquired through these four main types of mechanoreceptive afferents fibres that innervate the glabrous skin, each of which have end organs, of very different morphology, shaped according to a specific function (Johnson 2001) as described below. A schematic representation of the mechanoreceptors in the human glabrous skin is shown in Fig. 2.1.

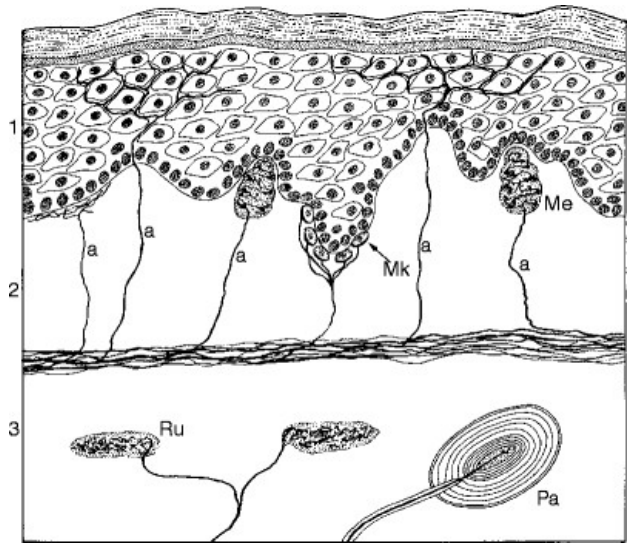

Fig. 2.1. Receptors in the glabrous skin: axon (a), Meissner corpuscle (Me), Merkel cell (Mk), Pacinian corpuscle (Pa), Ruffini corpuscle (Ru), epidermis (1), dermis (2), subcutis (3) (Brodal and Rinvik 1981).

2.2. Merkel cells (SA I afferents)

The Merkel discs are oval receptors located in the deepest part of the epidermis. They consist of specialised epidermal cells that enfold the unmyelinated ends of *slowly adapting type I* (SA I) afferent neurons. They respond to sustained indentation with a sustained, slowly adapting discharge that is linearly related to indentation depth (Blake et al. 1997, Johnson et al. 2000, Vega-Bermudez and Johnson 1999). However, they are much more sensitive to the temporal and spatial structure of a stimulus than to indentation, so that, for example, scanning a Braille dot with the finger evokes an impulse rate that is 10 times greater than that evoked by placing the finger on the dot without horizontal movement (Johnson and Lamb 1981). They are sensitive to local stress, thus associated with the sense of light touch and the discrimination of edges, corners, shapes and textures. They respond to vibrations up to 15 Hz, they have a receptive field diameter of 2-3 mm and a spatial resolution of 0.5 mm, the highest among the four main types of mechanoreceptors. Their linear response to skin deformation, over a very wide range of deformations (up to 1500 μm), makes SA I afferents to Merkel cells particularly suited for the fine representation of surfaces or objects(Johnson 2001).

It has also been shown that only SAI afferents provide the brain with a neural image of a curved surface that could be used for the perception of curvature (Goodwin et al. 1995). Furthermore the discrimination of the curvature is independent of contact force and contact area (Goodwin et al. 1991, Goodwin and Wheat 1992).

2.2.1. Meissner cells (FA I afferents)

In the dermal ridges, just below the epidermis, Meissner corpuscles consist of fluid-filled cell layers that cushion the endings of the *fast adapting type I* (FA I) afferent fibres. The Meissner corpuscle works as a filter and protect the FA I afferents from the confounding effects of large, static or low-frequency skin deformation required to grasp objects. Indeed, they are mainly responsible for detecting the slip between an object held in the hand and the finger. This high-pass filter behaviour is also the reason why one eventually stops feeling the clothing on the skin. They have the highest sensitivity for frequencies from 10 to

50 Hz and have a relatively poor spatial resolution (3–5 mm in diameter).The most important function of the FA I afferent nerves is to provide the feedback for the constant adjustment of the grip force, allowing us to manipulate objects delicately with a force not far above the force required to avoid the slip (Johansson and Westling 1984, Macefield et al. 1996, Srinivasan et al. 1990). Owing to their sensitivity for time varying stimuli, the FA I afferents are able to sense the vibrations produced when the finger is slid across a surface, thus allowing for the perception of texture (Katz 1925, Lederman 1981).

2.2.2. Ruffini cells (SA II afferents)

The Ruffini corpuscles are located into the collagen matrix of the connective tissue of the dermis, at the end of the *slowly adapting type II* (SA II) afferents. They innervate the skin less densely than other receptors, but their receptive field is larger. They are more sensitive to stretch than to indentation. Indeed, skin stretch evokes an impulse rate that is 2-4 times greater than that evoked by indentation (Edin 1992). Because of this, they play an important role in the perception of the direction of object motion when an object being held in the hand produces skin stretch. (Olausson et al. 2000). Along with muscle spindles skin stretch is also responsible for providing a neural image of hand shape and finger position (Collins and Prochazka 1996, Edin and Johansson 1995). The receptor's deep location seems to screen the afferents from the normal deformations produced by an object, enabling them to detect the object's motion and hand shape (Johnson 2001).

2.2.3. Pacinian corpuscles (FA II afferents)

The Pacinian corpuscles (or lamellar corpuscles) are located 2 mm under the skin and have a multi-layered, fluid filled structure that resembles an onion(Bell et al. 1994). The layers act as a selective filter (approximately between 20 and 250 Hz) protecting the unmyelinated terminal part of a single *fast adapting type II* (FA II) afferent neuron from large and slow stimuli(Brisben et al. 1999, Loewenstein and Skalak 1966). As they are located deep in the skin the FAII have a very poor spatial resolution as their perceptive field may include the entire hand (Johnson

2001). The FA II afferents are extremely sensitive, two order of magnitude more sensitive than the FA I. The most sensitive receptor responds to vibratory stimuli of 10 nm amplitude applied to the skin. Because of these properties, FA II receptors are responsible for the perception of vibratory stimuli transmitted by objects held in the hand. As Pacinian corpuscles mask the large and slow stimuli that accompany many manual tasks, they allow us to perceive events at the working end a tool (Brisben et al. 1999).

The cutaneous mechanoreceptors properties are reported in Table 2.1.

Table 2.1. Cutaneous mechanoreceptors properties.

Receptor	**Afferent**	**Approx. frequency range**	**Approx. Receptive field**	**Detection**	**Location**	**References**
Merkel's discs	SA I	Up to 15 Hz	Small (2-3 mm)	Touch Pressure Changes in texture	Superficial skin	(Goodwin et al. 1995, Goodwin et al. 1991, Goodwin and Wheat 1992, Johnson 2001)
Meissner's corpuscles	FA I	From 10 to 50 Hz	Small (3-5 mm)	Light touch Changes in texture Relatively slow vibrations	Superficial skin	(Johansson and Westling 1984, Macefield et al. 1996, Srinivasan et al. 1990). 1.1.
Ruffini endings	SA II	Low frequencies	Large	Hand shape and finger position	Deep skin	(Collins and Prochazka 1996, Edin 1992, Edin and Johansson 1995, Johnson 2001, Olausson et al. 2000)
Pacinian corpuscles	FA II	From 20 to 250 Hz	Large	Rapid vibratory pressure Events at the end of a tool	Deep skin	(Brisben et al. 1999, Johnson 2001, Loewenstein and Skalak 1966)

2.3. Tactile unit density and sensitivity

The number of tactile units innervating the glabrous skin area of one hand has been estimated as 17,000. Their densities and sensitivities are different within the sub-regions of the glabrous skin of the hand (Johansson and Vallbo 1979) (Fig. 2.2).

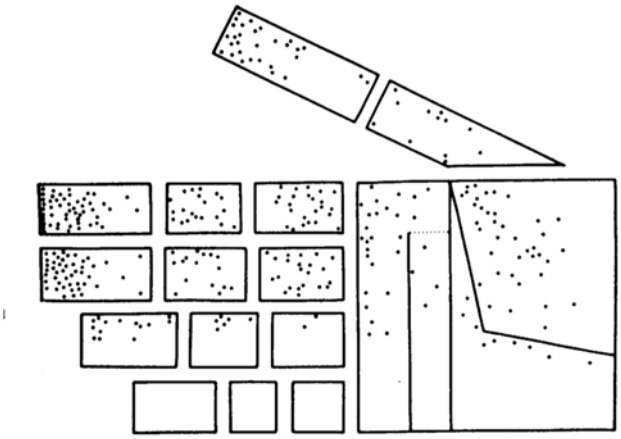

Fig. 2.2. Locations of receptive field centres of glabrous skin mechanoreceptive units (Johansson and Vallbo 1979)

Studies indicate that the tactile sensory organs density slightly increases from the palm to the fingers, and that it rapidly rises when reaching the fingertip. The FA I and the SA I are the units that exhibit the major increase in density, while the other two types of units are evenly distributed over the total skin area

Basic data on densities and sensitivities for the four tactile units are summarised in Fig. 2.3 (Vallbo and Johansson 1984).

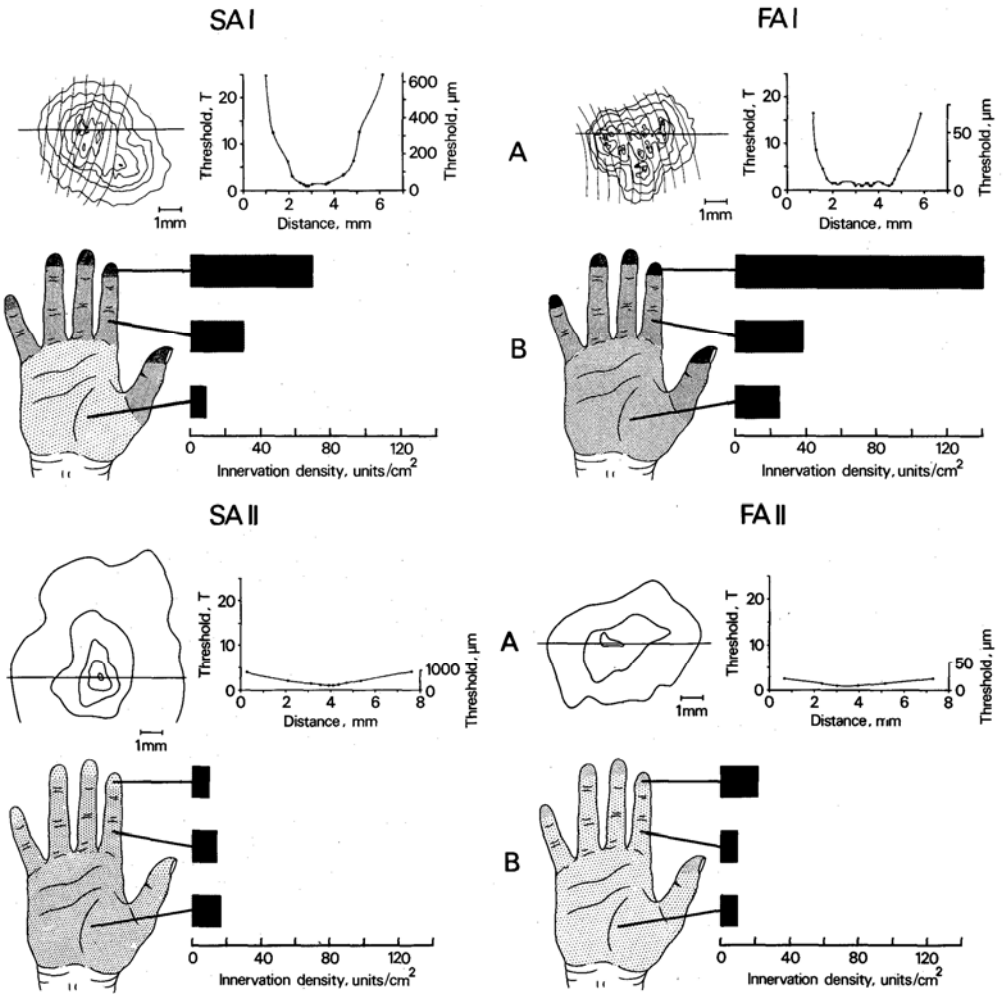

Fig. 2.3. Characteristics of the four mechanoreceptive units: sensitivity maps (A) and average density within the glabrous skin areas (Vallbo and Johansson 1984).

2.4. Chapter conclusions

The human hand is equipped with four functionally distinct types of tactile afferent fibres, which have different functionality, sensitivities and densities within the skin areas. Touch is a complex sense that integrates information from those tactile afferent fibres in order to infer physical properties of an object while it is contacted by the human skin.

Measuring the performance of this system requires methods for the assessment of the perceptual processes and devices able to provide suitable stimuli that will be described in the following chapters.

Chapter 3 Psychophysics of human perception

Psychophysics is a branch of psychology that investigates the relation between external stimulus and internal sensation in human perception. Ernst Heinrich Weber (1795–1878) was the first to investigate it with a quantitative approach. Weber, who is known for Weber's law, found that the smallest noticeable change in a stimulus increases linearly with the stimulus intensity (Weber 1834).

The term psychophysics was first used by Gustav Theodor Fechner, a scholar of Weber, who described the first principles and procedures used in psychophysical experiments in his "Elements of Psychophysics" (Fechner 1860). Fechner also used Weber's findings to put the law in the following mathematical form:

$$\Delta I / I = k \tag{3.1}$$

where I is the stimulus intensity, ΔI is the intensity variation needed for a stimulus of the same kind to be perceived as different and k is a constant. Later, Fechner showed that Weber's law could be explained by assuming that the external stimulus is scaled into a logarithmic internal representation of sensation (Fechner 1860).

Weber-Fechner works are the first attempts to mathematically relate the internal psychic and the external physical stimulations on the basis of experimental data. Although they focused on physical stimuli, it has been demonstrated that this law can also be applied to more abstract parameters, such as our sense of numbers (Shepard et al. 1975). Furthermore, records from neuron activity allowed to investigate the neural basis of the internal scale finding clear physiological evidence for Weber's law (Dehaene 2003).

3.1. Psychometric function

The curve used to relate the sensation to the physical quantity of a stimulus is the *psychometric function*. It shows the relationship between a given feature of the physical stimulus (which for example could be velocity, duration, brightness or weight) and the responses given by the subject. An example of psychometric function is shown in Fig. 3.1.

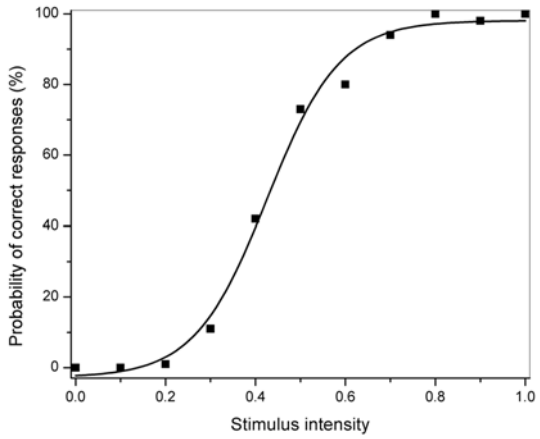

Fig. 3.1. Example of psychometric function

Usually the x-axis represents the stimulus intensity, while the y-axis reports the probability of correct responses provided during one of the specific tasks described in the following section (Klein 2001).

3.2. Psychophysical tasks

In order to collect consistent responses from the subjects during psychophysical experiments, diverse psychophysical tasks are implemented. Usually during a task one or more stimuli are presented to the subject, which is asked to judge them. The response is rated as positive, or correct, if it is coherent with the physical quantity presented, otherwise it is negative. The existing tasks can be divided in three main categories: *detection tasks*, *discrimination tasks* and *identification* or *classification tasks* (Fechner 1860, Gescheider 1997a, Krantz 2012).

3.3. Detection tasks

Detection tasks are used to calculate the *absolute threshold*, which is the smallest intensity needed for a stimulus to be perceived and to assess the psychometric function.

Yes-no procedure is when a stimulus is presented during an interval and the subject must indicate whether it has perceived the stimulus or not. The absolute threshold is defined as the value of the stimulus whereby 50% of the responses are positive.

Two alternative forced choice tasks require a stimulus to be presented during one of two intervals (time separated) or two possible locations (space separated). The subject must indicate in which interval or location the stimulus is present. The psychometric function ranges from 50% to 100%, because subjects respond randomly when the stimulus is below the threshold. The absolute threshold is defined as the stimulus intensity where 75% of answers are correct (Bogacz et al. 2006).

3.3.1. Discrimination tasks

Discrimination tasks are used to measure the *difference threshold*. The difference threshold or *just noticeable difference* (JND) is the minimal difference between two stimuli that can be perceived (Schacter et al. 2011).
In these tasks two stimuli are presented, a reference stimulus and a comparison stimulus. The subject must compare the two stimuli (Fechner 1860).

Two alternative forced choice tasks is when the observer does not know what the reference stimulus is. The subject has to choose the stimulus that possesses more of some quality (which could be for example the magnitude or duration) (Bogacz et al. 2006).

Discrimination task with reminder is when the subject is aware of a stimulus, which is the reference and has to say if the comparison is larger.

These two tasks are used to estimate the *point of subjective equivalence* (PSE) and the JND. The first is the stimulus that obtains 50% of positive responses while the latter corresponds to half the distance between the two stimuli that obtain respectively 25% and 75% of positive responses. Depending on the shape of the psychometric function, PSE and JND may or may not be the same (Schacter et al. 2011).

Same-different task is a variation of the forced choice discrimination task in which the subject must indicate whether he has perceived a difference between the two stimuli presented.

For this task the psychometric function ranges from 50% (chance level) to 100%.

The JND is defined as the stimulus difference that produces a given proportion (for example 75%) of the "different" responses.

3.3.2. Identification or classification tasks

In identification or classification tasks the observer must identify the stimuli among a group of more than two stimuli. Successive integers are assigned to an ordered set of stimuli. After certain amount of time, when the subject is familiar with the stimuli and the related numbers, each stimulus is presented in random order. The subjects must identify the stimulus by identifying the corresponding number (Krantz 2012).

3.4. Psychophysical methods

The responses collected during the tasks described above, are used to extract the psychophysical parameters (such as the JND). This requires the presentation of a series of stimuli to the subjects, the closer the stimuli are to the threshold, the more efficient and accurate is the measurement. Psychophysical methods have been developed in order to identify the values along the stimulus axis and the order that optimise the experiments (Snodgrass and Psychophysics 1975).

3.4.1. Classical psychophysical methods

Fechner in his works developed methods for the measurement of the internal psychic scales that date back to the very beginning of the psychophysics and are known as the *classical psychophysical methods* (Fechner 1860, Gescheider 1997b). Fechner's original methods are the following.

The method of constant stimuli: a number of selected values (typically from 5 to 9), evenly distributed along the stimulus range, are repeatedly presented in random order. The subject has to compare these stimuli with a fixed reference value.

The method of limits: the stimulus intensity varies in small ascending or descending steps from a level well below or above the threshold value. At each step the subject compares the stimulus with the reference. The stimulus level at which the subject

response changes is recorded for each trial. This method is usually employed for determining the JND, which is calculated as the average value of all the recorded values.

The method of adjustment is a variation of the method of limits. The subject can continuously vary the stimulus so as to set it to apparent equality with the reference. This experiment is mostly used to evaluate the PSE.

3.4.2. Adaptive psychophysical methods

In order to further improve the efficiency of the psychophysical measurements and to reduce the experiment time, adaptive methods use the results of previous trials to select the next best stimulus to present to the subject. The stimuli are selected during the trial according to an algorithm that drives the placement of the stimulus towards the measurement point that is the most informative. The most commonly utilised adaptive procedures can be placed in three different categories according to the method used to choose the stimuli during the experiment: *parameter estimation by sequential testing* (PEST), *maximum-likelihood procedures* (ML), *staircase procedure* (Leek 2001, Treutwein 1995).

PEST: the selected values of the stimuli is adapted to focus the trials at the most efficient location along the stimulus axis, stopping the trial when the estimate is considered adequate (Harvey 1986, Taylor and Creelman 1967). A block of trials, with the same intensity level is presented; if the percentage of correct responses is higher than a certain threshold the step level is reduced and a new block of stimuli is presented; if the percentage of the new block is lower than the threshold, which means that the level is too low, there is an increase of half the step. The intensity level is changed according to the observed probability and every change in direction produces a halving of the step. When a chosen step value is reached, the series terminates and the value of the final step is recorded as the threshold value.

Maximum-likelihood procedures: it's a modification of PEST, after each trial the results are combined to form a psychometric function, the points of the curve are fitted and a current sensory threshold is estimated. After each experiment the new

threshold value is used to place the next set of trials. An implementation of the procedure is the QUES (Watson and Pelli 1983).

3.5. Selection of the psychophysical characterisation method

The different characterisation methods described above typically have different levels of accuracy. The actual level corresponding to a different complexity of the implementation. In particular the classical methods require less sophisticated algorithms. For the sake of achieving a characterisation at a preliminary level, according to the needs of this first work on this new kind of tactile display, preference was given to the simplicity of implementation. This was to more easily give an initial indication on the efficacy of the proposed tactile technology, while postponing more accurate and more extensive characterisation to future investigations.

To this end, in this work we decided to evaluate the developed display by choosing a relatively simple psychophysical task and the most basic psychophysical method to evaluate the accomplishment of that task. In particular, we chose the psychophysical task referred to as ‘discrimination task with reminder’ described above and psychophysical method referred to as ‘method of limits’ described above.

3.6. Chapter conclusions

This chapter briefly presented the selection, among the most common types, of the specific psychophysical task and method used in this work to evaluate their accomplishment using the developed prototype display.

The actual implementation of the psychophysical characterisation is presented in Chapter 8 .

Chapter 4 Wearable Tactile feedback systems

Haptic feedback is the most recent and one of the least explored modality for human-machine interaction. As it is a complex combination of different types of physical information from the environment, such as force, pressure and temperature, a realistic rendering of this sensation is challenging. Most of the efforts have been directed to the development of kinaesthetic feedback systems that are able to provide forces to the fingers and the limbs; examples are the Geomagic Touch (Geomagic, USA) (Geomagic Inc. 2016) or the CyberGrasp (CyberGlove Systems LLC 2016a). However, the excellent force feedback provided by such systems is not complimented by the tactile sensation. Although systems intended for this purpose have been developed to be used on various parts of the body (such as head, shoulders, limbs and torso), the following sections describe only devices that are wearable (or that can be made wearable) and are able to stimulate the finger pad.

4.1. Mechanical devices

4.2. The Gravity Grabber

Only a few systems that are able to provide force to the finger pad have been proposed as they usually result in heavy and bulky devices. One of the most effective is the Gravity Grabber (Minamizawa et al. 2007): a wearable device that is able to deform the finger pad so as to simulate the grip sensation and the gravity sensation. It consists of two motors and a belt (Fig. 4.1 a and b). The operating principle being that if the motors rotate in opposite directions, they roll up the belt and produce a vertical pressure stress (as shown in Fig. 4.1c), if the motors rotate in the same direction, the belt is rolled up on one side and rolled out on the other side (Fig. 4.1d), thus generating a shearing stress. By wearing the devices on the index finger and the thumb, users are able to perceive the grip force, gravity and inertia of a virtual object (Minamizawa et al. 2007).

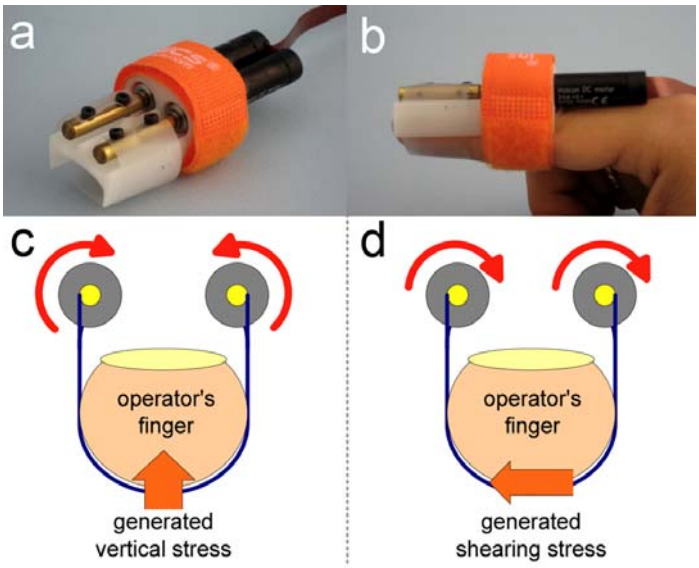

Fig. 4.1. The Gravity grabber prototype (a,b) and methods for generating vertical stress (c) and shearing stress (d) (Minamizawa et al. 2007).

4.2.1. Lateral skin stretch stimulation

Skin stretch is a feedback modality in which a shear force is applied to the finger pad of the user. The force can be applied by a single actuator, consisting of a small position device, or by an array of stimulators. The difference between the two approaches is that a single actuator allows for significantly more force and displacement while an array is capable of producing programmable and more detailed strain fields.

A skin stretch device consisting of a single tactor was presented by Schorr et al. (Fig. 4.2)(Schorr et al. 2013),.

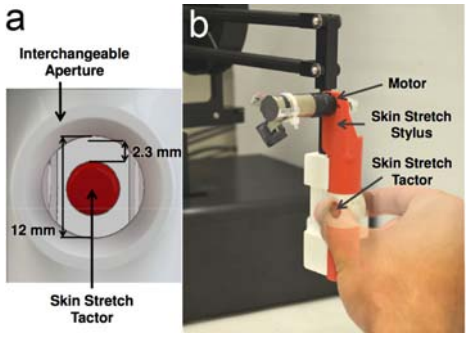

Fig. 4.2. Skin stretch devices. Small position device (a) and experimental setup (b). (Schorr et al. 2013).

An array of pins using piezoceramic actuators was presented by Hayward and Cruz-Hernandez (Fig. 4.3 a and b) (Hayward and Cruz-Hernandez 2000) and piezoceramic bending cantilevers was presented by Pasquero and Hayward (Fig. 4.3 c and d) (Pasquero and Hayward 2003) and Wang and Hayward(Fig. 4.3 e and f) (Wang and Hayward 2010).

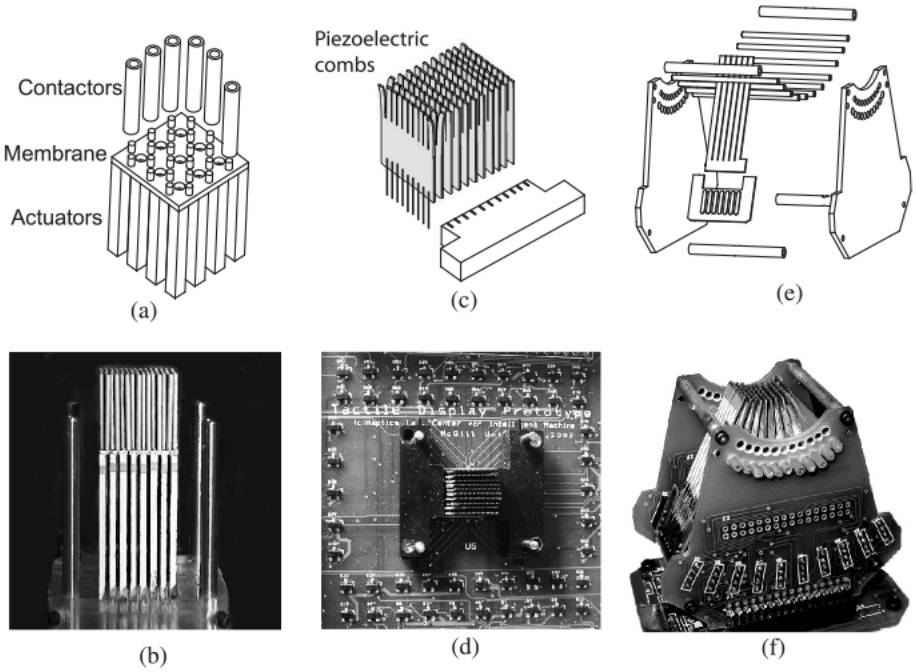

Fig. 4.3. Membrane architecture described by Hayward and Cruz-Hernandez (2000) (a), (b). Cantilever architecture as in Pasquero and Hayward (2003) (c), (d) and Wang and Hayward (e), (f).

Other approaches to the skin stretch are those proposed by Knoop and Rossiter using pins actuated by dielectric elastomer (Fig. 4.4 a and b) (Knoop and Rossiter 2015b) and bars actuated by shape memory alloys elastomer (Fig. 4.4c) (Knoop and Rossiter 2015a).

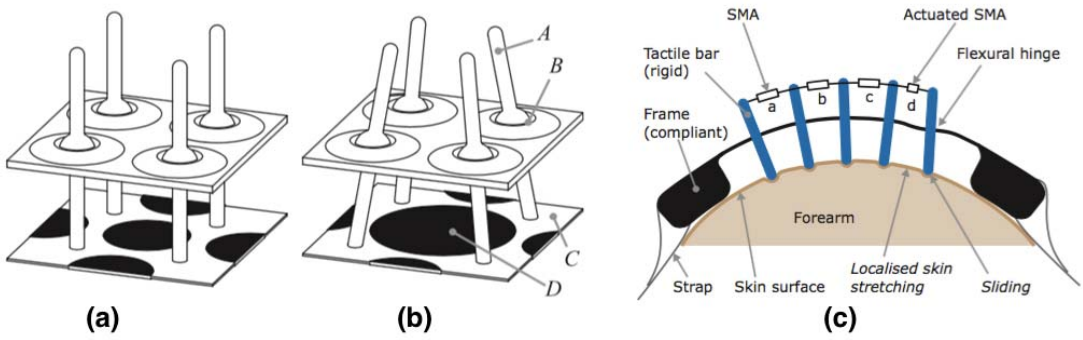

Fig. 4.4. Mechanisms for laterotactile stimulation. Device based on DEA shown at rest (a) and with an actuated DEA element. SMA based stimulator (c)(Knoop and Rossiter 2015b, Knoop and Rossiter 2015a).

The skin stretch has been demonstrated to be a solution for tactile feedback as effective as that using normal stimulation of the skin. As skin stretch is a tactile sensation experienced in everyday life, devices based on this stimulation strategy are described as pleasant and natural, so they do not require any particular advanced training. Also, this approach allows the user to identify the direction of any applied stimulus (Knoop and Rossiter 2015a).

Owing to high sensitivity of the human skin for this kind of stimuli skin stretch appears to be an intuitive substitute for force feedback (Knoop and Rossiter 2015b, Schorr et al. 2013).

4.2.2. Vibrotactile devices

Instead of providing them with mechanical force, the tactile receptors that innervate the skin can be stimulated by mechanical vibrations of different frequencies. Frequencies up to 250 Hz would activate the Pacinian receptors while values from 0 to 50 Hz would stimulate the others. A commercial device exploiting this stimulation mechanism is the CyberTouch system (CyberGlove Systems LLC 2016b). It consists of a glove integrating 6 vibrotactile stimulators, one on the inside of each finger and one on the palm of the hand. The stimulators can be programmed to generate continuous vibration or pulses at different strengths, so as to tune the touch sensation. The CyberTouch II is shown in (Fig. 4.5)

Fig. 4.5. CyberTouch II glove (CyberGlove Systems LLC 2016b).

4.2.3. Arrays of actuated pins

These displays consist of arrays of pins able to displace exploiting various kinds of actuation systems. Usually, each pin can be controlled allowing for a local stimulation of the finger pad. Lee et al. described an array of pins based on dielectric elastomer actuators (Fig. 4.6a)(Lee et al. 2014). The display was lightweight and compliant, produced a maximum force of about 120 mN and a maximum stroke of 350 μm. Due to its relatively small size, the tactile display could be integrated into a haptic glove system.

Kim et al. proposed a tactile display consisting of an array of pins driven by linear ultrasonic actuators (sub-miniature motors that uses the piezoelectric effect) (Fig. 4.6b). The display can generate various types of texture sensations such as ridges, grooves, and surface roughness using static indentations or through the vibration of each pin(Kim et al. 2008). While the display was designed in the attempt to make it embeddable in portable devices, it requires further improvements in terms of reduction of the size.

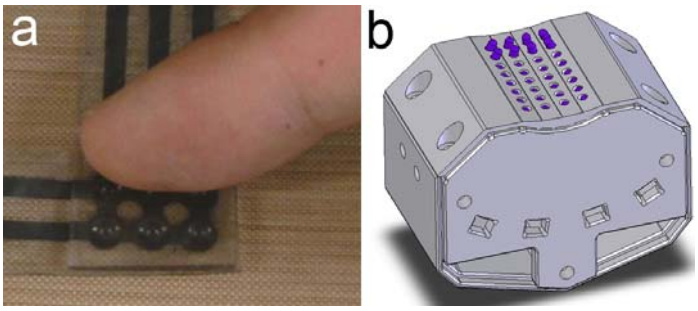

Fig. 4.6. Examples of tactile displays consisting of array of pins. Device based on dielectric elastomer actuators (a) and tactile display module using ultrasonic actuators (b)(Kim et al. 2008, Lee et al. 2014).

4.3. Electrotactile devices

Electrotactile displays for the fingertip have been developed that can elicit a tactile sensation through electrocutaneous stimuli. The tactile sensation is produced by electrically activating the fibre innervating the mechanoreceptors (Altinsoy and Merchel 2012). The nerves of each type of receptors can be independently stimulated by selecting the signal frequency, either by a single or by an array of electrodes. Combining the stimulation of the different receptors allows to obtain different sensation, such as pressure, softness and vibration (Tezuka et al. 2016). .Fig. 4.7 shows an example of electrotactile display composed by an array of micro needles

(Kajimoto et al. 2001, Kitamura et al. 2015).These systems have to be improved, as the tactile sensation provided is often reported as not "natural". Investigations have to focus on the control and delivery of the electrical stimuli.

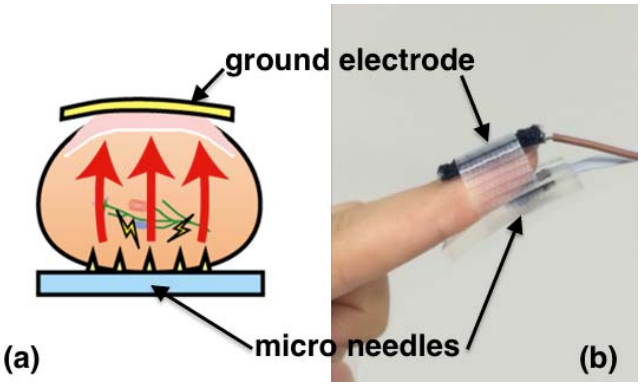

Fig. 4.7. Electrotactile display: schematic representation of the principle of operation (a) and display arranged at the fingertip (Tezuka et al. 2016).

4.4. Airborne tactile display

Although not properly wearable, due to its non-contact mechanism, airborne tactile displays are quite promising as a method of conveying tactile information to the finger pad. It exploits a nonlinear phenomenon of ultrasound: the acoustic radiation pressure. When an ultrasound beam is reflected by an object's surface, the surface is subjected to a force in the direction of the incident beam. The display consists of an ultrasonic phased array able to generate a focal point of airborne ultrasound pressure (Fig. 4.8). The phased array is used to control the position of the focal point according to the position of the hand, while the acoustic pressure amplitude can be continuously modulated to generate a vibrotactile stimulation (Hoshi and Shinoda 2016, Iwamoto et al. 2008)(Carter et al. 2013).

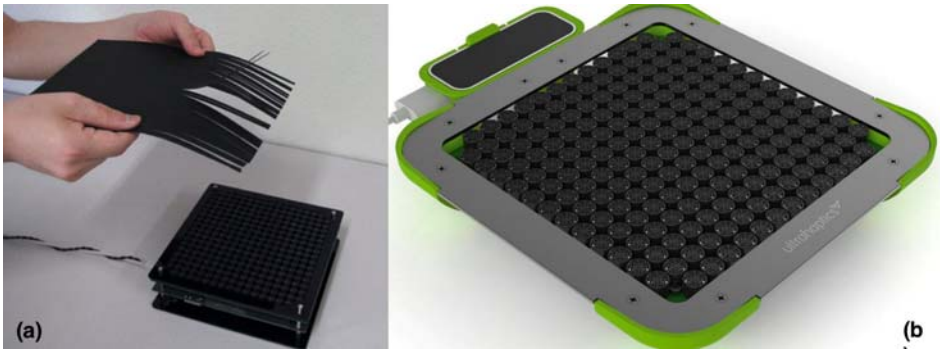

Fig. 4.8. The focused ultrasounds can flip up thin paper strips (a) (Hoshi and Shinoda 2016) and the commercially available Ultrahaptic display (b)(*Ultrahaptics, UK*).

4.5. Sensory substitution for tactile feedback

The term *sensory substitution* (SS) is mainly used when referring to assistive technologies for visually impaired people or prosthetic limbs capable of providing sensory feedback. In general, a SS system transforms a stimulus of one sensory modality into a stimulus of another sensory modality. A well-known SS system is the Braille code, where information, that is usually acquired visually, is acquired through touch. Another example might be a prosthetic hand equipped with sensors that, by applying vibrations to the remaining part of the limb, can convey a sense of touch from the sensors. SS is enabled by the plasticity of the central nervous system that permits the integration of inputs from one sensory channel, allowing for the learning of a new mode of perception. SS can obviously occur across sensory systems, such as touch-to-sight or within a single sensory system such as touch-to-touch (Bach-y-Rita and Kercel 2003, Lenay et al. 2003).

4.6. Need for a different technology

Tactile haptic devices interact with users through the stimulation of the skin. Wearable versions of such devices aim to provide this function whilst being worn. As the definition of wearability can be ambiguous, for our purposes we are concerned here with the ability of a device to be small, easy to carry, comfortable and not impair the motions of the user. So, the device should not burden the user mechanically (therefore it should be compact and light in weight), as well as acoustically and thermally (so it should not generate perceivable noise and heat). If we are to consider the placement of wearable tactile devices upon individual fingertips, the requirements of compactness and weight become even harder to facilitate.

Furthermore, if the device is aimed at providing tactile stimulation, it should be based on an actuation technology capable of generating large and quasi-static displacements at moderate forces (as opposed to high-frequency small vibrations at high forces), as this modality is compliant with the natural way of encoding tactile information.

Considering these requirements, it should be not surprising that tactile feedback appears to be still underutilised in wearable devices for virtual- or augmented-reality

systems aimed at mimicking realistic interactions. Indeed, the greatest majority of approaches today is based on the use of vibrations.

This fact is likely due to a lack of adequate actuation solutions to generate large and quasi-static displacements and moderate forces via compact, light in weight, silent and energy efficient technologies.

Indeed, even for the non-vibratory systems, current designs appear to be burdened by their underlying actuation technology, as shown above. For example, whilst the use of servomotors mounted on the top of the finger to move an interface (such as a band or a plate) has been shown to be able to create adequate renderings of tactile interactions, the form factor seems too large to be viable for multiple fingertips simultaneously (in order for example to simulate grasping).

The other common non-vibratory approach of using pneumatic actuation requires a relatively complex, bulky and noisy system of pumps, regulators and air lines, which tends to limit wearability and portability.

Therefore, aimed at overcoming such limitations of conventional systems, a new soft actuation technology is needed. This work is aimed at addressing this need, by describing a completely different approach.

4.7. Chapter conclusions

This chapter outlines the state of the art of conventional wearable technologies to create tactile feedback. It shows how the limitation of such approaches cause the need for rethinking the enabling actuation technologies, which represents the motivation for the work described in this thesis.

Chapter 5 Perception of softness

5.1. Introduction

The degree of compliance (or softness) of an object is a mechanical property that can be roughly defined, with reference to an elastic body, as the amount of deformation caused by a unit measure of applied force. Softness can be objectively measured and it mainly depends on the properties and the structure of the material.

The human perception of softness is related to the object mechanical properties. However, the tactile interaction with an object is more complex and involves diverse mechanisms.

In particular, when touching a deformable object two different elements are involved in the perception of the compliance (or softness) : the first is the force that is applied to the object and the second is the extent of the deformation of the finger and finger pad. The associated haptic information can be of two kinds: *kinaesthetic information* and *tactile information*. The first is related to the position and the force exerted by fingers and limbs and is provided by the proprioceptive receptor (muscle spindle and the SA II receptors in the skin). The second is related to the deformation of the finger pad and is mediated by the mechanoreceptors innervating the glabrous skin of the finger pad (Srinivasan and LaMotte 1995). The key role played by the tactile component can be explained by considering that the finger pad contact area while touching a soft object is larger than the contact area while touching a hard object when the same force is applied to the two objects (Fujita and Oyama 1999). This is an example of how the force alone is not sufficient for the recognition of an object's softness. Indeed, it must be complemented by the information provided by the contact area.

Experiments aimed at investigating its role with respect to kinaesthetic and tactile information are described below.

5.2. The role of kinaesthetic and tactile information

In order to assess the relative significance of tactile and kinaesthetic information in the perception of softness, it is necessary to design experiments that are able to isolate the contribution of each component, to study the two effects independently.

Srinivasan and LaMotte performed several psychophysical tests using two kind of test samples: rubber test samples, having a compliant contact surface and test samples composed by a spring cell, with a rigid contact surface (Fig. 5.1). This was done so as to provide two kinds of tactile sensations. Both types of samples underwent a deformation when probed by the users. The finger was able to indent and deform the rubber sample, while the spring cell sample could only be displaced. The force and the contact area between each of the test samples and the finger pad were measured, both in *active touch* (which is when the finger is free to move when probing the object) and in *passive touch* (which is when the finger position is fixed and the object is displaced to touch the finger, so as to exclude the kinaesthetic part). Furthermore, in order to investigate the kinaesthetic sensation alone, half of the experiments in active touch were conducted with a local anaesthesia to the finger pad (Srinivasan and LaMotte 1995).

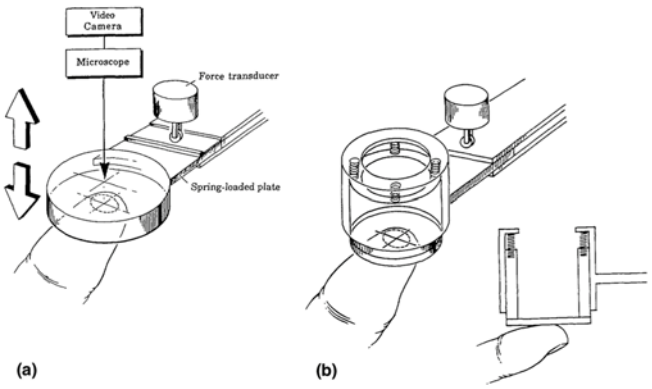

Fig. 5.1. Schematic of the devices for the experiments conducted by Srinivasan and La Motte. Rubber sample (a), spring cell sample (b)(Srinivasan and LaMotte 1995)

It has been demonstrated that, for objects having a compliant surface, the kinaesthetic component alone is unable to discriminate between the softest and the hardest sample. Furthermore they found that the discrimination probabilities were approximately the same with both the components and when only the

tactile information was available. This can be explained by considering that, while the finger indent into a soft object with deformable surface, for a given contact force, the spatial distribution of pressure and the contact area depend on the object compliance.

This suggests that tactile information alone (and in particular the variation of contact area) may be sufficient to discriminate compliant objects. Indeed, for a semi-infinite elastic medium (such as a the rubber sample shown in Fig. 5.1a) the object conforms to the finger pad shape, increasing the contact area.

Conversely, for a rigid body on a Winkler foundation (whereby the elastic mean is simplified by arrays of springs placed underneath the body), as for the spring cell shown in Fig. 5.1b, the variation in the distribution of pressure and the skin deformation depend mainly on the contact force and the compliance of the finger pad, as the object's surface does not deform. Therefore, in this case, the tactile component does not add information for the discrimination other than the force perceived.

The key role played by the tactile information in the perception of the softness has also been experimentally demonstrated by Fujita and Ohmori (Fujita and Ohmori 2001). They designed a system able to exclude the effect of the proprioceptive component during the perceptual task, allowing the subjects to focus only on the tactile information. The system consisted of a fluid filled cylinder with a rubber membrane at its top. The fingertip contact area was dynamically tuned by changing the volume of fluid according to the force exerted by the finger, which was recorded by a load cell (Fig. 5.2). Tests performed on real and simulated samples allowed for confirming the efficacy of the softness display. The experiments demonstrated that softness could be rendered by controlling the fingertip contact area both in active touch and in passive touch.

Fig. 5.2. Close-up of the device developed by demonstrated by Fujita and Ohmori (Fujita and Ohmori 2001)

A further contribution in the investigations on how the cutaneous and kinaesthetic information influence the perception of softness has been given by Scilingo el al. (Scilingo et al. 2010). Similarly to Srinivasan and LaMotte, and Fujita and Ohmori, they compared psychophysical tests on both real and simulated soft objects, using silicone samples and a pneumatic device able to tune the force and contact area (Fig. 5.3). According to the results of their work, the integration of tactile and kinaesthetic information allows for the highest recognition ratio, for both real and rendered softness. As expected, using one of the two components alone causes a decrease of the recognition ratio, however when considered in isolation the tactile component appears to provide more information than the kinaesthetic. In particular, the difference in performance was even more evident when the softness was simulated, rather than for real samples. Whilst the authors did not provide any explanation, the results supported the conclusion that for haptic displays purely kinaesthetic information is inferior in softness discrimination with respect to tactile.

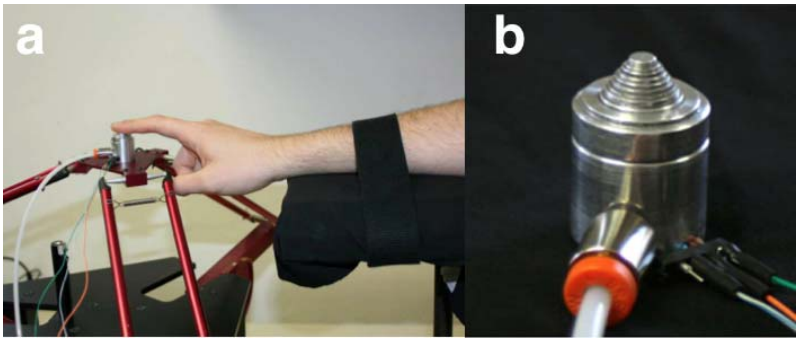

Fig. 5.3. The integrated haptic display (a) and the softness display (b) described by Scilingo el al. (Scilingo et al. 2010)

It has also been observed by Fujita and Oyama that, in human pinch of an unknown compliant object, the peak contact area is independent from the object softness perceived (Fujita and Oyama 1999).

5.3. Chapter conclusions

According to the experimental findings reported in this chapter, the contact area is fundamental for the tactile perception of the softness of an object. In particular, the contact area spread ratio plays a key role in the recognition of the mechanical properties of the object.

Contact area and pressure distribution are also affected by the compliance of the skin, which allows the finger to adapt and conform to different object shapes. However, it has been found that that during the grasp the pressure distribution is fairly smooth with no localised pressure peaks over the contact area (Knoop et al. 2017).

These findings allow for an assumption to be made that an adequate softness sensation can be simulated by controlling the rate of contact area increase, without the need for a force feedback.

This kind of displays might be able to evoke a reliable sensation of softness, enabling better discrimination than purely kinaesthetic displays. Moreover, it has been demonstrated that a tactile display may be effectively used to substitute kinaesthesia in applications such as robotic controllers for surgery and hazardous environment, where precision and stability of the feedback system is critical (Prattichizzo et al. 2010).

Whilst displays described above are able to actively tune the contact area, they lack portability, as they were bulky and only intended for bench tests. Thus a display with light weight and ease of integration could enable wearable devices. Furthermore, a display inherently soft, thus able to conform its shape to the finger, might enable more realistic strategies for the rendering of softness.

Most of these properties are shown by the so-called “smart materials” which are described in the next chapter.

Chapter 6 Smart material-based actuator technologies

6.1. Introduction

Smart materials (sometimes known as intelligent materials) are materials that are designed to change some of their properties in response to a specific stimulus (such as temperature, light, pH, stress, magnetic field or electric field).

Smart material-based actuators are mainly used for robotic and mechatronic applications, however, they can enable applications that are precluded to conventional actuators.

In this chapter, the main classes of smart materials and some of their applications are described.

6.2. Shape memory alloys (SMAs)

Shape memory alloys (SMAs) are a class of materials that is able to return to their original form when heated beyond a certain temperature (Jani et al. 2014). The material can be deformed at low temperature, and it recovers its original form when heated. This phenomenon is called the "shape memory effect", and can be exploited to produce actuation.

SMAs are attractive as they can develop high stresses (around 230 MPa) and, when arranged as spring, considerable strains (up to 10 %). Owing to their thermal capacity, which slows the heating and cooling, the actuation frequency SMA-actuators is limited (Hunter et al. 1991).

They have a high elastic modulus of tens of GPa (D.E.Hodgson et al. 1990), which is not suitable for soft actuation. However, they can be shaped into springs (Fig. 6.1). This provides the structure with good compliance and with suitable design can increase the actuation strain to as much as a 50 % linear contraction (Kim et al. 2009).

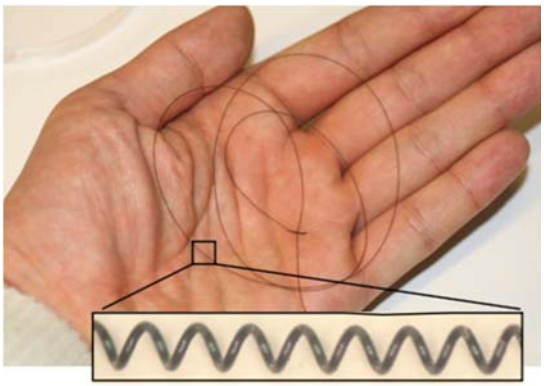

Fig. 6.1. SMA spring (diameter 400μm and length 50 cm)(Kim et al. 2009).

SMAs are mostly used in biomimetic robotic applications such as underwater locomotion, inchworms and flying robots. Fig. 6.2 shows some examples of those robots.

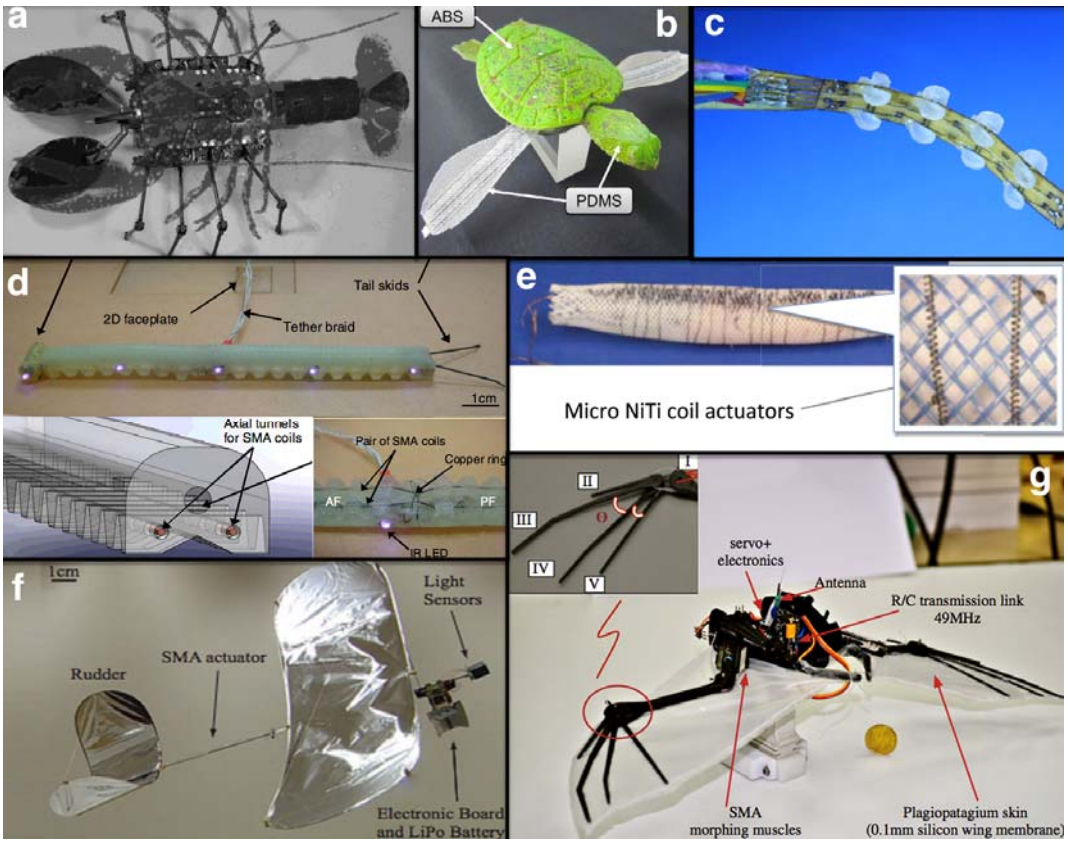

Fig. 6.2. Pictures of SMA soft actuator robots: (a) biomimetic underwater robot (Ayers and Witting 2007), (b) Turtle-like swimming robot (Kim et al. 2012), (c) robotic fish fin (Cho et al. 2008), (d) caterpillar-inspired soft-bodied rolling robot (Lin et al. 2011), (e) peristaltic soft robot with antagonistic coil actuators (Seok et al. 2013), (f) SMA-actuated micro-glider (Kovac et al. 2007) and (g) bat wings using SMA actuators (Colorado et al. 2012)

SMAs are also used for tactile displays and in particular for arrays of pins (Fig. 6.3), as they allow for the fabrication of compact actuators (Matsunaga et al. 2005, Velazquez et al. 2005).

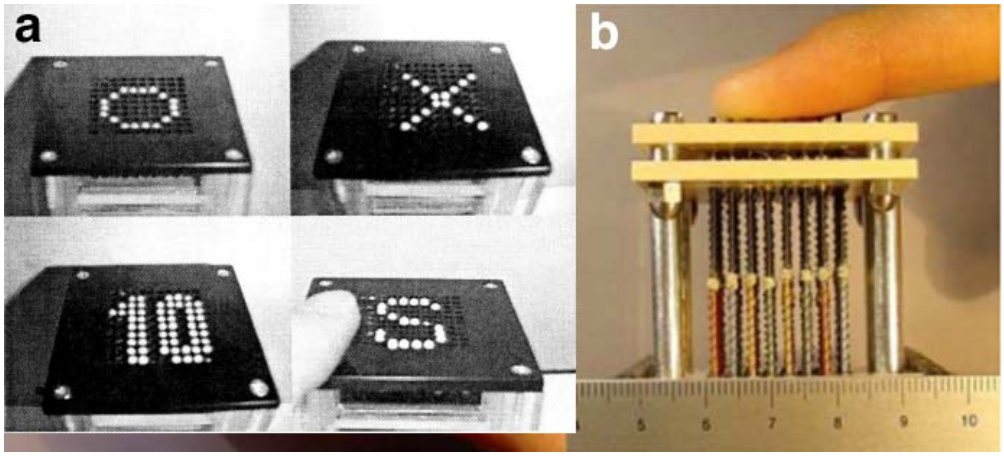

Fig. 6.3. SMA based tactile displays consisting of array of pins. Adapted from (Matsunaga et al. 2005, Velazquez et al. 2005)

The most attractive features of SMA reside in their compact design and low weight. This allows for a miniaturisation of the SMA based device. However, they have a low energy density as most of the power is dissipated by the heat required to exploit the shape memory effect. Furthermore, whilst they can be actuated relatively quickly by resistive heating, the time required by the alloy to cool and return to , rest position limits the operating frequency.

6.3. Pneumatic elastomeric actuators

Pneumatic elastomeric actuators consist of one or more chambers that expand when pressurized by a fluid, so as to produce diverse kind of actuations that depend upon their structural configuration. Linear contractile actuators that exploit this working principle are the McKibben artificial muscles (Daerden and Lefeber 2002). They consist of an elastomeric bladder inside a woven fabric mesh. When the bladder is pressurized it radially expands. The geometry of the mesh translates the radial expansion into a linear contraction (Fig. 6.4).

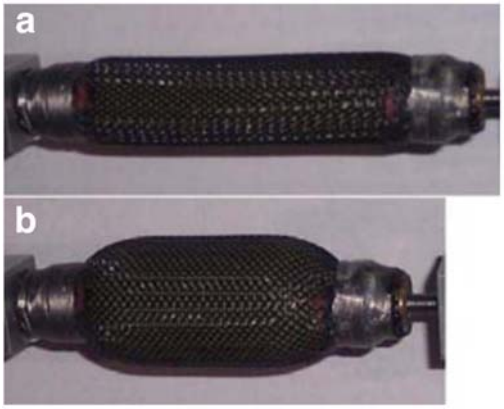

Fig. 6.4. Pictures of the McKibben artificial muscle in the rest state (a) and when pressurization produces the contraction (b) (Kang et al. 2009).

The recently introduced PneuNets (pneumatic networks) are a new class of pneumatic elastomeric actuators that consist of a series of chambers and channels that inflate when pressurized. Several kind of motion can be achieved by changing the geometry of the chambers of by combining material with different mechanical properties (Ilievski et al. 2011). As an example, adding a flexible but non stretchable layer to a series of chambers resulted in a bending actuator that was used in a legged robot (Shepherd et al. 2011)(Fig. 6.5).

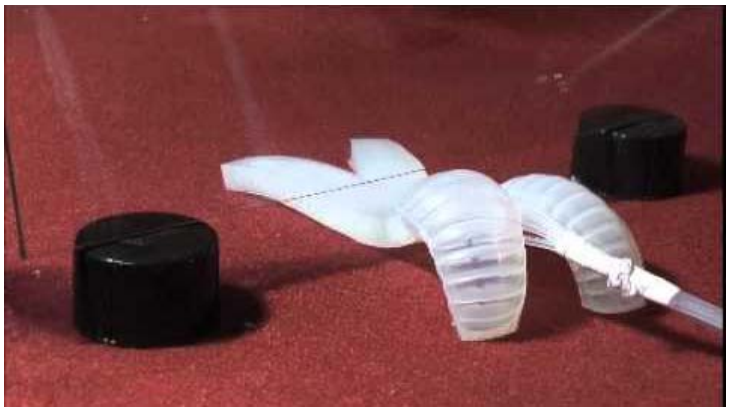

Fig. 6.5. Picture of the legged soft robot (Shepherd et al. 2011).

Pneumatic actuation has been also proposed as a mean of actuation for tactile displays. The tactile stimulation can be provided by circular elastomeric membranes that are inflated by application of a pneumatic pressure (Yun et al. 2016). Furthermore, tangential stimulation can be provided by displacing the touch surface, which is in contact with the finger pad (Yoo et al. 2015, Yun et al. 2016).

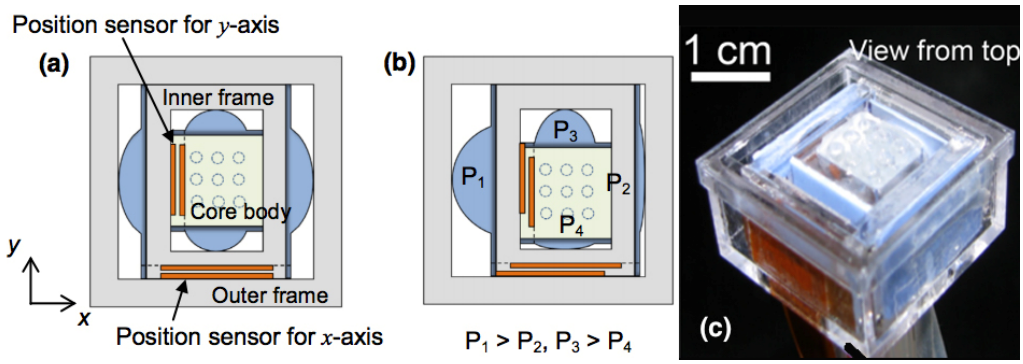

Fig. 6.6. Schematic representation and picture of the pneumatic tactile display (a, b) and picture of the device (c) (Yun et al. 2016).

While this kind of actuator are versatile and can produce considerable forces, they require an external pump, which makes them hard to integrate in portable devices, because of encumbrance and power consumption.

6.4. Magnetorheological devices

A magnetorheological (MR) fluid is a material that responds to an applied magnetic field with a change of viscoelastic properties. The applied field can precisely control the yield stress and by removing it, the fluid return to its liquid state (Kordonsky 1993). Although MR fluids are typically used in devices such as shock absorber, dampers and valves, the properties of these fluids have also been exploited to mimic the compliance of different materials (Lee and Jang 2011, Scilingo et al. 2003a). Two haptic displays have been proposed: one can be used to simulate the pinch-grasp behaviour of different rendered materials (Fig. 6.7a), the other, the so-called Haptic Black Box, is a container filled with a MR fluid where once a hand has been introduced to interact with the fluid, the fluid viscosity is controlled locally by a matrix of vertical solenoids (Fig. 6.7b).

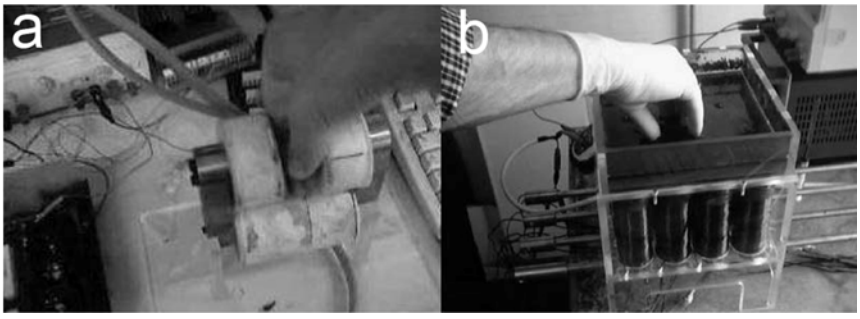

Fig. 6.7. Magnetorheological pinch-grasp device (a) and Haptic Black Box (b) (Scilingo et al. 2003b).

The devices in Fig. 6.7 were demonstrated to be effective in mimicking the compliance. However, the need for strong magnetic fields limits their application, as they are both heavy and bulky. Furthermore, the driving of the solenoids implies high power consumption.

6.5. Electroactive polymers (EAPs)

Electroactive polymers (EAPs) are an emerging class of smart materials that are capable of changing shape in response to an electrical stimulus**.** EAPs are referred to as "artificial muscles" as they combine actuation, sensing and stiffness control, showing functional analogy with natural muscles. According to their major mechanism of actuation, EAPs are divided in two main classes: ionic, in which the actuation is caused by the displacement of ions inside the polymer and electronic, that are activated by electrostatic forces (Bar-Cohen 2004, Brochu and Pei 2010, Carpi et al. 2008, Carpi et al. 2011c).

Table 6.1 EAP classification.

EAP class	Materials	Reference
Ionic EAPs	Polymer gels (PG)	(Tanaka et al. 1982)
	Ionic polymer-metal composites (IPMC)	(Asaka et al. 1995)
	Conjugated polymers (CP)	(Baughman 1996)
	Carbon nanotubes (CNT)	(Baughman et al. 1999)
Electronic EAPs	Piezoelectric polymers (PP)	(Nalwa 1995)
	Electrostrictive polymers (EP)	(Zhang et al. 1998)
	Dielectric elastomers (DE)	(Pelrine et al. 2000b)
	Liquid crystal elastomers (LCE)	(Lehmann et al. 2001)

6.6. Ionic EAPs

In ionic EAPs the actuation is caused by the displacement of ions in and out the polymer matrix. Examples of Ionic EAPs are: polymer gels, ionic polymer-metal composite, conjugated polymers, carbon nanotubes.

Polymer gels have the capability to expand or contract in response to external stimuli such as temperature, pH, solvent, ionic strength and electric field. The contraction

and expansion depend on the diffusion of water (or solvent) in and out the polymeric matrix (Feil et al. 1992, Osada 1987, Tanaka et al. 1982).

Ionic polymer–metal composites (IPMCs) consist of a polyelectrolyte membrane (such as Nafion) whose surfaces are coated with conductors (introduced by chemically plating with platinum or gold). As is shown in Fig. 6.8, when a voltage is applied, the ion migration and redistribution of water produces a swelling of the electrolyte in the vicinity of the cathode side and a shrinking close to the anode side, resulting in a bending deformation (Asaka et al. 1995, Jo et al. 2013)

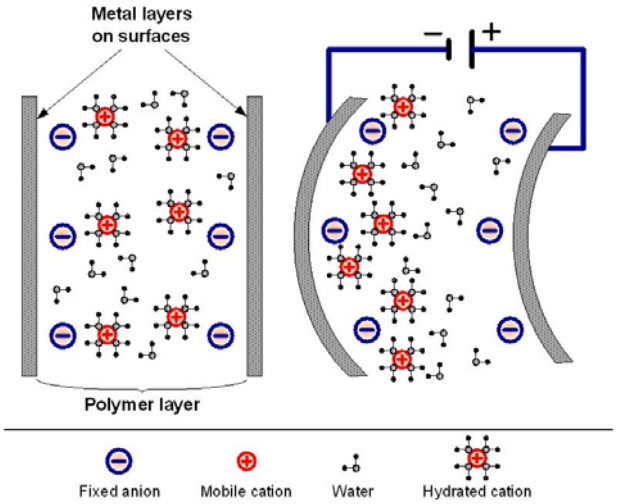

Fig. 6.8. Schematic representation of a IPMCs actuator working principle. (a) The actuator in a rest state. (b) The actuator shown with a voltage applied (Nam and Kwan 2012).

Fig. 6.9 shows how the volume of the conjugated or conducting polymers (CP) changes when the material is electrochemically oxidized or reduced. This results in an insertion and extraction of counter ions into the CP that cause an expansion or a contraction of the polymer, which lead to the actuation (Baughman 1996, Jager et al. 2000, Smela 2003)

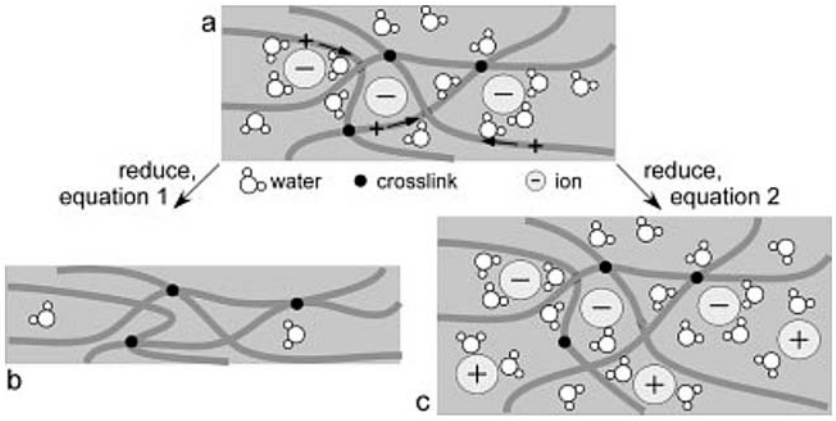

Fig. 6.9. Mechanism of volume change in CPs (Smela 2003).

Carbon nanotubes (CNT) exploit the following principle of operation. A voltage applied between the CNT and a counter electrode attracts ions to the CNT. The accumulation of charges on the surface is balanced by an electronic charge removal or injection within the CNTs. The variation in the charge on the carbon atoms produces a changes in the length of the covalent bond, which results, in an expansion and contraction of the CNTs according to the charge polarity (Baughman et al. 1999).

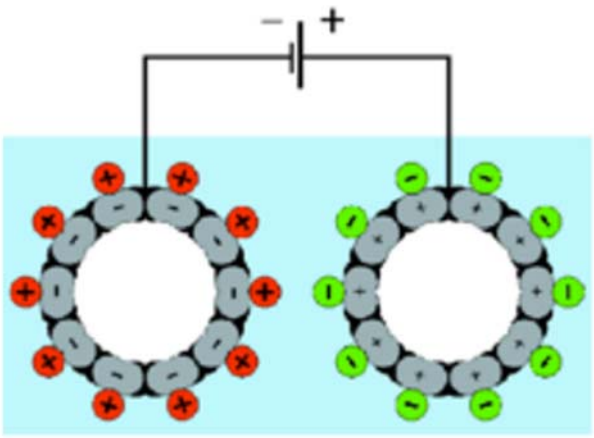

Fig. 6.10. Schematic illustration of charge injection in a nanotube-based electromechanical actuator (Baughman et al. 1999).

The actuation of ionic EAPs requires just a few volts, however a significant current is required to generate the ionic flow and a power is required to maintain the actuation. They usually require a solution that allows for the ions to migrate. Ionic EAPs achieve limited actuation strains and their actuation speed is relatively slow as

the actuation mechanism depends on the diffusion of relatively bulky chemical species.

6.6.1. Electronic EAPs

In Electronic EAPs the deformation is caused by electric field or Coulomb forces. Examples of electronic EAPs are: piezoelectric polymers, electrostrictive polymers, dielectric elastomers, and liquid crystalline elastomers.

Piezoelectric and electrostrictive polymers deform when an electrical field, which is parallel to the direction of polarization of the electrical dipoles in the structure of the polymer, generates an elongation of the material with respect to the field direction. The torque generated by the electrical field increases the alignment of the dipoles producing a change in length (Nalwa 1995, Zhang et al. 1998)

Dielectric elastomers actuators (DEAs) deform in response to an electric field. They consist in a soft elastomer sandwiched between two compliant electrodes. When a voltage is applied between the two electrodes, the electrostatic pressure produced results in a thickness squeezing and consequent surface expansion (Bar-Cohen 2004, Carpi 2010, Carpi and Smela 2009)

Liquid crystal elastomers (LCE) consist of long crosslinked polymer chains that are also liquid crystalline (LC). In their natural shape, the chains are ordered and, when the order is lost (by a range of different actuation processes that can include: heating; illumination or the application of an electric field), they reversibly contract (Dorkenoo et al. 2012, Lehmann et al. 2001)(Fig. 6.11).

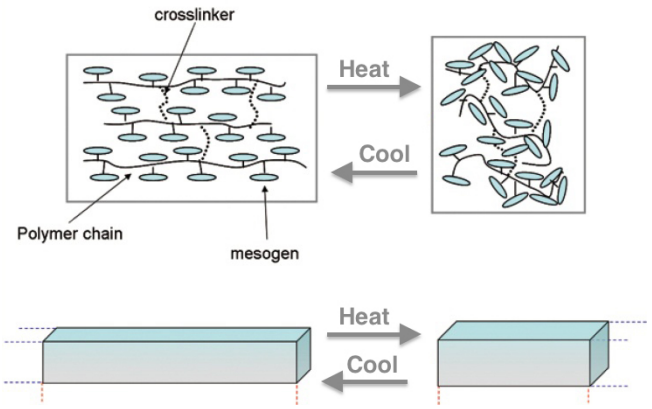

Fig. 6.11. Contraction of a LCE in response to heating. Microscopic point of view (top), macroscopic point of view (bottom) (Dorkenoo et al. 2012).

Fig. 6.12 shows a range of different EAP actuator applications.

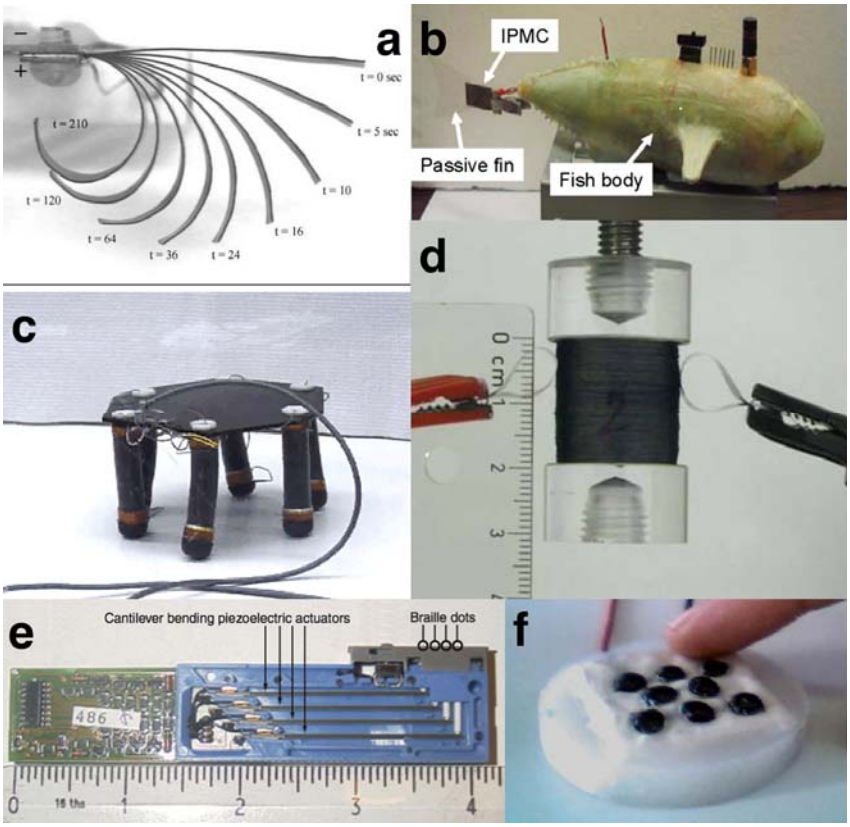

Fig. 6.12. EAP actuator applications. a) Successive photos of an IPMC bender (Nemat-Nasser and Wu 2003). b) Prototype of IPMC based robotic fish (Chen et al. 2010). c) MERbot: six-legged robot with 2-DOF DEA bases legs (Pei et al. 2003). d) DEA-based stacked linear contractile actuator (Kovacs et al. 2009). e) Lateral view of a typical piezoelectric driven bimorph Braille cell (Runyan and Carpi 2011). f) Prototype array of actuators based on DEAs (Carpi et al. 2009).

6.7. Chapter conclusion

Among the smart actuation technologies EAPs are increasingly being chosen as they offer solutions for an expanding range of applications that are precluded to other smart material-based actuation technologies (Carpi and Smela 2009).

Within the EAP family, DEAs are emerging as they are fast, lightweight, exhibit comparable or larger actuation strains, high energy density and high efficiency (Brochu and Pei 2010, Carpi et al. 2010a, Carpi et al. 2008, Pelrine et al. 2000b).

These properties, as well as their compliance make them a perfect candidate for lightweight and portable soft tactile displays. Indeed, the unique properties offered by DEAs can enable a wide range of applications in the field of soft actuation, allowing for new mechanism and designs. Furthermore, the intrinsic compliance of the end effector can be beneficial for the comfort of the user when in direct

interaction with the human body. In the following chapter, we will review these kinds of actuators.

Chapter 7 Dielectric elastomer actuators

7.1. Actuation working principle

While the deformation of a solid material stimulated by electricity was first observed in the late 18th century (Roentgen 1880), the working principle of DEAs was reintroduced in the late 1990s (Pelrine et al. 1998).

DEAs consist of a thin dielectric elastomeric membrane sandwiched between two compliant electrodes, so as to form a soft capacitor. When a voltage is applied, the opposing charges that are induced on the electrodes of the capacitor produce an electrostatic pressure. The attraction between opposing charges on the two electrodes and the repulsion of like-charges on the same electrode result in a thickness squeezing and consequent surface expansion as the material is practically incompressible (Bar-Cohen 2004, Carpi 2010, Carpi and Smela 2009). Fig. 7.1 represents the actuation mechanism of a dielectric elastomer actuator.

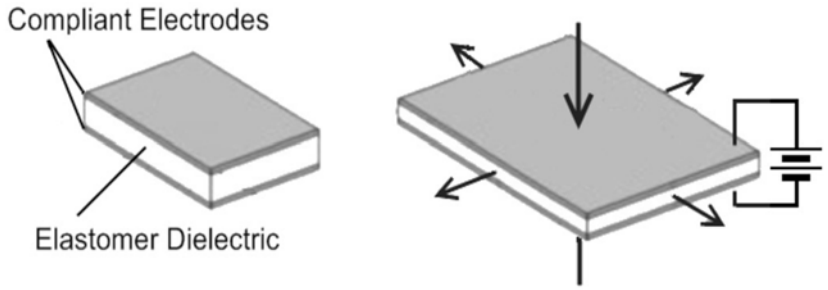

Fig. 7.1. Actuation principle of dielectric elastomers (DEs)(Anderson 2011).

The electrostatic pressure *p,* which is responsible for the actuation, is known as Maxwell stress and can be calculated in reference to the planar DEA shown in Fig. 7.1 as follows.

The first law of thermodynamics is stated as

$$dU = \delta Q - \delta W \tag{7.1}$$

where δQ is the amount of heat added to the system, and δW is the work done by the system (Hentschke 2013). Supposing that the DEAs is a thermodynamic system held

at a constant temperature and that the Maxwell stress *p,* orthogonal to the electrodes (having area *A*), produce a change in thickness of *dz*, then it can be stated that

$$\delta Q = 0 \tag{7.2}$$

and

$$\delta W = -pAdz \tag{7.3}$$

By substituting eq.(7.2)and(7.3) into eq. (7.1) gives

$$dU = pAdz \tag{7.4}$$

so that

$$p = \frac{dU}{Adz} \tag{7.5}$$

The electrostatic energy *U* stored in the deformable capacitor *C* when a voltage *V* is applied is

$$U = \frac{1}{2}CV^2 = \frac{1}{2}\varepsilon_0\varepsilon_r\frac{A}{z}V^2 \tag{7.6}$$

whereε_0 is the dielectric permittivity of vacuum, ε_r is the relative dielectric constant of the elastomer.

The change in the electrostatic energy *dU* can be written as its derivative with respect to the two variables: the thickness *z* and the area *A* of the planar DEA.

$$dU = \frac{\partial U}{\partial z}dz + \frac{\partial U}{\partial A}dA \tag{7.7}$$

And, as the elastomers can be considered as being essentially incompressible. Therefore,

$$Adz + zdA = 0$$

(7.8)

so that

$$\frac{dA}{A} = -\frac{dz}{z}$$

(7.9)

which represents the area expansion resulting from a thickness reduction.
By substituting eq.(7.9) into eq. (7.7) we obtain

$$dU = \left(-\frac{1}{2}\varepsilon_0\varepsilon_r\frac{A}{z}V^2\right)dz + \left(-\frac{1}{2}\varepsilon_0\varepsilon_r\frac{A}{z}V^2\right)dz = -\varepsilon_0\varepsilon_r\frac{A}{z}V^2dz$$

(7.10)

Finally, by substituting eq.(7.11) into eq.(7.5) is obtained

$$p = \varepsilon_0\varepsilon_r\left(\frac{V}{z}\right)^2 = \varepsilon_0\varepsilon_r E^2$$

(7.11)

which relates the Maxwell stress to the voltage applied, and the thickness of the dielectric elastomer layer (Pelrine et al. 2000b).

7.2. Elastomer materials

Among the several elastomers for DEAs, which include acrylics, silicones, fluoroelastomers, polyurethane, polybutadiene, and polyisoprene (Pelrine et al. 2000a, Pelrine et al. 2000b), the two most commonly used are the acrylics and the silicones.

The acrylic elastomer VHB (3M, USA) is a commercially available bonding tape well known for the large actuation strains offered. The VHB films are available in rolls of different thickness (500 μm and 1 mm), which allows for an easy and fast production of devices, as there is no need to fabricate the elastomer. However, the VHB film is not optimized for DEA applications. One issue being that it exhibits a high viscoelasticity, which limits the response speed and the reliability (Liu et al. 2014). Indeed, unlike ideal elastomers, real substances show a viscoelastic

behaviour, which consists in an elastic component and a viscous component. In a viscoelastic material the strain rate depends on time and there is a loss of energy when a stress is applied.

Some of the drawbacks and limitations of the VHB are overcome when using silicone elastomers. Indeed, they exhibit faster response speed due to a lower viscosity (Kornbluh et al. 2000, Maffli et al. 2015, Michel et al. 2010).. They are usually available in the non-polymerized form, which allows for the production of films with any required thickness. However, their maximum actuation strains are typically lower, because of a lower dielectric strength, which limits the maximum applicable electric field..

7.3. Electromechanical instability

Electromechanical instability (or the pull-in instability) is one of the most important mechanisms that lead to the failure of the DEAs. While for relatively stiff dielectric materials the deformation is limited by the electrical breakdown, for soft DE the actuation is limited by the electromechanical instability. Electromechanical instability arises as a consequence of the following mechanism. When a voltage is applied, the elastomer thickness decreases. According to eq. (7.11), the Maxwell stress and the electric field increase, causing a further thickness reduction. As a result of this mechanism, if the electric field growth is faster than the stiffening of the elastomer then the thickness will keep decreasing to a point where the material will fail either mechanically or from dielectric breakdown (Anderson et al. 2012, Carpi et al. 2008). So, the electromechanical instability may or may not occur depending on the voltage-stretch curve exhibited by the elastomer. Three types of DE have been distinguished according to their voltage-stretch curve $\Phi(\lambda)$ with respect to the breakdown voltage-stretch curve $\Phi_B(\lambda)$ (Zhao and Suo 2010)(Fig. 7.2).

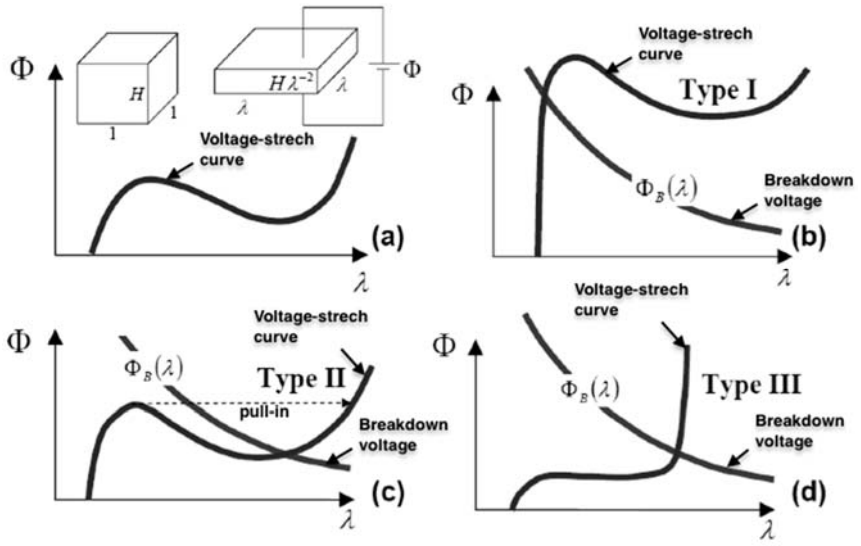

Fig. 7.2. Three types of DE are distinguished according to their voltage-stretch curve $\Phi(\lambda)$ with respect to the breakdown voltage-stretch curve $\Phi B(\lambda)$. Voltage-stretch of a generic DE (a). Type I DE, the voltage-stretch curve intersects the breakdown curve prior to the electromechanical instability occurs (b). Type II DE, the DE is softer than type I and it thins down excessively according to the pull in mechanism, so the elastomer reaches the breakdown (c). Type III DEs offer large deformations while eliminating the electromechanical instability by reaching a stable state before the electrical breakdown (d) (Zhao and Suo 2010).

In type I DEs the stiffness increases rapidly, so the electrical breakdown occurs prior to the electromechanical instability. Owing to their high stiffness the type I DEs are capable of small deformations. Type II DEs are softer than the type I and allow for higher deformations, however they thin down excessively and, according to the pull in mechanism described above, they reach the electrical breakdown. Type III DEs offer large deformations while eliminating the electromechanical instability by reaching a stable state before the electrical breakdown

This implies that it is possible to avoid the electromechanical instability by properly tailoring the elastomers mechanical properties.

7.4. Pre-stretch

Most of the elastomer materials used in DEAs undergo a significant pre-stretch phase, prior their actuation. The pre-stretch increases the Maxwell stress, according to eq. (7.11), as it thins the elastomer layer. Moreover, it increases the breakdown strength and suppresses the pull-in instability (Kofod et al. 2003, Zhao and Suo 2010), thus further increasing the electromechanical transduction.

The pull-in instability is reduced or removed as the stiffening of the material (caused by the pre-stretch) shifts the voltage-strain curve of the elastomer. As a result,

actuation can occur for strains that are beyond the zone where the instability appears (Koh et al. 2011, Suo 2010, Zhao and Suo 2010).

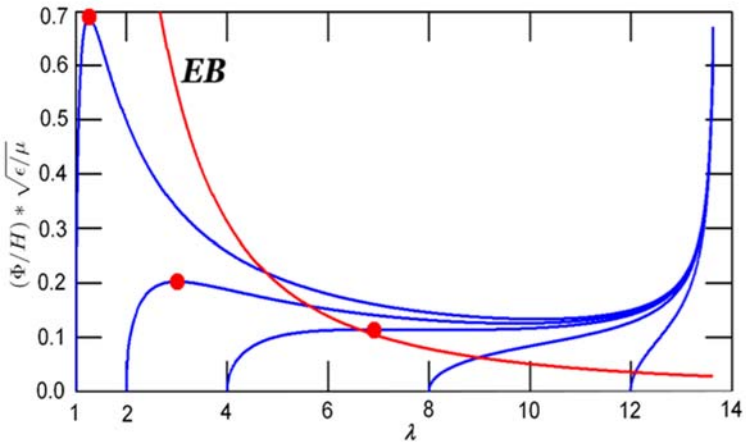

Fig. 7.3. Voltage-stretch response of DE membrane at various prestretches λ (blue lines), with electromechanical instability denoted with solid red dots, and electrical breakdown denoted by the intersection between the blue and the red lines. The prestretch, which corresponds to λ for a null voltage, affects the voltage stretch curve of the elastomer. This shift the intersection with the electrical breakdown curve allowing for higher deformations (Koh et al. 2011).

The main disadvantage of the pre-stretch is the need for a rigid structure that is used to maintain an adequate tension in the elastomer. This requirement can increase the complexity, the encumbrance and the weight of the device. In order to overcome this drawback, new elastomers having 'chemically locked-in' prestrain have been proposed. To the prestretched elastomer matrix is added a more rigid component silicones that act to preserve the prestrain in the host network. This allows for free-standing prestrain-locked elastomers that don't need rigid structures supporting the prestretch(Brochu et al. 2013).Also, elastomers displaying the 'type III' behaviour shown above have been synthesised (Niu et al. 2013).

7.5. Electrode materials

The electrodes have to be conductive, as they have to hold the charge. Also, they have to be compliant otherwise they will reduce the electromechanical transduction. Furthermore, their conductivity must remain relatively stable at the large actuation strains exhibited by the DEAs.

The most commonly used electrodes are based on carbon powder, which can be used as it is or can be mixed with other materials, such as greases or silicones. The main

carbon-based compounds reported in literature for the fabrication of compliant electrodes for DEAs are the Vulcan XC72 (Carpi et al. 2007) by Carbocrom (Italy), the Ketjenblack EC-300J (Aschwanden et al. 2008) and the Ketjenblack EC-600JD (AkzoNobel polymer chemistry, The Netherlands) (Kovacs and During 2009, Rosset and Shea 2013).

The loose carbon powder can be deposited directly onto the surface of the elastomer, either using a brush or a spray. Owing to the weak bonding force between the carbon agglomerates, the contribution of this kind of electrodes to the stiffness of the membrane is negligible (Kovacs et al. 2009, Rosset and Shea 2013). However, this kind of electrode can be easily damaged or removed, as it is not properly bonded to the elastomer.

Carbon grease (a mixture of carbon black and grease) allows for a better adhesion and ease of deposition, when compared to the carbon powder, but it also rubs off easily (Huang et al. 2012).

Carbon black can be mixed with a non-polymerized elastomer then cured to form a solid electrode (Bozlar et al. 2012, Yurekli et al. 2001). Carbon black filled elastomeric electrodes are robust and offer a good adhesion to the elastomer. However, their stiffness is no longer negligible and as a consequence they have to be processed in appropriately thin layers. The increase of sheet resistance caused by the reduction of thickness might affect the actuation. Indeed, the sheet resistance of the electrode increases when the thickness decreases. Nevertheless, pad printed electrodes having a thickness in the μm range have been demonstrated (Poulin et al. 2015), even though they have been only tested for actuators with limited electrode area.

7.6. Actuating configurations

The thickness squeezing and surface expansion exhibited by a generic planar DEA can be exploited in a variety of actuating configurations (Carpi et al. 2008, Kornbluh et al. 2002). The planar expansion can be used to obtain a linear extender (Fig. 7.4b). Rigid constraints at the periphery of a circular membrane lead to an out-of-plane actuation (Fig. 7.4c). Contractile actuators can be developed by stacking several elastomer layers or by folding a single elastomer stripe, so as to the exploit the thickness squeezing exhibited by the DEAs (Fig. 7.4 d and e). A multi degree-of-

freedom actuator can be obtained by rolling an elastomer layer with patterned electrodes (Fig. 7.4 f and g) (Pei et al. 2004).Planar actuators can be coupled to rigid frames so as to produce force and displacement (Fig. 7.4 i and j).

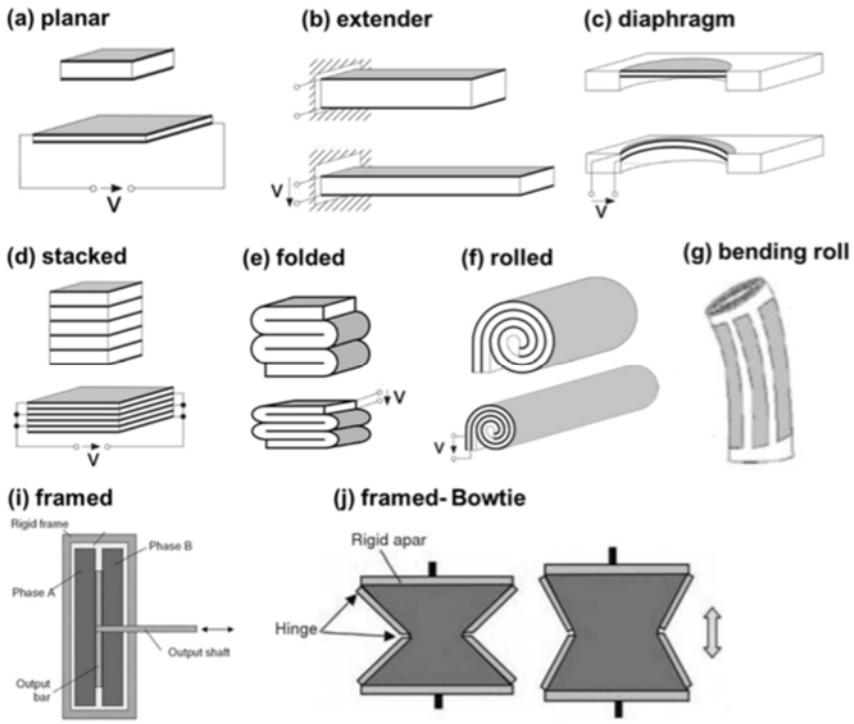

Fig. 7.4. DEAs basic configurations (Carpi et al. 2008).

These basic actuating configurations have been used in several applications. The sequential actuation of four planar DEAs has been exploited either in a laser speckle reducer (*Optotune website* , Blum et al. 2012) and in a rotary motor (Anderson et al. 2010). Tuneable optics have also been developed by exploiting the out-of-plane actuation (Niklaus et al. 2010) and by coupling a soft polymeric lens to a planar annular actuator (Carpi et al. 2011b, Maffli et al. 2015). Furthermore, stacked actuators have been demonstrated to lift weights over 2kg (Kovacs et al. 2009).

Recently, hydrostatically coupled DEAs have been introduced, which exploit a fluid coupling between a DEA and one or more passive elastomeric parts (Carpi et al. 2010b). The fluid that works as hydrostatic coupling transmits the actuation from the active part to the passive parts. This enables actuating configuration such as the contractile actuator (Carpi et al. 2012) and the bubble-like actuator (Carpi et al. 2009) shown in Fig. 7.5. The contractile actuator consists of a fluid filled chamber delimited by two rigid disks and a cylindrical layer of DEA. The disks are provided with a precompression (either by an internal spring as in Fig. 7.5b or an external

load) that provides the membrane with outward curvature. When a voltage is applied, the surface expansion of the DEA increases the outward bulge, causing the structure to contract.

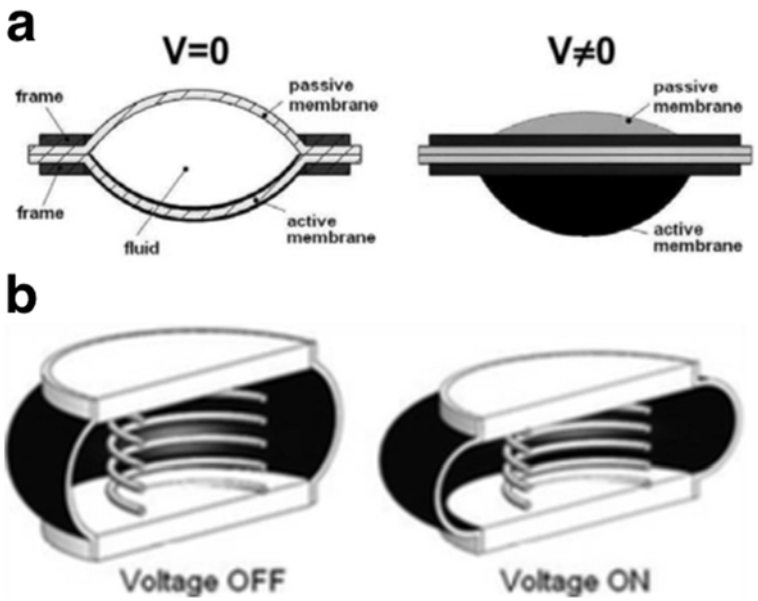

Fig. 7.5. Examples of HC-DEAs: a) Bubble-like actuator (Carpi et al. 2010b). b) Contractile actuator (Carpi et al. 2012).

The bubble-like actuator consists of two bubble shaped elastomeric layers clamped by two rigid rings. The electrical driving of this actuator results in a buckling of the active membrane and which causes the passive membrane height to decrease. The working principle of the actuator is extensively described in the following chapter.

7.7. Chapter conclusions

Dielectric elastomer actuators (DEAs) are transducers consisting of an elastomeric membrane sandwiched between two compliant electrodes. When a voltage difference is applied between the electrodes, the electrostatic force that is generated squeezes the membrane. This simple working principle can be exploited in several actuator configurations, which were shown in this chapter.

In particular, the push-pull actuating mechanism shown by the bubble-like HC-DEA has been proposed as a potential tactile stimulator (Carpi et al. 2009, Lee et al. 2014). The extensive validation of that concept, in terms of actuator working

principle, its fabrication and its use as an actual tactile display are the subject of this thesis and are described in the next chapters.

Chapter 8 A tactile feedback system: structure, material and methods

8.1. Introduction

This chapter describes a proposed new design of tactile display and the methods that were used for its fabrication and the assessment of its electromechanical and psychophysical performance.

The tactile display design that has been adopted in this work was based upon the bubble-like hydrostatically coupled DEA (HC-DEA) technology, whose general operational principal was described in Chapter 6 . The tactile stimulation is obtained by exploiting the push-pull actuation typical with this kind of actuator.

The fabrication process that was conceived specifically to develop this new device is described. The details of the specific design solution that was used to create and to enclose the actuator and which allowed the finger to be maintained in its correct position are also described in detail.

Finally, the electromechanical and psychophysical tests performed to assess the capability of the actuator to generate adequate mechanical stimuli are explained.

8.2. The tactile display

8.3. Actuator structure

The DEA-based tactile stimulator was devised using a bubble-like HC-DEA technology. This approach relies upon an incompressible fluid that hydrostatically couples a DEA-based active membrane to a passive membrane, which is in contact with a user's fingertip.

In particular, the structure includes two circular membranes. One membrane is passive while the other, the active membrane, is made active by coating both of its faces with compliant electrodes. The active membrane is electromechanically active as it exploits the DE actuation principle. Both membranes are clamped by

two rigid circular frames that have the following three functions. Firstly, the frames are responsible for sustaining the prestretch in the membrane that is required for optimal actuation. Secondly, they maximize the actuation in the out-of-plane direction, as they act as a peripheral constraint that inhibits the radial expansion of the active membrane. Thirdly, they work together to seal an incompressible fluid that is contained between the two membranes as shown in Fig. 8.1. The fluid, which provides each membrane with the shape of a portion of a spherical cap, is also responsible for the transmission of the actuation from the active to the passive membrane, using the mechanism described in the following section.

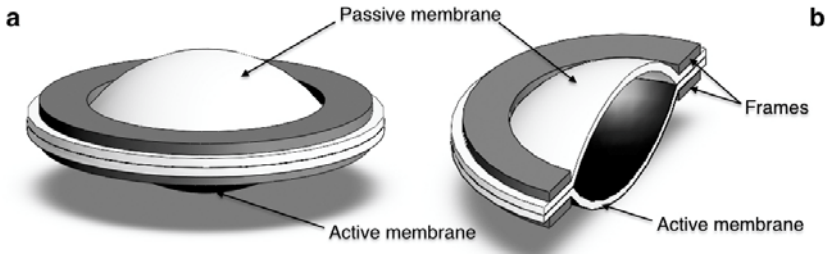

Fig. 8.1. Structure of the HC-DEA device used to obtain the tactile display: 3D renderings showing an axonometric view (a) and a sectional view (b).

8.3.1. Actuator principle of operation

When a voltage is applied to the electrodes, as a consequence of the resulting Maxwell stress, the active membrane expands its surface area. As a consequence of the initial pre-curvature and the constraint provided by the circular frames, the active membrane buckles outwards. Thus, as the fluid's volume is constant, the passive membrane moves inwards (Carpi et al. 2010b). So, a fluid-mediated hydrostatic transmission between the two membranes is established, as demonstrated in Fig. 8.2. The application of an alternating voltage produces a push-pull action.

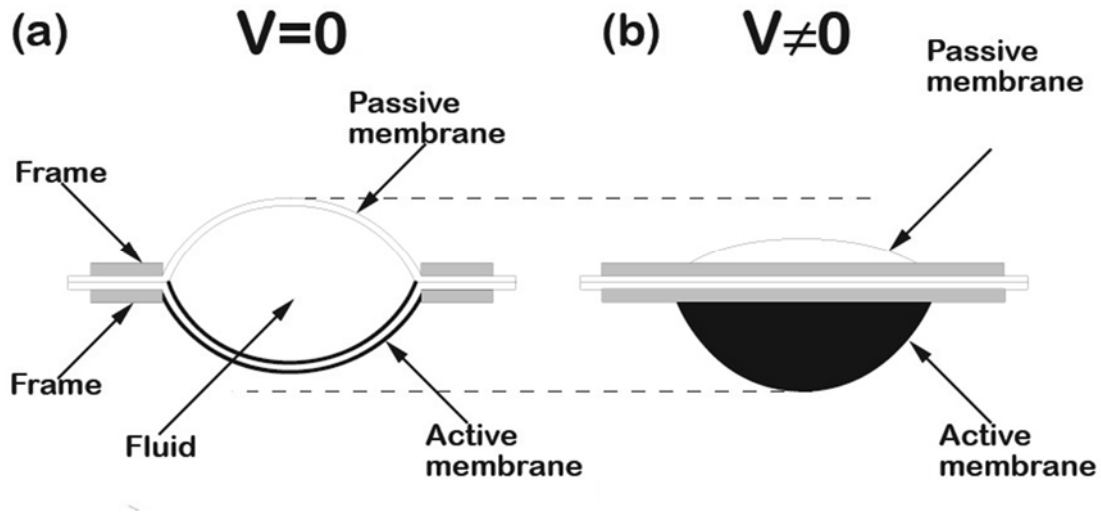

Fig. 8.2. Schematic drawing of the HC-DEA configuration: (a) lateral section of the device in the rest state; (b) lateral view of the device in an electrically induced state, due to an applied voltage difference V.

The fluid mediated actuation allows for two attractive features. First, the user can touch the passive membrane, which works as the end effector, without being exposed to the high voltage that feeds the active membrane, allowing for an electrically safe transmission of actuation. Second, any distortion of the passive membrane introduced by the finger is evenly distributed to the active membrane. Indeed, the hydraulic transmission maintains a suitable uniformity of the active membrane's curvature. This avoids any localised perturbation of the thickness that could lead to premature electrical breakdown (Fig. 8.3). Such a self-compensation effect preserves the functionality and increases the electrical robustness of the device (Frediani et al. 2014).

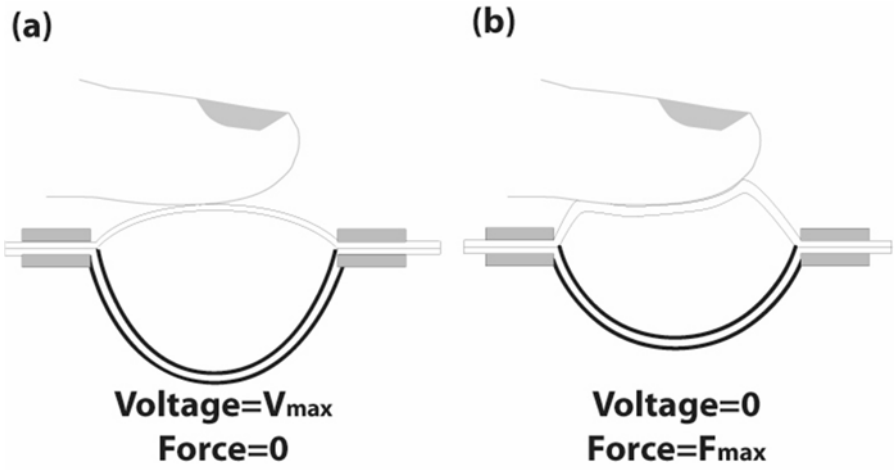

Fig. 8.3. Schematic drawings of the interaction between a finger and the soft tactile display. Loading of the passive membrane of a bubble-like HC-DEA: the internal redistribution of the fluid ensures that the active membrane keeps a uniform profile, both at rest (c) and when a voltage is applied (d).

8.3.2. Actuator fabrication

The bubble like HC-DEA consisted of two membranes made of an acrylic elastomer film (VHB 4910, 3M, USA). The use of this elastomer, which is the most widely used and studied material in the DEA field (Carpi et al. 2008), was justified especially as a result of its good self-adhesion properties, which simplified the manufacturing process, as described below.

Both membranes were radially pre-stretched to a radial extension ratio of four using the custom-made apparatus shown in Fig. 8.4.

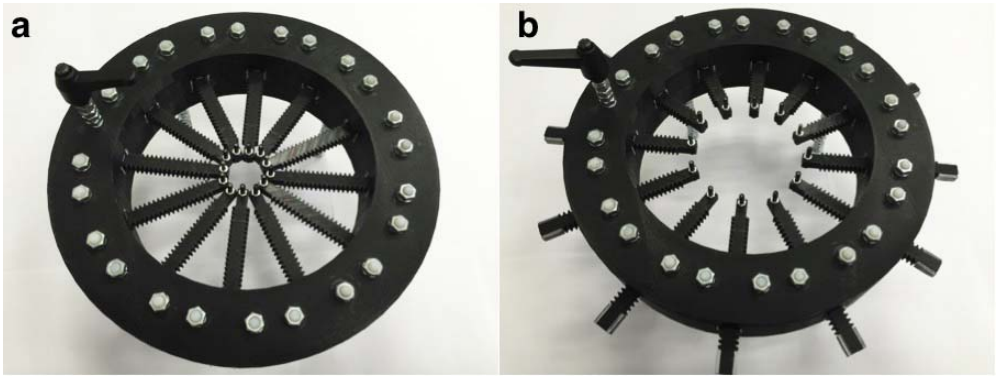

Fig. 8.4. Radial stretching tool in the null stretch (a) and in stretch state (b).

That tool consisted of a circular frame with 12 sliding arms. The elastomer, in the unstretched state, was fixed to the pins located at the end of the arms. By rotating the handle, the arms slid outwards radially stretching the elastomer.

The film thickness reduction, as an effect of the pre-stretch, was calculated as follows. Let us consider a cylinder of elastomer having initial thickness t_0 and base radius r_0 (Fig. 8.5).

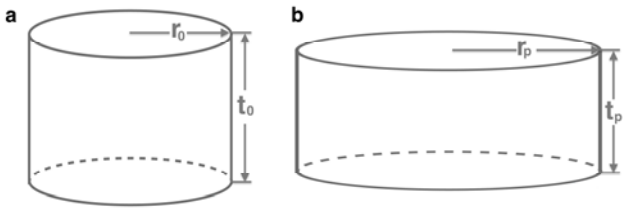

Fig. 8.5. Elastomer cylinder in an initial state (a) and after a radial pre-stretch (b).

The initial volume of the cylinder is:

$$Vol_0 = \pi r_0^2 t_0$$

(8.1)

As a result of the radial pre-stretch λ_r, the cylinder base radius r_p becomes

$$r_p = r_0 \lambda_r$$

(8.2)

and the corresponding volume Vol_p is

$$Vol_p = \pi r_p^2 t_p$$

(8.3)

As the volume of the elastomer is constant, we can write

$$Vol_0 = Vol_P \quad \pi r_0^2 t_0 = \pi r_p^2 t_p = \pi r_0^2 \lambda_r^2 t_0$$

(8.4)

A solution of eq.(8.5) can be written as:

$$t_p = t_0 / \lambda_r^2$$

(8.5)

As the membrane's initial thickness t_0=1 mm and the pre-stretch ratio λ_r=4, then the thickness after pre-stretch resulted in a thickness t_p=62.5 μm.

The elastomer was then transferred onto a plastic ring to facilitate handling throughout the rest of the fabrication process (Fig. 8.6).

Fig. 8.6. The elastomer is transferred onto a plastic ring used to keep the film pre-stretched during the fabrication process.

One membrane was purely passive while the other was made active by coating both of its faces with compliant electrodes. The electrode material consisted of a

carbon conductive grease (846, M.G. Chemicals, Canada), which combined good conductivity and compliance with ease of use as it was easily applied to the surfaces (Fig. 8.7).

Fig. 8.7. The carbon grease electrode is smeared onto the elastomer surface using a brush.

Each electrode had a circular shape with a radius of 10 mm.

The pre-stretched passive membrane was placed over an empty chamber having a circular hole of the same size of the electrode. A depression was created in the film by the application of a vacuum in the chamber, which was generated using a syringe. As shown in Fig. 8.8, this depression in the membrane created a cavity that was then filled in with 1 ml of a dielectric silicone grease (8462, M.G. Chemicals, Canada). The silicone grease was mainly chosen for its viscosity, as it avoided any leakage between the two membranes, which might have resulted in a failure of the device. Also, the chemical incompatibility between the silicone and the acrylic elastomer prevented the diffusion of this medium through the membrane, which might have affected its electrical and mechanical properties. While the high viscosity of the grease was expected to decrease the speed of actuation, it was the best choice at the moment, considering that the first prototypes fabricated using silicone oil had a really short lifetime (about 1 day).

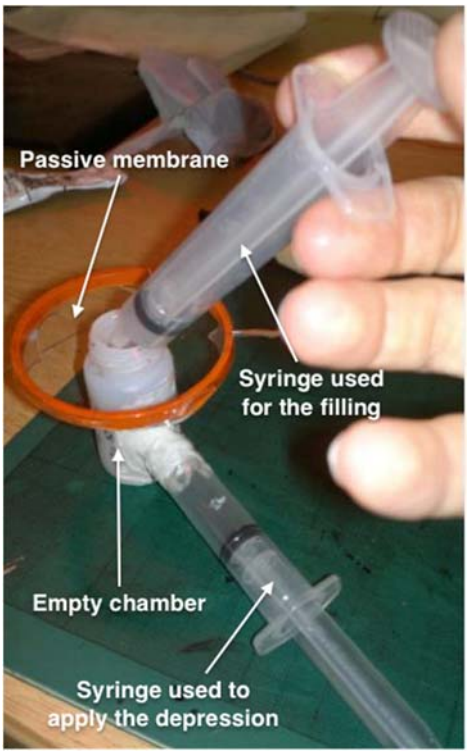

Fig. 8.8. The depression created by the application of a small vacuum which forms a cavity in the passive membrane which is then filled in using a dielectric silicone grease applied through a second syringe.

The active membrane, which was already coated on each surface with the carbon grease electrodes to which electrical contacts, made from aluminium strips, was then coupled to the other membrane (Fig. 8.9).

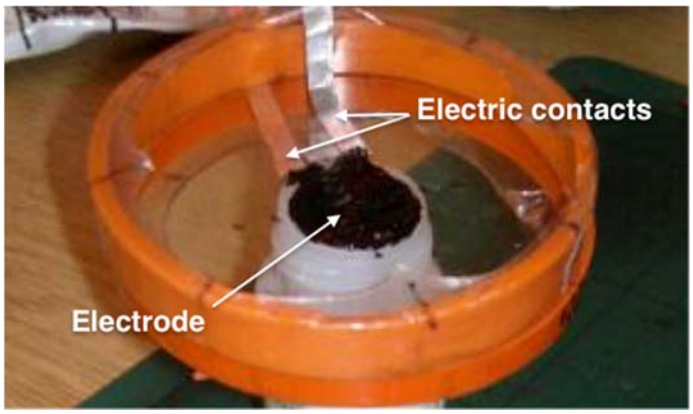

Fig. 8.9. The active membrane being coupled to the passive membrane. The figure also shows the two aluminium strips that are used as electrical contacts to the electrodes.

The adhesiveness of the VHB film facilitated effective bonding between the two layers. After a hold time of 10 minutes, the bonded membranes were removed from the vacuum chamber, and bonded to a stiff plastic frame.

Fig. 8.10 shows the fabrication steps.

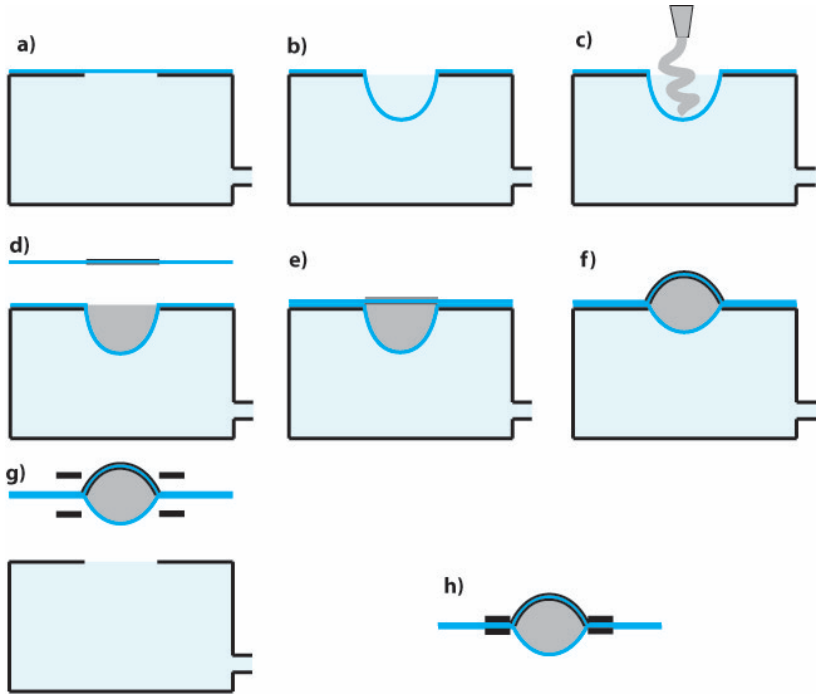

Fig. 8.10. Fabrication steps for a bubble-like HC-DEA: (a) the passive membrane is placed over an empty chamber with a circular hole. (b) A vacuum is applied in order to deform the membrane and create a cavity. (c) The cavity is filled with silicone grease. (d) The active membrane is coupled to the other membrane. (e) They are bonded together. (f) The vacuum is released. (g) The membranes are removed from the vacuum chamber. (h) They are bonded to a plastic frame.

The resulting final shape (Fig. 8.11) of each membrane was a spherical cap having a height of 7 mm and a base radius of 10 mm.

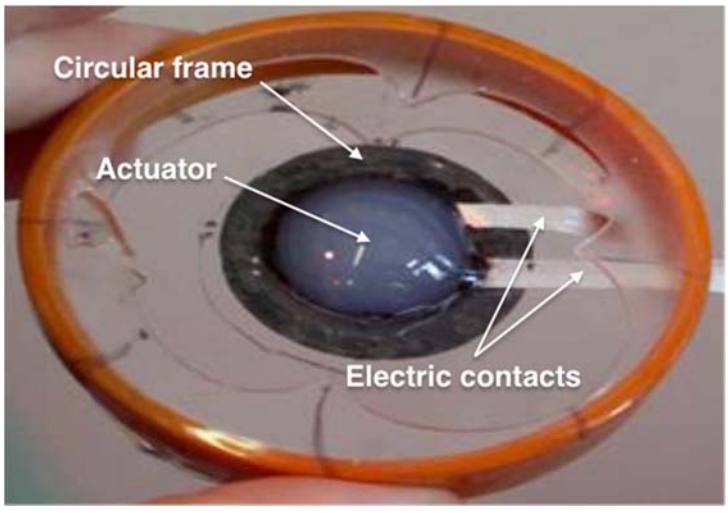

Fig. 8.11. The depression is removed and the actuator is bonded to a circular frame.

The two most critical steps of this fabrication process are the filling of the cavity (Fig. 8.8) and the accurate positioning of the active membrane (Fig. 8.10d). Indeed, it is important to avoid the filling grease spilling out of the cavity, as this

would inhibit the membrane adhesiveness, thus preventing proper bonding between the two membranes. This issue is also important during the coupling of the two membranes.

8.3.3. Actuator casing

The previous section described the manufacturing of a generic bubble-like actuator. However, for the wearable tactile system, the actuator frame was designed also to properly lodge the finger, so as to allow for the finger pad to be in contact with the passive membrane (Fig. 8.12).

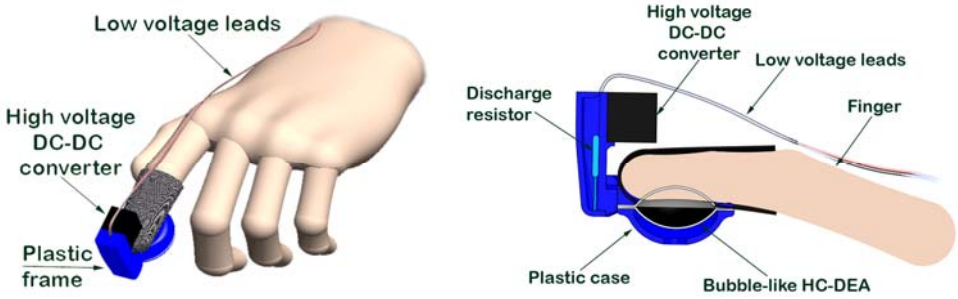

Fig. 8.12. Schematic drawings of the fingertip wearable tactile display.

To this end, a special casing for the actuator was conceived as follows. It consisted of a modification of the two circular frames described in section 8.3. The top frame was properly shaped so as to lodge the fingertip (Fig. 8.13a), while the bottom part was designed to work as a cover for the active membrane, so as to prevent any contact between it and the user (Fig. 8.13 b).

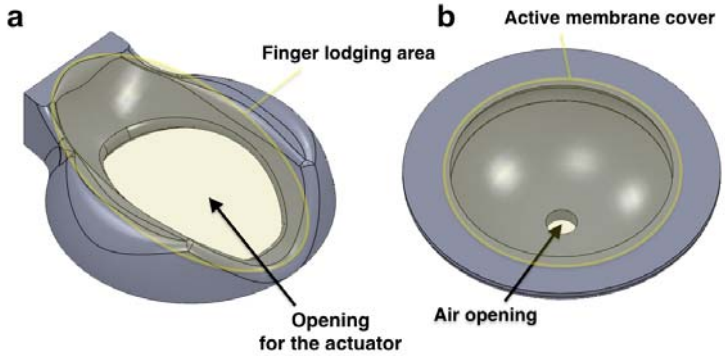

Fig. 8.13. Particulars of the display's top (a) and bottom (b) frames.

The bottom part also had an opening, which was used to let air to flow out when, as a result of the actuation, the active membrane expands.

The finger part of a glove, made of an elastic fabric, was used to keep the finger in place.

Fig. 8.12 also shows another part of the plastic case that was designed to accommodate a high-voltage DC-DC converter used to drive the active membrane (represented by the black cube in figure) above the fingertip. The position of the converter was chosen so as not to interfere with the finger movements. The converter used in this application was an EMCO Q50 (EMCO High Voltage, USA). This device was fed with a 0-4.5 V signal, which in turn generated a 0-4.5 kV input for the actuator. The plastic case also hosted a high-voltage discharge resistor, whose function is described in the following section.

Fig. 8.14 shows all the parts of the display in an exploded view.

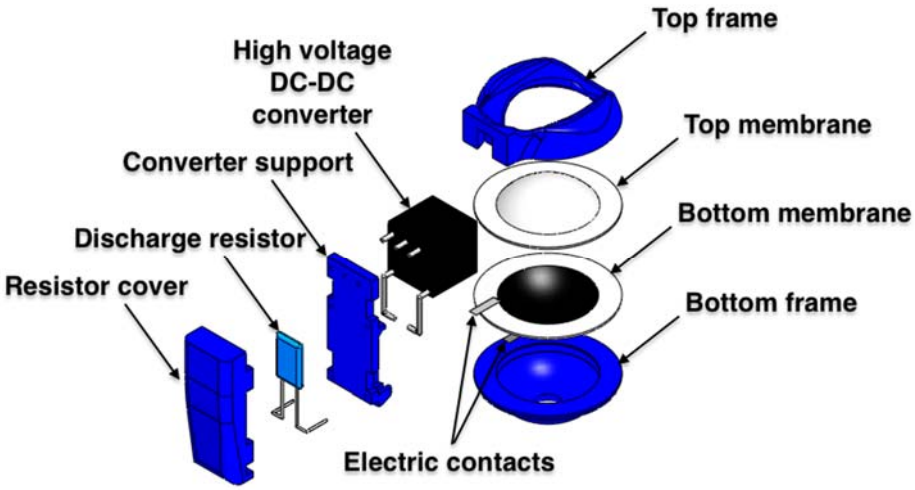

Fig. 8.14. Exploded view of the tactile display.

The support for the converter and the top frame were designed so that a trapezoidal pin extended from the support and a recess with a similar shape was cut into the top frame so as to create a sliding joint (Fig. 8.15). This allowed for easy disassembly of the two parts, in order to replace the actuator.

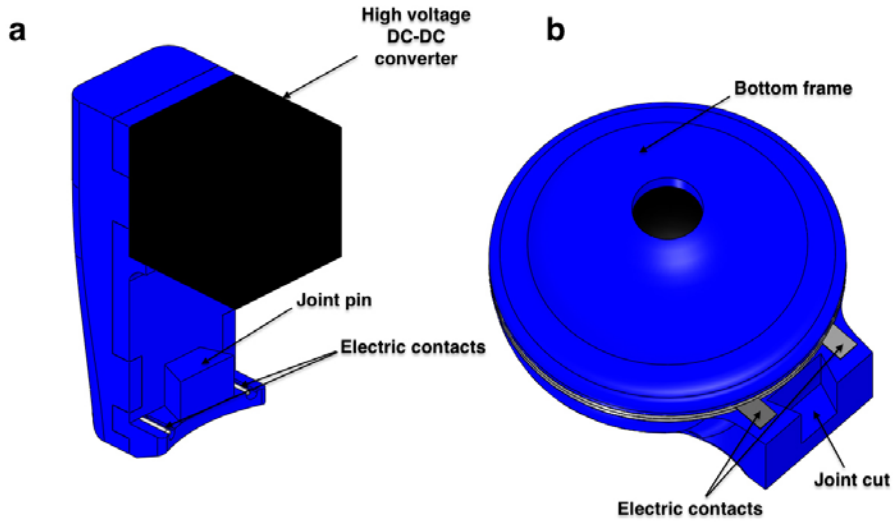

Fig. 8.15. Views of the support for the high voltage converter (a) and of the case for the actuator (b) that show the joint between the two parts, as well as the electrical contacts.

The joint also served to make an effective electrical connection by allowing to clamp the actuator aluminium strips between the metal wires from the high voltage circuitry and the plastic frame (Fig. 8.16).

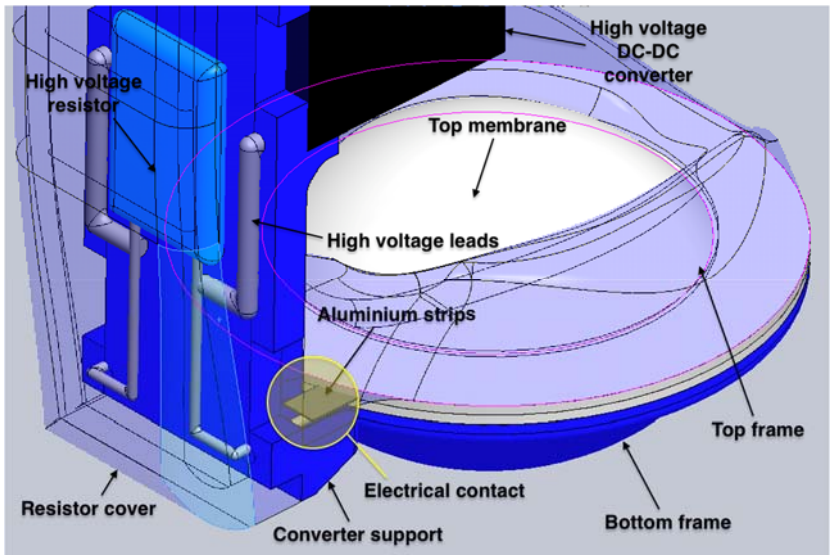

Fig. 8.16. A close up of the electrical contacts between the high-voltage circuitry and the actuator. The resistor cover and the top frame are made transparent so as to allow for a view of the electrical contact.

The development of the casing underwent several iterations in order to progressively 'optimise' the shape, size and function of all the various components. Fig. 8.12 shows the version used to perform the mechanical tests and psychophysical experiments described in the next sections.

8.4. High voltage driving systems

Whereas several systems that are able to provide high voltages are available on the market, none of them has been developed specifically to drive DEA. However, devices are able to generate the driving signal required for the actuation. In particular, the high voltage sources that were used during the testing of the device are described in the following sections.

8.4.1. Trek model 615-10

Fig. 8.17 shows the high voltage amplifier Trek model 615-10 (Trek Inc., USA) used for some of the electromechanical testing in this work.

Fig. 8.17. Trek model 615-10±10 kV high-voltage AC/DC generator.

These types of bench-top generator / amplifier are very expensive (at around ten thousand pounds). The high performance provided allows them to adapt to various tasks other than simply driving DEA devices (for example: electrical insulation testing, dielectric material evaluation, electrospinning). They can have a bandwidth of the order of kHz and provide currents of the order of tens of mA, which make them oversized for most of the typical DEA applications.
It combines an AC/CD generator with a ±10 kV high voltage amplifier. The high voltage output can either be manually set via knobs located on the device or via a low voltage analog input. It features the remote monitoring of voltage and current, which is useful for testing and control purpose.

In addition to the high cost, the main drawbacks of this kind of generators are represented by their excessive dimensions and weight (10-20 kg), which make them suitable for benchtop operation and device development only.

8.4.2. EMCO Q50

The miniaturised DC/DC converter EMCO Q50-5 (5 kV output, 5 V input; 0.5 W; EMCO High Voltage, USA) was integrated within the tactile display case and provided the voltage needed for the actuation for the majority of the work described in this thesis.

Fig. 8.18. Picture of the DC-DC converter (EMCO Q50-5).

The EMCO Q50-5 can provide up to 5kV. The module used was compact (2 cm^3) and lightweight (4 gr). The output is directly proportional to the input voltage and is linear from 0.7 V to the maximum input voltage. For input voltage values up to 0.7 V the output voltage is null. So, 0.7 V can be defined as a de facto ‘activation threshold’.

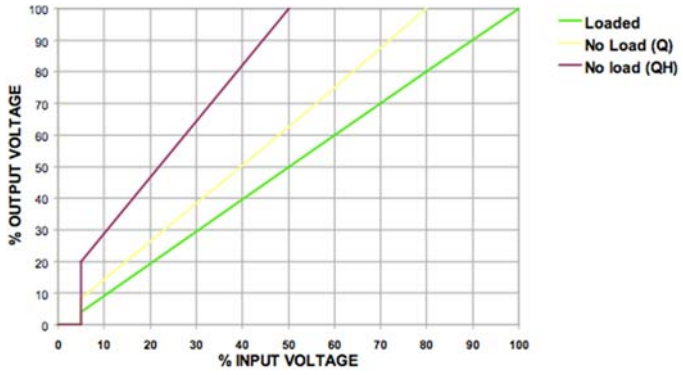

Fig. 8.19. Typical input versus output voltage for the EMCO Q series DC/DC converters (*EMCO high voltage Q Series datasheet* 2016).

As the output power is limited, they can provide a maximum current of 100 μA. The price is typically around £300.

Furthermore, owing to the internal circuitry, they require an external high-voltage discharge resistor, to be connected in parallel to the converter's output, which has the following two functions. Firstly, it allows the converter to operate in the full load status (therefore the output current is close to the maximum that the device can provide) whilst maintaining an output that is proportional to the input (**Error! Reference source not found.**) (EMCO high voltage Q Series datasheet 2016). The second reason for using a parallel resistor is to facilitate a faster discharge of the actuator when the voltage is reduced or nulled. Indeed, without any discharge resistor the characteristic high output impedance shown by the EMCO converter would make the actuator discharge excessively long. Even with a discharge resistor the operation frequency is still limited to a few Hz.

The high voltage resistor (HB Series, TE Connectivity Ltd, Switzerland) (Fig. 8.20) used in parallel to the actuator had a value of 50 MΩ.

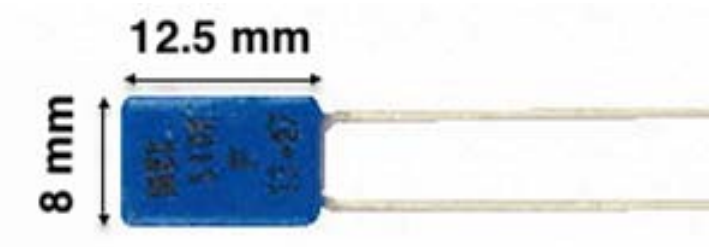

Fig. 8.20. Picture of the high voltage resistor (TE Connectivity, HB Series.)

In order to allow for the converter to operate in the "full-load condition", the value of the resistor was chosen as follows. The actuator properties defined the

maximum voltage V_{Max} to be provided by the converter, which was 4.5 kV. The converter datasheet (EMCO high voltage Q Series datasheet 2016) indicated that the maximum output current I_{Max} to be ensured in order to let the converter work in the "full-load condition" was 0.1 mA. So, in order to guarantee the full-load condition, the necessary resistance value R was calculated as follows:

$$R = \frac{V_{Max}}{I_{Max}} = \frac{4500}{0.1\ 10^{-3}} = 45\ M\Omega \tag{8.6}$$

With the aim of reducing the encumbrance of the support for the high voltage converter, we chose the closest resistor among those commercially available, so as to have one single load resistor. Indeed, the resistance values (in the range of our interest) that are available in the HB series were 5, 20 and 50 MΩ. The calculated value of 45 MΩ could have been obtained with a series of 3 resistors (two of 20 MΩ and one of 5 MΩ). However, this would have increased the dimensions of the high voltage support. So, we opted for the closest value available as a single resistor, which corresponded to 50 MΩ. With this resistance value, the nominal full-load condition (which arises when the output current close to I_{Max}) was only obtained at the maximum driving voltage. Indeed for voltages lower than the maximum, the current provided by the converter was lower than the maximum. However, with a single resistor only one choice is possible.

In order to verify the input-output curve reported in the EMCO datasheet and that the full load condition was achieved with the selected resistor value, the voltage generated by the EMCO Q50-5 was measured for different load resistors ranging from 10 to 100 MΩ. The voltage converter was driven by a low voltage signal varying from 0 to 5 V with steps of 0.5 V. The high voltage output was acquired using a high voltage probe (TT-HVP 40 high voltage probe, TESTEC Elektronik GmbH, Germany). The measurement was repeated three times for each load resistor, reporting the average value. This allowed for an assessment of the slope of the input-output curve (Fig. 8.21).

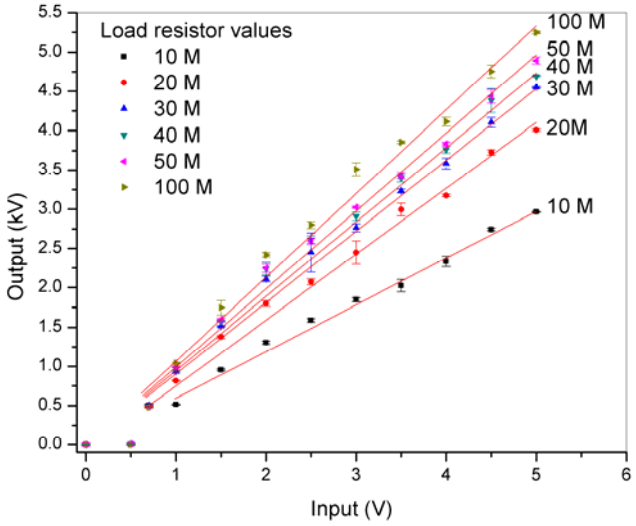

Fig. 8.21. EMCO Q50-5 input versus output voltage for different load resistors. The red lines represent a linear fitting. Error bars represent 95% of confidence interval.

For the selected resistor value of 50 MΩ the input-output curve was also measured with the actuator placed in parallel to the resistor, so as to compare the behaviour of the EMCO with and without the actuator load (Fig. 8.22).

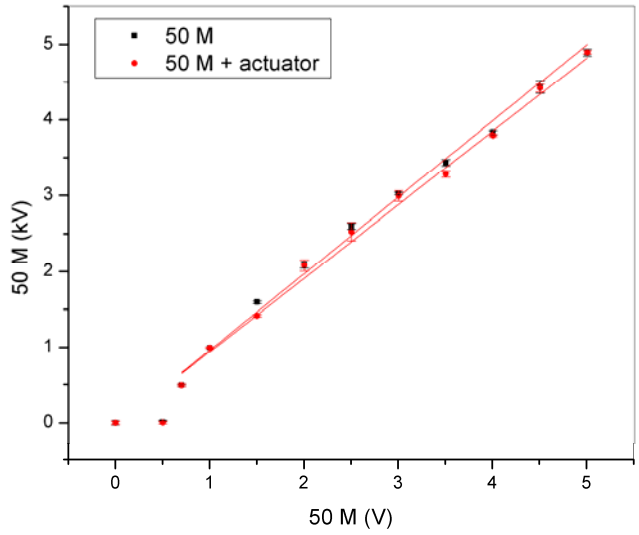

Fig. 8.22. EMCO Q50-5 input versus output voltage for a 50 MΩ load resistor and with the actuator in parallel to the resistor (The red lines represent the linear fitting).

Also, a ramp ranging from 0 to 1 V was used to detect the activation threshold (0.7 V according to the datasheet) at which the input-output curve begins to be linear. Results are reported in Table 8.1, which also shows the slope of the input versus output characteristic curve for the different resistors.

Table 8.1. Input versus output voltage slope and threshold for an EMCO Q50-5

Resistance (MΩ)	Fitted slope (kV/V)	Activation threshold (V)
10	0.59	0.89
20	0.84	0.75
30	0.92	0.67
40	0.97	0.63
50	0.99	0.63
50 + actuator	0.97	0.63
100	1.08	0.63

The results show that the load resistor affects both the input-output voltage and the activation threshold. Although the chosen load resistor did not correspond to the optimal value, the full-load condition was still obtained. Furthermore, the actuator connected in parallel did not significantly affect the linearity of the input-output voltage characteristic, which was still linear from the activation threshold to the maximum value with a fitted slope of about 1 kV/V.

A more sophisticated approach intended to obtain the full-load condition for the entire range of voltages (rather than only at the maximum one) would have required an adaptive device able to adjust the resistance value actively, according to the voltage to be supplied. Such a strategy was not considered, as according to the results it was not needed (because the linearity is ensured) and it would have made the whole system excessively complex, bulky and expensive.

The value chosen for the resistance also prevented the nominal maximum output voltage (5 kV) from being exceeded. Differently, for instance Fig. 8.21 shows that for a load resistor value of 100 MΩ the converter provided a voltage of about 5.25 kV, which could have damaged the actuator or, in the long term, could have resulted in a failure of the converter.

8.4.3. Remarks on the choice of the high voltage source

Whereas the bench generators offer the best performance in terms of power and bandwidth, they are not portable as they are also heavy, cumbersome and

expensive. Conversely, the DC/DC converters have a lower performance. These types of device use a high frequency inverter (typically operating at frequencies ranging from 20 to 100 kHz) to produce the high voltage. This can result in a ripple noise in the output that can create interference within the application (which can then effect the read out from sensors that are placed close to the device).

In conclusion, the high voltage sources available are selected according to the application requirements and the available budget. While for laboratory testing high performance amplifiers were preferred, low cost, small size and low weight converters were used for several of the DEA applications, especially when high speeds of actuation were not required.

Finally, the need for a high-frequency operation in a range of portable devices is not yet resolved. This is constraining the development of devices for use in high frequency applications.

8.5. Control hardware

The external controller used to provide the low voltage signal to the high voltage converter was an Arduino UNO board (Fig. 8.23).

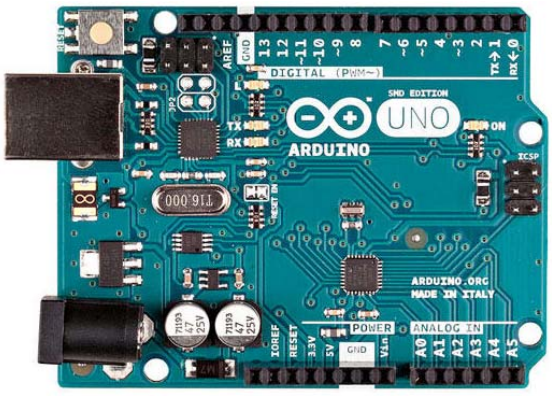

Fig. 8.23. Picture of the Arduino UNO board

The Arduino boards are part of an open source project and are widely used to easily prototype and experiment with electronics. The Arduino project provides several microcontroller-based boards and an integrated development environment (IDE) for programming the microcontroller. The Arduino UNO board used provides 14 digital input/output pins, six of which can produce pulse

width modulated (PWM) signals, and six analogue inputs. The board features the Universal Serial Bus (USB) communication interface, which is used for programming and for communicating with a computer (*Arduino UNO overview* 2016).

The low voltages used to feed the high voltage converter were generated by one of the PWM pins of the device. As the Arduino board could only output PWM voltages, a capacitor-resistor smoothing circuit was employed to smooth the signal. Furthermore, the PWM maximum output current of 20 mA (*Arduino UNO overview* 2016) is not sufficient to directly drive the high voltage converter, as it requires up to 400 mA when driven at full-load. To interface the controller with the high voltage DC-DC converter, the smoothed signal was fed to a buffer (TCA0372 1.0 A output current, dual power operational amplifiers, Motorola, USA)(Fig. 8.24) that was powered by an external regulated 5V-1A, power supply. The buffer interfaces the signal smoothed by a filter with the high voltage converter (EMCO Q 50-5).

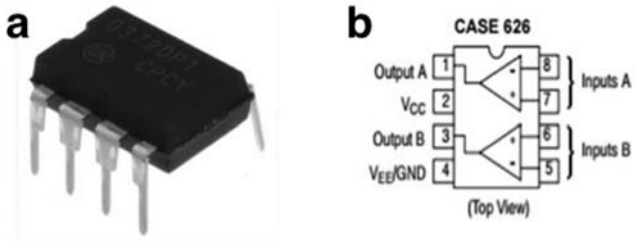

Fig. 8.24. TCA0372 operational amplifier: monolithic integrated circuit case (a) and pin connections (b)

Fig. 8.25 shows the schematic of the driving circuit.

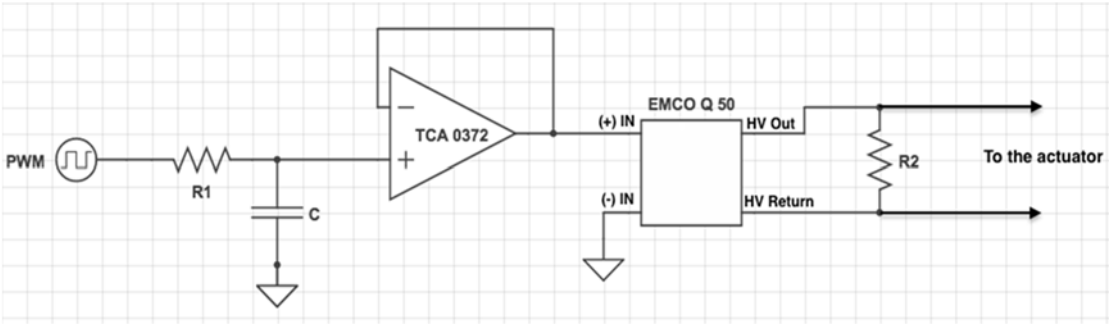

Fig. 8.25. Schematic of the driving circuit. The high voltage resistor R2=50 MΩ (needed by the converter to work properly and by the actuator to discharge fast) is also shown.

We found that smoothing the 490 Hz PWM signal with a low pass filter (made of a 4.7 µF capacitor and a 150 Ω resistor) enabled linear control of the high voltage driving signal.

The component values were empirically selected as a (non-optimised) trade-off between the need for maximising the response speed and the need for minimising the ripple to a magnitude that was not perceived at the fingertip by the users.

8.6. Electromechanical characterisation

8.6.1. Introduction

To assess the static electromechanical performance of the tactile display, free stroke and blocking force were measured at the apex of the passive membrane. Furthermore, in order to take into account for the viscoelasticity exhibited by the VHB elastomer, and to quantify the effect on the actuator performance, a stress relaxation test was performed. Finally, the mechanical response to sinusoidal signals at different frequencies was measured to quantify the capability of the display to generate time variant stimuli. For all the electromechanical tests, the voltage was generated by the high voltage amplifier (Model 615-10, Trek Inc., USA) described in section 8.4.1 as the DC/DC converter described in section 8.4.2 was not able to investigate the required range of test frequencies.

8.6.2. Free stroke and blocking force

In order to characterise the static electromechanical performance of the tactile display, voltage induced free stroke and blocking force were measured with a double-column dynamometer (Z005, Zwick Roell, Germany) according to the following procedure. A cylindrical indenter was attached to a load cell mounted on the mobile crossbar of the machine. The indenter had a diameter of 12 mm, so as to fit with the internal part of the plastic case of the tactile display (Fig. 8.26).

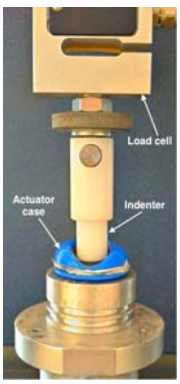

Fig. 8.26. Electromechanical characterisation setup.

The crossbar was then moved so as to bring the indenter in contact (with a negligible force) with the actuator's passive membrane, as shown in Fig. 8.27a. A voltage was then applied to the actuator, so as to cause the displacement the passive membrane's apex (Fig. 8.27b). The tool was brought in contact again with the actuator (Fig. 8.27c). The distance covered to restore contact was considered as the active displacement (free stroke). Subsequently, the voltage was turned off, without changing the position of the tool. As a result of this, the release undergone by the actuator while trying to recover its rest shape generated a force, whose steady-state final value was considered as the blocking force (Fig. 8.27d). Finally, the crossbar was brought back to the initial position, and the actuator was allowed to fully recover its original shape. This measurement was performed for different driving voltages up to 4.5 kV, which was used as a safe limit to avoid electrical breakdown. The test was repeated for five actuator samples.

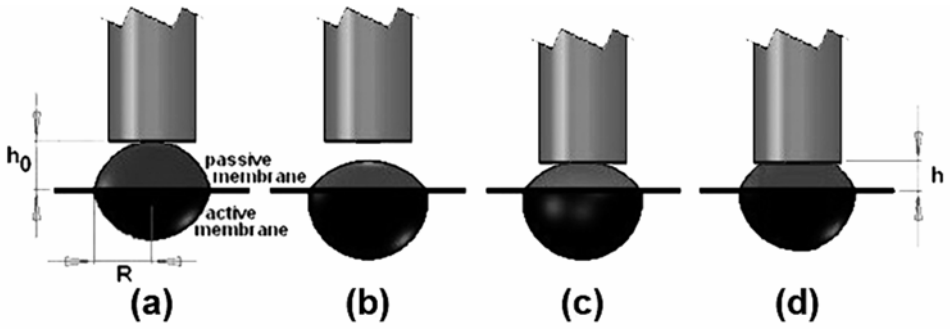

Fig. 8.27. Schematic representation of sequential steps of the testing procedure adopted to measure free stroke and blocking force: (a) contact with negligible force between measurement tool and actuator at rest; (b) electrical activation of the actuator; (c) contact with negligible force between measurement tool and activated actuator; (d) de-activation of the actuator.

This test is not representative of the tactile interaction and transduction, which occur when the fingertip touches the tactile display, owing to the following two reasons.

First, the way of measuring a force experimentally via load cells has nothing in common with the natural counterpart, which adopts mechanoreceptors having different properties (for example they are distributed and not concentrated, they are microscopic and not macroscopic) and of course transduce the force in a different way.

Second, the indenter did not have the same shape, size and mechanical properties (compliance) of a finger pulp. The variability among individuals of shape/size

and compliance of finger pulps would force to choose (more or less arbitrarily) those parameters of the indenter. As a consequence, the indentation results would be biased accordingly. Hence, instead of attempting to mimic a (non-standardised) finger pulp, we opted for using the simplest form of indenter, consisting of a rigid flat body.

Owing to these reasons, these characterisation tests were aimed at quantifying the actuator performance (in terms of blocking force and free stroke), rather than attempting to estimate the tactile perception experienced by the user. The latter need was addressed, via psychophysical characterisation described in section 8.7.

It is worth noting that preference was given to a characterisation in terms of force rather than pressure according to the following considerations. As measuring a force experimentally via load cells is different than the natural generation of tactile perception, from that point of view neither a force nor a pressure determined from any indentation test (with any device) would be indicative of a real tactile perception. Therefore, the force, rather than the pressure was prioritised to enhance the data reliability. Indeed, quantifying the pressure requires estimating the contact area, which inevitably introduces experimental errors that increase the uncertainty of the overall performance measures, as compared to the simpler force measurements.

8.6.3. Blocking force with constant deformation

The test performed in the previous section provided a standard estimation of the actuator's performance. However, when the actuator is used as tactile display, the finger is held in a fixed position with respect to the actuator and the top membrane pushes against the finger pad. Indeed, the casing for the fingertip is designed to keep the fingertip in contact with the top membrane.

To estimate the actuator's performance in that condition, a blocking force test with constant deformation was performed for five actuator samples as follows. While driving the actuator at the maximum voltage (4.5 kV), the indenter was brought in contact with the displaced top membrane and maintained in that position throughout the entire test. In that condition the measured force was negligible, whereas for decreasing voltage values, the partial release of the actuator displacement caused the top membrane to push against the indenter. The

steady-state blocking force was then recorded for each voltage value. The experiment, which was aimed at reproducing the condition in which the finger impedes the passive membrane to fully recover its original shape, allowed for a more reliable estimate of the voltage dependent force provided to the finger pad.

8.6.4. Stress relaxation

As the VHB 4910 elastomer used to fabricate the actuator shows a significant viscosity, which was expected to affect the mechanical properties of the actuator, an estimate on the force variation over time was needed.

To this end, while in the previous measurement only the steady-state value of the force was considered, here we present a measurement in which the indenter was brought in contact with the membrane driven at the maximum voltage investigated (4.5 kV, as described in the previous section), and maintained in that position for the entire test. The voltage was then switched off and the force produced by the actuator while trying to recover its shape was recorded for 10 min.

This amount of time was intentionally significantly much longer than is likely to be encountered in practice. Indeed, the actuator is designed for applications where it is unlikely that the same stimulus intensity is delivered for several minutes. So, this time of application was considered as a potential worst case.

8.6.5. Dynamic response

The frequency response of the actuator was tested by measuring the displacement of the top passive membrane using a laser displacement sensor (ILD1402-5, Micro-Epsilon, Germany) (Fig. 8.28).

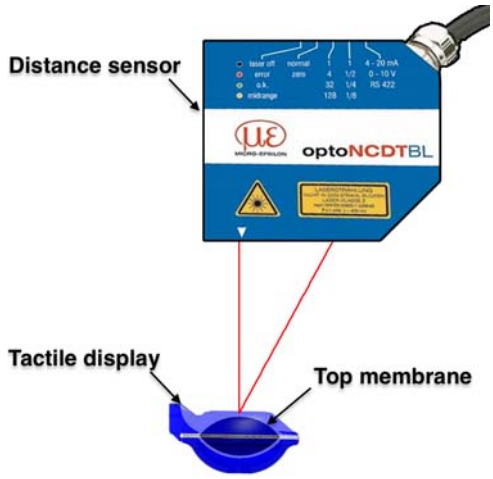

Fig. 8.28. Schematic representation of the experimental setup used to measure the frequency response.

The actuator was driven with a signal consisting of a sinusoidal wave, which had an amplitude of 2 kV and a mean value of 2 kV. So, the resulting signal was entirely positive and ranged from 0 to 4 kV and can be expressed as:

$$V = V_*(1 + \sin \omega t) \tag{8.7}$$

Where V_* is the amplitude of both continuous and sinusoidal parts, and as the deformation D is proportional to the square of the driving voltage V we can write:

$$D\ \alpha\ V^2 \rightarrow D\ \alpha\ V^*(1 + \sin \omega t) \tag{8.8}$$

so that

$$D\ \alpha\ V_*^2 \left(1 + \frac{1 - \cos 2\omega t}{2} + 2\sin \omega t\right) \tag{8.9}$$

Eq. (8.9) shows that the quadratic deformation-vs-voltage law typical of DE actuation introduces a second order harmonics distortion. However, since the second harmonic amplitude is four times smaller than the first, the distortion introduced does not substantially affect the peak-to-peak estimate of the actuator displacement (Fig. 8.29). The peak-to-peak value was chosen as a measurement of the actual maximum displacement provided by the actuator when driven by a variable signal.

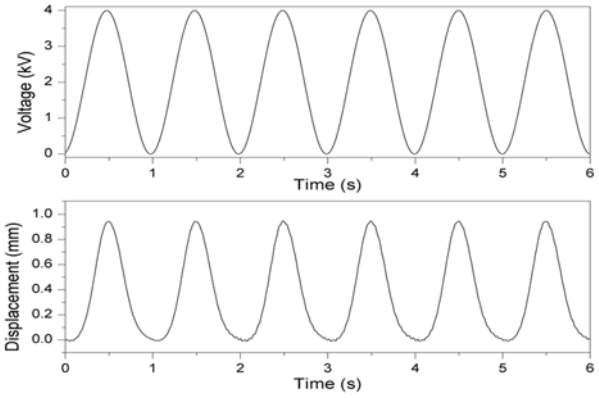

Fig. 8.29. Example of dynamic response of an actuator (bottom panel). In particular the driving signal (top panel) consisted of a sinusoidal wave at 1 Hz having amplitude of 2 kV and mean value 2 kV.

The top membrane actuator membrane displacement of two actuators was measured for frequencies ranging from 0.1 to 300 Hz.

Also, in order to estimate the mechanical time constant, using the same experimental setup, the step response of one actuator was recorded.

8.7. Psychophysical tests

8.7.1. Introduction

In order to assess the performance of the system as a means to convey tactile stimuli to the user's finger pad, psychophysical tests were performed. Two types of experiments were designed with the aim of investigating the ability of the display to simulate contacts with soft objects. The first test simulated contact with a virtual soft plane, while in the second test the ability of the display to render the softness was tested within a virtual environment. The experimental procedures described in the following sections were approved by the Ethical Committee of Queen Mary University of London as described in Appendix B.

The device used for these psychophysical tests was the tactile display described in section 8.2 and 8.3, which consisted in the soft actuator driven by the DC/DC converter described in section 8.4.2.

8.7.2. Virtual plane test

8.7.2.a. Experimental setup

While wearing the tactile display on their dominant hand's index finger, the subjects had to interact with a virtual plane. They were asked to lift and lower their hand as if they were probing a surface.

The fingertip position was continuously tracked by an infra-red-based distance sensor (IR reflective distance sensor 10 cm, Phidgets Inc., Canada) (Fig. 8.30).

Fig. 8.30. Infra-red reflective distance sensor 10 cm, Phidgets Inc., Canada

The users were instructed to move their hands perpendicularly to the sensor. However, the sensor interaction area was wide enough to allow for a certain misalignment of the fingertip. Furthermore, even an unwanted misalignments, did not affected the experiment as, in that case, the user was not provided with any stimulus.

Fig. 8.31 shows a schematic representation of the experimental setup.

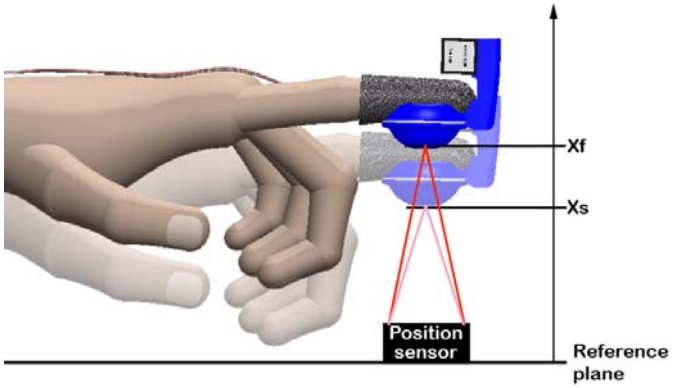

Fig. 8.31. Schematic representation of the movement that volunteers were asked to perform during the psychophysical test.

A virtual contact occurred whenever the fingertip distance x_f reached a certain distance x_s, corresponding to the position of the virtual plane. When the contact with the virtual plane was detected, the display switched from the maximum driving voltage V_0 to one of the five reference voltages V1-V5. When the driving voltage was V_0, the membrane was not in contact with the finger pad, as it was at its maximum displacement; V1-V5 corresponded to five different stimulus intensities that were mapped using the approach described below.

The voltage-force measurements obtained from the Blocking force with constant deformation test described in section 8.6.3. were fitted with a second-degree polynomial function (Fig. 8.32).

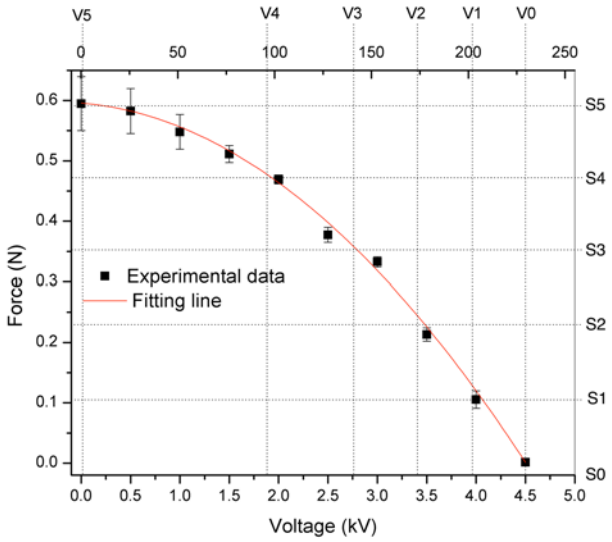

Fig. 8.32. Force-voltage characteristic curve averaged over five actuator samples. The stimuli S_0-S_5 used for the psychophysical test are indicated. The fitting line of the experimental data is used to extrapolate the five voltages V1-V5. The voltage values (bottom axis) are mapped to integer values (top axis) for the control system. Error bars represent a 95% confidence interval.

The five voltages V_1-V_5 were extrapolated so that they corresponded to five equally spaced values (S_1-S_5) along the force range provided by the display (Fig. 8.32).

The voltage values were then mapped the to the linear integers 0-255 and then sent via a serial connection to a microcontroller (UNO board, Arduino, Italy), which was used to generate the low voltage required to drive the DC/DC converter that generated the high voltage, as described in section 8.4.

Table 8.2 shows the five reference stimuli that were equally spaced along the force range provided by the display, the extrapolated analogue voltage values and the related digital values set on the Arduino UNO via serial communication.

Table 8.2. Values of voltage used during the psychophysical tests and the corresponding calculated forces.

Stimulus		**Voltage**		
Reference	Corr. force value (N)	Reference	Extrap. value (kV)	Digital value
S_0	0	V_0	4.5	230
S_1	0.13	V_1	3.9	199
S_2	0.25	V_2	3.4	173
S_3	0.38	V_3	2.8	140
S_4	0.51	V_4	1.9	97
S_5	0.64	V_5	0	0

8.7.2.b. Perceptual task

Ten right-handed subjects were involved in the experiment (7 males and 3 female, age 28.6 ±3.4). The participants were instructed to lift and lower the hand several times along the direction orthogonal to the plane, so as to reproduce the movement of probing a surface, as sketched in Fig. 8.31.

After the subject had familiarised themselves with the reference stimulus, the driving voltage was slowly increased. The subject, who kept probing the virtual plane, was asked to report when a difference with respect to the initial reference stimulus was perceived. The corresponding driving voltage value was then recorded. The test was repeated by randomly changing the reference voltage and thus the related stimulus. For each value, the test was performed two times with each volunteer. The data collected were used to compute the so-called Just Noticeable Difference (JND). As described in Chapter 3 , JND is the minimum difference in stimulation that a person can detect and represents a figure of merit of the sensory system efficiency.

8.7.3. Virtual reality test

8.7.3.a. Experimental setup

In this second type of tests, instead of probing the distance from a simple virtual plane, each user was asked to explore a more structured virtual environment. As for the previous experiment, the user had to wear the tactile display on the index finger of their dominant hand. The position and gesture of the entire hand (via a mapping of the finger joints) was obtained in real time by tracking the hand (within a certain work space) with via an optical sensor (Leap Motion controller, Leap Motion, Inc., USA) (Weichert et al. 2013), which was connected to a laptop using a USB connector. An Arduino UNO board was used again as described in section 8.4 to generate a low voltage signal driving the DC-DC converter described above. The equipment used in the experiments is shown in Fig. 8.33.

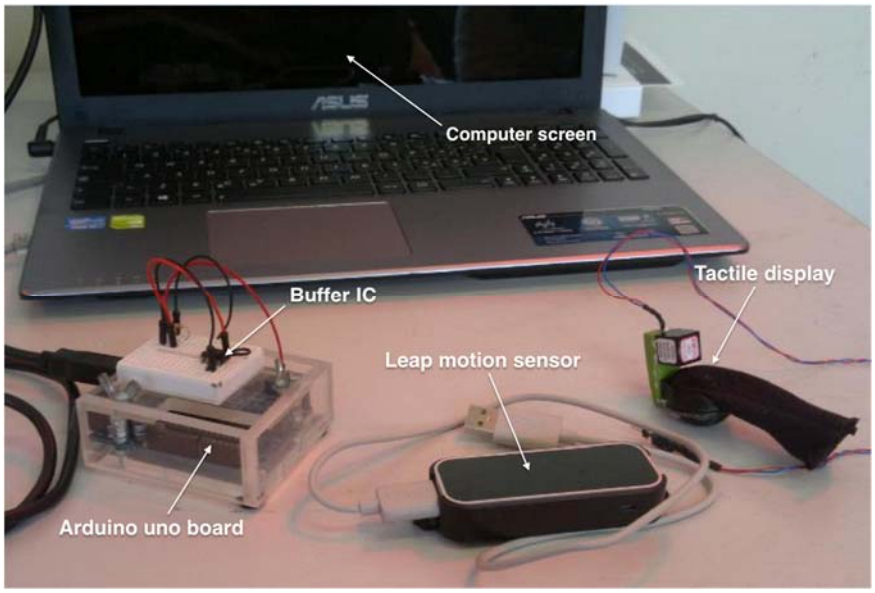

Fig. 8.33. Experimental equipment used for the virtual reality testing.

Data related to the position and gesture of the user hand were obtained by using the Leap Motion sensor and the software already available for it (Weichert et al. 2013) (Fig. 8.34).

Fig. 8.34. Picture of the Leap Motion hand tracking system (a) and exploded view of the system (b).

The Leap Motion controller is designed to be placed on a desktop in front of the user. It can track both hands using two infrared cameras and three infrared LEDs. The device interactive 3D space is a roughly hemispherical area to a distance of about 80 cm (Fig. 8.35).

Fig. 8.35. Leap Motion interaction area.

The tracking system is based on a patented software that uses the stereoscopic monochromatic images acquired by the two cameras (Fig. 8.36a) to reconstruct the 3D position of the hands and fingers (Fig. 8.27b) (How Does the Leap Motion Controller Work? 2016, Weichert et al. 2013).

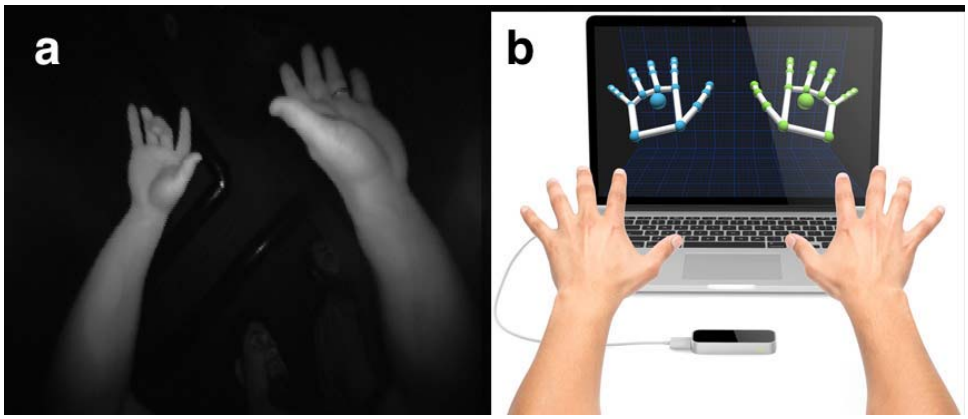

Fig. 8.36. Example of the monochromatic image taken by one of the infrared cameras (a) and example of 3D reconstruction of finger and hand positions operated by the Leap Motion system (b).

While several optical systems are available for 3D fingertip tracking, such as the Kinect by Microsoft (*Kinect for Windows* 2010) and the Duo MLX by Code laboratories (*Duo MLX embeddable stereo imagining for high performance 3D sensing* 2015), we opted for the Leap Motion system as we envisaged our fingertip tactile display being used for interaction with virtual models and scenes at a desktop interaction scale, in a way that is currently not achievable with other systems. Furthermore, other advantages of the Leap Motion tracking system are represented by its relatively low cost and the availability of a large programming support community.

Guna et al. have published a detailed analysis of the precision and reliability of the Leap Motion tracking system (Guna et al. 2014). They compared the Leap against a higher cost high precision optical motion tracking system (Qualisys Motion Capture) for both static and dynamic tracking scenarios. Results from that study demonstrated that for static situations the Leap could record fingertip positions with a sub 0.5 mm standard deviation, but under dynamic scenarios less reliable values were obtained, especially at the extremities of the device's field of view.

Notwithstanding the tracking system accuracy, when the users were wearing the display, the precision in the definition of the fingertip positions was dramatically

decreased. Although the reconstruction algorithm has not been disclosed, we can presume that the circular shape and the dimensions of the tactile display did not allow the system to identify the finger accurately. Furthermore, it is likely that the size of the display limited the view of the other fingers, preventing the system being able to reconstruct the positions of the other fingers.

To overcome these limitations, the Leap Motion sensor was programmed to detect the palm of the hand. While this strategy improved the accuracy of tracking movement as a whole, it did not allow accurate tracking of the fine movements of the finger. This resulted in a less realistic simulation, as the user had to keep the hand open during the experiment in order to allow the sensor to track the movements (Fig. 8.37).

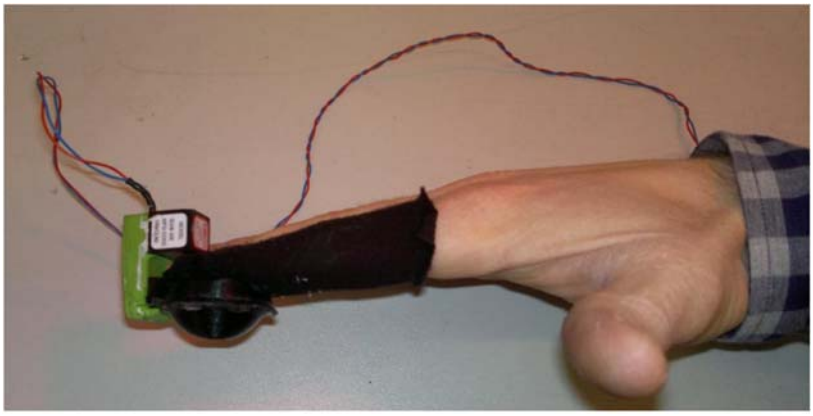

Fig. 8.37. Tactile display worn on the dominant hand's index finger during a psychophysical experiment.

8.7.3.b. Perceptual tasks

Fifteen volunteers (ten males and five females, age 25.5 ± 2.6) were enrolled to perform the perceptual tasks described in the following section. Out of the fifteen volunteers, two volunteers were left-handed and none had physical limitations that could affect the experimental outcomes.

Two experiments were performed. They were aimed at assessing the differential threshold and the psychometric function. Both experiments consisted in presenting objects with different softness that were visually rendered within a virtual environment and simulated by the tactile display.

First experiment: JND

The aim of the first type of experiments was to obtain JND. In order to calculate the JND, the following procedure was performed. A visual output was generated to accompany the haptic interaction. The object to be probed and the fingertip were represented in the 3D environment respectively by a box and a sphere (Fig. 8.38).

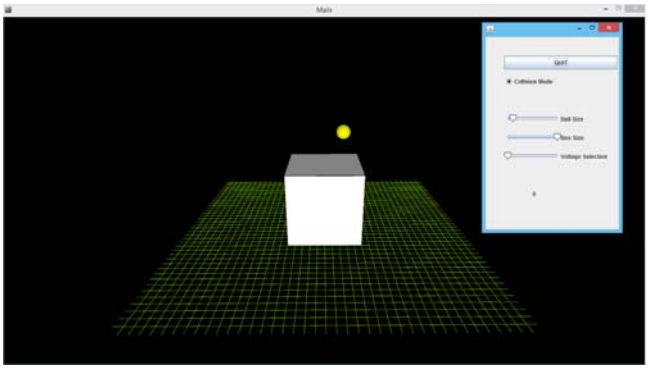

Fig. 8.38. Visual output provided during the first type of perceptual experiment: the white box is the virtual soft object and the yellow sphere represent the position of the finger.

While in the JND test described in the previous section users did not have any visual feedback of the contact with the virtual plane, here users could explore a simple virtual environment in which the position of the fingertip and the virtual object were rendered. This was a first implementation of the system in which the display was used in closed loop with a virtual environment. It allowed us to investigate on the integration of the display with an off-the-shelf hand-tracking device and on how the visual feedback affected the tactile performance.

The JND test was implemented according to the so-called 'method of limits', as follows. Whenever the yellow sphere (the user's finger) reached the virtual object, the driving voltage of the tactile display was switched from 4.5 kV (V_0 in Table 8.2) to one of the five reference voltages V_1-V_5 extrapolated as described in section 8.7.2.a. After the subject familiarised with the reference stimulus, the voltage was slowly increased. The subject was asked to report when a difference with respect to the initial reference stimulus was perceived. The voltage value at which the difference between the reported stimulus and the reference was perceived was recorded.

Second experiment: Psychometric curve

This second experiment was carried out using only a 2D virtual environment, as, during the experiment described in the previous section, some users found it difficult to locate the fingertip position within the virtual environment. So the scene was here simplified from 3D to 2D. The user's fingertip, whose movement was tracked using the Leap Motion sensor, was displayed in the virtual environment by a yellow circle (acting as a 2D analogue of the 3D sphere used in the previous experiment), while two green circles represented two objects, corresponding to different tactile stimuli: a standard and a reference stimulus. A screenshot of the test is shown in Fig. 8.39.

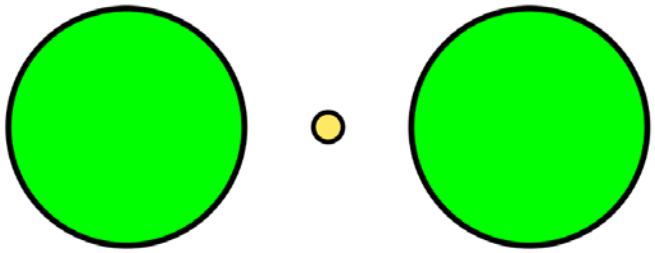

Fig. 8.39. Screenshot of the perceptual task related to the second type of experiment: the small yellow circle represents the 2D motion of the finger while the green circles are the reference and the comparison objects.

In this experiment volunteers had to report whether a stimulus was perceived "harder" or "softer" than the given reference. The comparison stimuli were presented in random order. When no interaction between the user's fingertip and the two circles was detected, the actuator driving voltage was set to the maximum allowed (4.5 kV) which corresponded to the minimum force condition. During the test the user, wearing the tactile display, probed the left circle, which was associated with the standard stimulus (and to the standard voltage for the entire duration of the test); then the volunteer probed the right circle corresponding to a comparison stimulus.

Eleven equally spaced voltage values V_1-V_{11} were used to extrapolate the stimulus values P_1-P_{11} from the voltage-vs-force curve shown in Fig. 8.32 according to a procedure analogous to that described in section 8.7.2.a.

With respect to the JND tests described above, in this case the number of voltage values was increased so as to allow for a more accurate detection of the *point of* subjective equivalence (PSE). As shown in Table 8.3, the force range used to map the reference voltages ranged between 0.32 N and 0.60 N. Values lower

than 0.32 N were discarded, as preliminary tests showed that they were always perceived by the users to be lesser than the standard stimulus. The reference stimulus P_6 was the median point along the chosen force range so as to have five stimuli that were "harder" and five that were "softer". P_6 corresponded to a calculated force level of 0.52N.

Table 8.3. Voltages and digital values used during the psychometric curve test.

Stimulus		**Voltage**	
Reference	Corr. Force value (N)	Reference	Value (kV)
P_1	0.60	V_1	0
P_2	0.59	V_2	0.29
P_3	0.57	V_3	0.58
P_4	0.56	V_4	0.88
P_5	0.54	V_5	1.17
P_6	0.52	V_6	1.46
P_7	0.49	V_7	1.76
P_8	0.45	V_8	2.05
P_9	0.42	V_9	2.35
P_{10}	0.37	V_{10}	2.64
P_{11}	0.32	V_{11}	2.94

The eleven comparison stimuli were presented twice randomly during the test. For each of the comparison stimuli, the participant could probe the two stimuli as long as needed and then report verbally whether the comparison stimulus was judged greater than the reference, so the answer was recorded as 1; otherwise, the recorded value was 0. The experimental phases of the test are shown in Fig. 8.40. The figure also shows the change that occurred to the colour of the circle (from green to blue) when the contact was detected, which served as a visual cue as to which object is being touched.

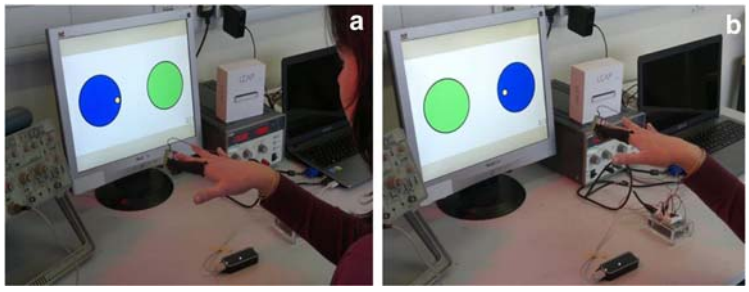

Fig. 8.40. Psychometric curve experiment: (a) the user probes first the reference stimulus, (b) the user probes the comparison stimulus.

8.8. JND calculation

The data collected during both the JND tests described above were used to calculate the corresponding JND values as follows.

With respect to a reference a stimulus force S_N (related to a voltage V_N) as defined above; let us call here S_{JND} (related to a voltage V_{JND}) the stimulus force from which the users started to perceive a difference. The S_{JND} value was obtained by extrapolation (using the V_{JND} value) from the fitted voltage-force curve described above.

The JND was then calculated as follows.

$$JND = \left|S_N - S_{JND}\right| \tag{8.10}$$

Repeating this calculation for different S_N allowed us to obtain a JND curve.

It is worth stressing again that, as already remarked in section 8.6.2, the voltage-force curve used to extrapolate the stimulus intensity values was obtained with a bench testing setup, which provided a only quantitative characterisation of the users' perception during the actual usage of the display.

8.9. Chapter conclusions

This chapter described the tactile display in terms of its design, actuation technology, fabrication and the electronics and hardware systems used to control it. The methods for its electromechanical and psychophysical characterisation were described as well. The results of the tests performed according to those methods are reported in the next chapter.

Chapter 9 The tactile feedback system: results and discussion

9.1. Introduction

The tactile display has been demonstrated to be able to provide tactile stimulation to the finger pad via a soft interface. By enabling the generation of significant forces and displacements with a single membrane of DEA, the adopted actuator configuration allowed for the design of a lightweight, silent and wearable tactile display that was comfortable for the users.

In this chapter, the results of the characterisation tests are presented. The electromechanical tests provided information on the actuator's performance from a general standpoint, while the psychophysical tests were used to assess the ability of the display to generate tactile stimuli.

9.2. The tactile display

Fig. 9.1 shows prototypes of the tactile display used for these tests. The case parts were 3D printed in ABS using the design described in Chapter 8 .

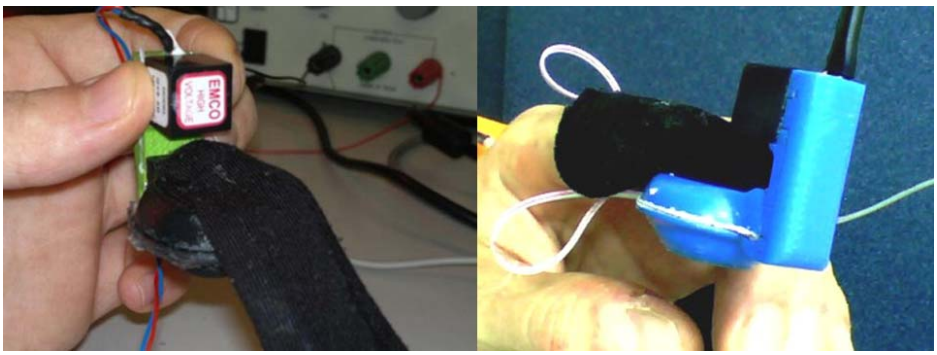

Fig. 9.1. Pictures of the prototype display.

Notwithstanding the results obtained, the psychophysical tests raised a fundamental issue regarding the integration of the display with hand tracking systems. Indeed, as described in section 8.7.3.a the shape and the dimensions of

the display did not allow the Leap motion hand tracking system to properly define the fingertip position.

This limitation can be overcome by redesigning the system using an approach that is described in Chapter 12

9.3. Electrical time constant

The dominant time constant is the electrical discharge time constant τ_e, as it is assumed that the actuator is charged through a resistance that is smaller than the 50 MΩ discharge resistor used for the driving electronics of the tactile display

This can be made by reasonably assuming that the series resistances of the contacts and electrodes are negligible with respect to the discharge resistor, whilst the output resistance of the high voltage converter is greater than that.

It is also possible to geometrically estimate the actuator's capacitance by assuming the actuator's active membrane as an ideally spherical cap, as represented in Fig. 9.2

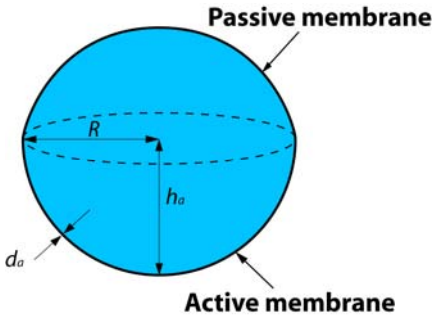

Fig. 9.2. Schematic representation of the actuator's membranes represented as ideally spherical caps.

The active membrane has a thickness d_a. A simple geometrical analysis of the structure allows for estimating d_a from measured values of the cap height h_a (as defined in Fig. 9.2).

Prior to providing it with a three-dimensional shape (while manufacturing the device), the active membrane initially consisted of flat circular elastomeric layer having a radius R and an initial thickness after pre-stretch $d_{a,0}$. So, its initial surface S_0 and volumes $Vol_{a,0}$ is:

$$S_0 = \pi R^2$$

(9.1)

$$Vol_{a,0} = S_0 d_{a,0}$$

(9.2)

During the fabrication of the device, the membrane is deformed, such that is final shape can be assumed as an ideal spherical cap, whose surface area S_a is given by the following expression:

$$S_a = \pi\left(R^2 + {h_a}^2\right)$$

(9.3)

Furthermore, by assuming that the thickness of the membrane is negligible with respect to the cap height and base radius, the final volume of the membranes Vol_a can be approximated as follows:

$$Vol_a = S_a d_a$$

(9.4)

Moreover, assuming that during the deformation from flat to spherical each membrane maintains its volume constant, from (9.2) and (9.4) we can write:

$$S_0 d_{a,0} = S_a d_a$$

(9.5)

Therefore, from (9.3) the final thickness of the membrane is obtained as:

$$d_a = d_{a,0} \frac{R^2}{\left(R^2 + {h_a}^2\right)}$$

(9.6)

The capacitance C_s of a spherical capacitor consisting of concentric spherical electrodes can be calculated as:

$$C_s = \frac{4\pi\varepsilon_0\varepsilon_r}{\frac{1}{r_i} - \frac{1}{r_e}}$$

(9.7)

Where r_e is the radius of the external electrode, r_i the radius of the internal electrode and ε_0 the permittivity of vacuum and ε_r the relative permittivity of the material in between the two spheres.

And, by assuming again that the thickness of the membrane is negligible with respect to the cap height and base radius, the capacitance C_a of the active membrane, which is assumed to be a spherical cap can be calculated as a portion of the entire sphere:

$$C_a = C_s \frac{S_a}{S_s} \tag{9.8}$$

Where S_s is the surface of the sphere that can be calculated as:

$$S_s = 4\pi R^2 \tag{9.9}$$

So, by assuming that

$$r_e = r + \frac{d_a}{2} \; and \; r_i = r - \frac{d_a}{2} \tag{9.10}$$

Where r is the cap radius that can be calculated as:

$$r = \frac{R^2 + {h_a}^2}{2h} \tag{9.11}$$

Finally, by combining eqs. from (9.3) to (9.11), and by considering a relative permittivity ε_r=4.8, a cap base radius R=10 mm, a cap height h_a=7 mm and an initial thickness after pre-stretch $d_{a,0}$=0.0625 mm, we can estimate the actuator's capacitance in about 240 pF.

Finally, the estimated electrical discharge time constant can be expressed as τ_e=RC=12 ms. This time constant is lower than the mechanical time constant, whose estimate is presented in section 9.4.3.

9.4. Electromechanical performance

9.4.1. Free stroke and blocking force

The voltage-induced response of the actuator is shown in Fig. 9.3 in terms of displacement and in Fig. 9.4 in terms force. The maximum displacement of the passive membrane apex at 4.5 kV was about 3 mm while the active force was about 0.57 N.

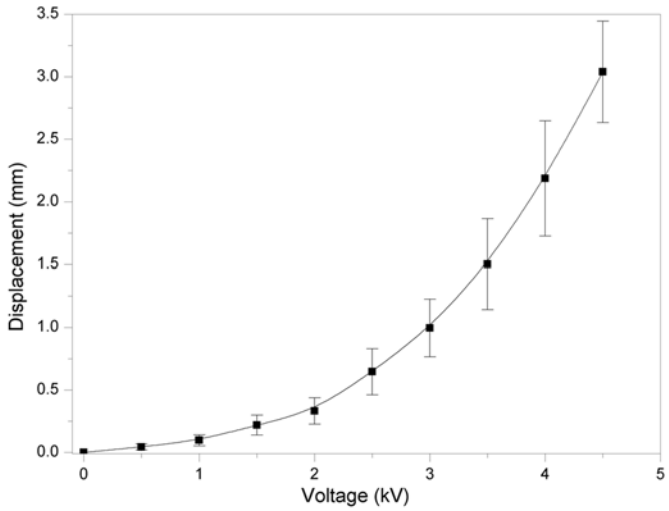

Fig. 9.3. Voltage-induced free stroke of the top passive membrane averaged over five samples. Error bars represent a 95% confidence interval. The fitting line is used as a guide for the eye.

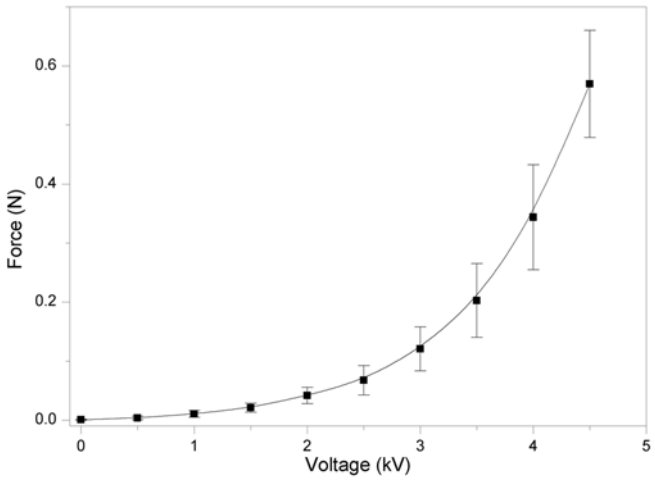

Fig. 9.4. Voltage-induced blocking force versus voltage averaged over five samples. Error bars represent a 95% confidence interval. The fitting line is used as a guide for the eye.

Fig. 9.5 shows the dependence of the blocking force on the voltage for a constant deformation equal to the maximum active displacement (3 mm) measured during the free-stroke test.

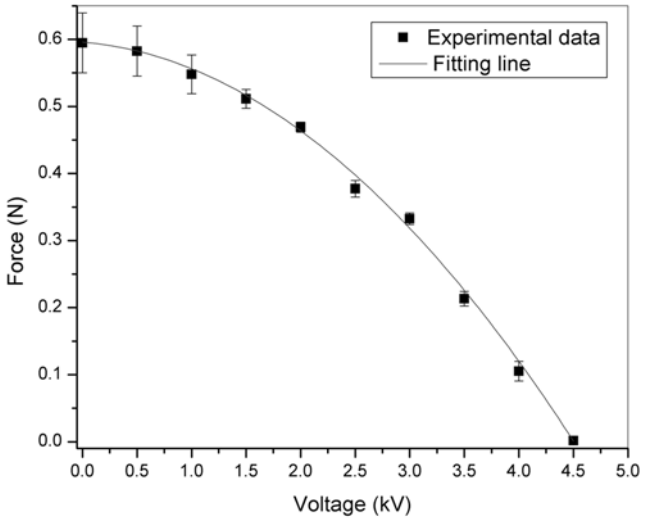

Fig. 9.5. Force generated by the tactile display as a function of the applied voltage while the indenter is kept at a constant position corresponding to the maximum displacement that the actuator is capable of producing. Error bars represent a 95% confidence interval. A fitting line of the experimental data is used as a guide for the eye.

As shown in figure, the maximum force is delivered when no voltage is applied, while a null force is produced at the maximum voltage. The maximum force provided by the display was about 0.6 N.

While it might be adequate for a tuneable delivery of tactile stimuli it is likely that this level of force and the way it is delivered will not be sufficient to simulate the diverse range of conditions that are encountered in real interaction tasks. Indeed, during the manipulation of objects the human tactile system can be stimulated by forces greater than those provided by the display (e.g.: when handling heavy objects). Furthermore, the stimulation rarely occurs in a direction that is just perpendicular to the finger pad, so skin stretch and shear force must be taken into account for a truly realistic tactile simulation. However, for some applications the values of force provided by this display are considered adequate.

According to Schorr et al, for specific applications, such as teleoperation, high levels of force feedback may cause annoying and unsafe contact 'bounce' resulting in an instability of the system that could worsen the accuracy and safety of the operation (Lawrence 1993, Schorr et al. 2013).

Moreover, it has been found by Smith et al. that, when exploring a surface, the whole finger typically uses an average normal force of about 0.6 N (Smith et al. 2002). This suggests that for exploration of soft tissues, such as rendered or simulated organs, that value of force might be appropriate.

Nevertheless, some applications might still require higher forces. In such cases, the force could be increased by increasing the stiffness of the whole actuator. This could be obtained by either using a stiffer elastomer or by creating a multi-layered structure (Fig. 9.6).

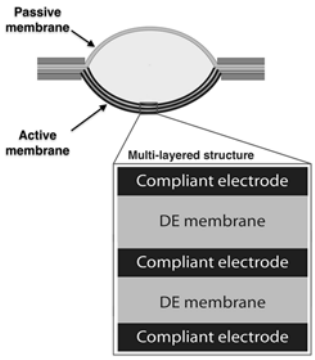

Fig. 9.6. HC-DEA with a multi-layered active membrane.

9.4.2. Viscoelastic performance

Fig. 9.7 presents the variation in the force exerted on the measurement tool during the stress relaxation test. The force was found to drop from 0.639 to 0.630 N in 10 minutes, corresponding to a relative variation of 1.4%.

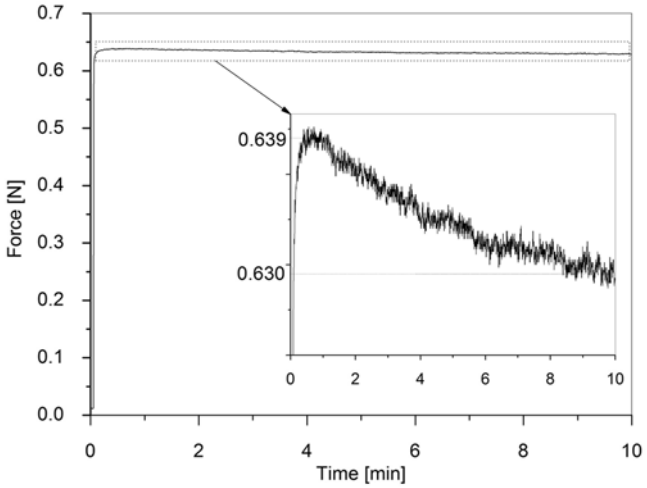

Fig. 9.7. Stress relaxation test over 10 minutes. The inset shows a magnification in the range of variation.

The elastomer material used, the VHB 4910, is one of the most studied commercially-available materials for DEAs (Carpi et al. 2011a, Pelrine et al. 2000b). It was used as it allows for significant electromechanical strains and stresses; also, its adhesive properties simplified the manufacturing process.

However, since it has been developed for use primarily as an adhesive bonding tape it has not been optimised to work as a DEA. Indeed, it shows significant creep and stress relaxation, which is an effect also well described in the DEA literature (Liu et al. 2014). Despite poor viscoelastic properties being described in the literature, this viscoelastic stress relaxation test showed that the force provided by the display was not significantly affected over the 10-minute duration of this test. This might be due to the relatively low stress experienced by the material for the applied constant deformation. The performance of the display in this viscoelastic test makes it highly suitable for applications where the tactile stimulus intensity is not changed over time periods in excess of a minute.

For more specific applications requiring higher actuation speeds, the strong viscoelastic effect exhibited by the material might become more relevant.

So, the selection of materials with lower mechanical loss (such as silicone rubber), instead of the 3M acrylic elastomer (Maffli et al. 2015), and a less viscous filling fluid, could lead to faster actuators which might be able to also provide an even more stable force.

9.4.3. Dynamic response

The peak-to-peak measurement of the top membrane displacement is plotted in Fig. 9.8 as a function of frequency, for two tested samples.

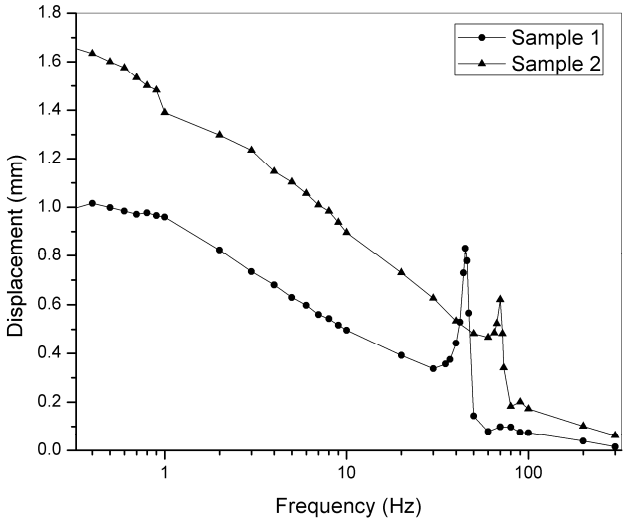

Fig. 9.8. Peak-to peak displacement versus frequency for two samples

Also, the peak-to-peak displacement normalised by the value at 0.1 Hz is plotted in Fig. 9.9.

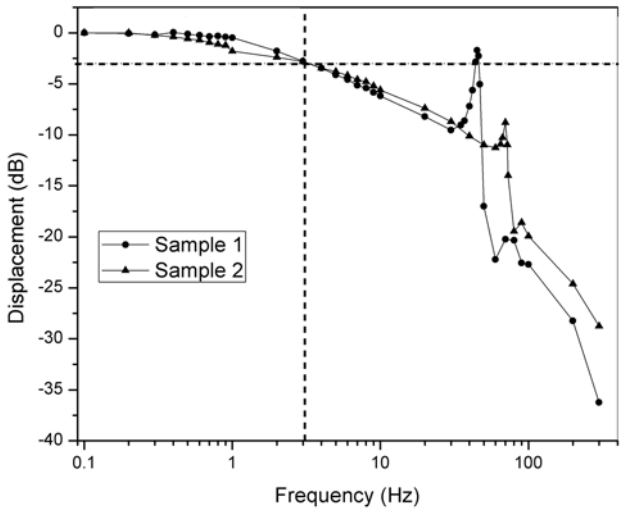

Fig. 9.9. Peak-to peak displacement (normalised by the value at 0.1 Hz) versus frequency for two samples tested.

The data show that the two samples had a similar response, characterised by a resonance frequency around 50-70 Hz and a -3dB cut-off frequency of 3 Hz.

The difference in resonance frequency could be caused by different final prestretches in the actuator's membrane. The fabrication process (which was mainly manual) might have introduced differences in the initial prestretch or in the volume of filling grease. Both these parameters might have affected the final prestretch, thus the actuation performance. Indeed, greater prestretches concur to

increase both the active displacement (as a consequence of the decrease in the thickness of the elastomer membrane) and the resonance frequency (caused by the stiffening of the membrane). These two concomitant effects are confirmed by the frequency response shown in Fig. 9.8 where the sample with the higher low frequency displacement also has a resonance peak at a higher frequency.

As for any DEA, it was expected that the cut-off frequency was primarily dominated by the material's viscoelastic behaviour. Therefore, in order to verify this, it was necessary to compare the electrical and mechanical time constants. The former is presented in section 9.3. The determination of the latter is presented below.

The actuator displacement curve, which was obtained in response to a voltage step of 4.5 kV (Fig. 9.10), was fitted with the following exponential function:

$$D(t) = A_1\left(1 - e^{t/\tau_{m1}}\right) + A_2\left(1 - e^{t/\tau_{m2}}\right) \tag{9.12}$$

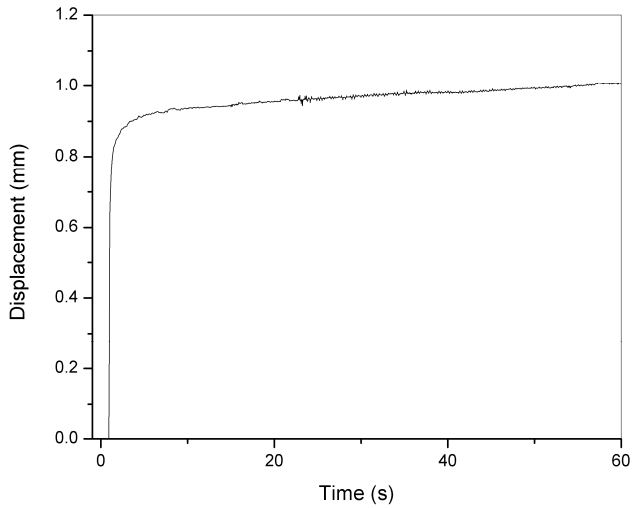

Fig. 9.10. Step response for one actuator sample.

The fitting returned the following values for the two mechanical time constants: τ_{m1}=0.16 and τ_{m2}=3.8 s. The first-time constant is related to the initial stage, which is typically referred as *transient creep* and shows a relatively high displacement rate, whilst the second time constant is related to a secondary stage, which is typically referred as the *steady-state creep* and shows a nearly constant strain rate.

Both the mechanical time constants are respectively one and two orders of magnitude greater than the electrical time constant τ_e=12 ms (reported in section 9.3). This confirms the dominant effect of the material's mechanical properties on the actuator's dynamic response.

Furthermore, by reasonably assuming that, during the sinusoidal driving, the actuator works mainly in the transient creep stage and by approximating the actuator to a first order mechanical system, we can use the mechanical time constant τ_{m1} to calculate the related mechanical cut-off frequency f_{mc} as

$$f_{mc} = \frac{1}{2\pi\tau_{m1}} \tag{9.13}$$

The resulting mechanical cut-off frequency f_{mc}=1Hz is consistent with the value of around 3 Hz shown by the measured frequency response (Fig. 9.9). The difference might be due to the first order approximations behind eq (9.13).

9.5. Psychophysical tests results

9.5.1. Virtual plane test

In this section the results from the first psychophysical tests are reported. The JND values were calculated from the recorded voltages as described in section 8.8 and are plotted as a function of the five equally spaced reference stimuli S_1-S_5 defined in section 8.7.2.

Fig. 9.11 shows the JND values (for each subject and each stimulus intensity value) recorded during the experiment.

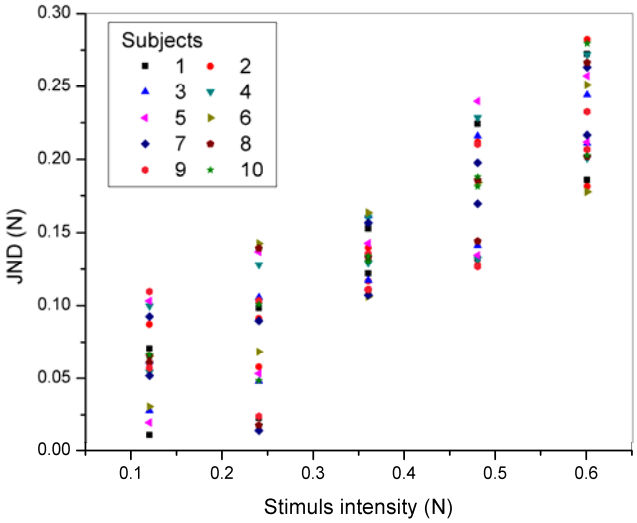

Fig. 9.11. JND test values for each of the ten subjects involved in the virtual plane test.

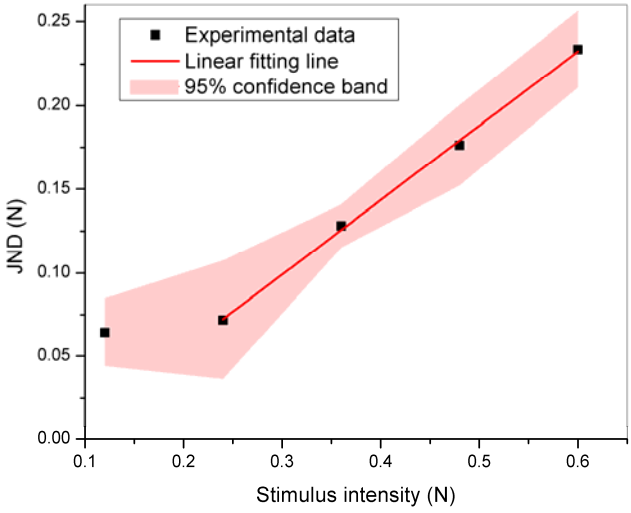

Fig. 9.12. JND as a function of the stimulus intensity.. The fitting line is used to calculate the Weber ratio and the pink shading its 95% confidence band.

As an overall measure of the ability of the device to generate small differences in stimuli that can be perceived by the user, the Weber constant (slope of the curve) was calculated from a linearization over the last four data points. It was found to be k=0.38.

A one-way ANOVA was used to evaluate the variability of k values among the different volunteers that tested the system. The analysis showed no statistically significant differences (F=1.04, p=0.404).

9.5.2. Virtual reality tests

First experiment: JND

The values of JND values were estimated again from the voltage values related to the answers provided by the subjects during the experiment, as described in section 8.8 Fig. 9.13 shows the JND values for each subject and each estimated stimulus value.

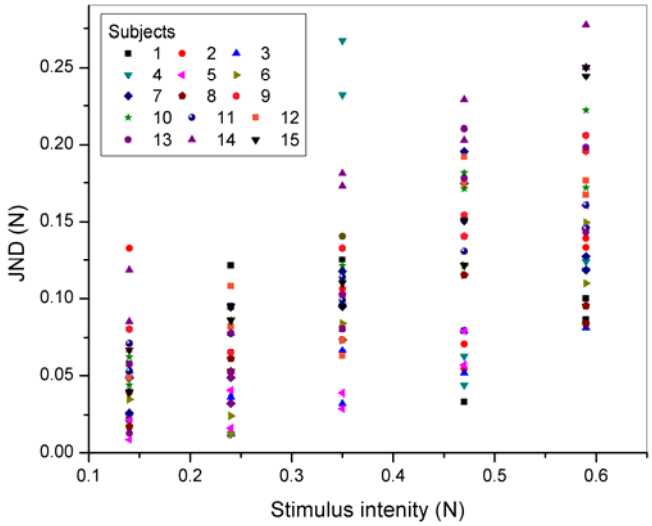

Fig. 9.13. JND test values for each of the fifteen subjects involved in the virtual reality JND test.

The results of each trial, for each reference force, were averaged over the 15 participants. Fig. 9.14 shows results from the psychophysical test. JND values were plotted as a function of the five reference stimulus intensities.

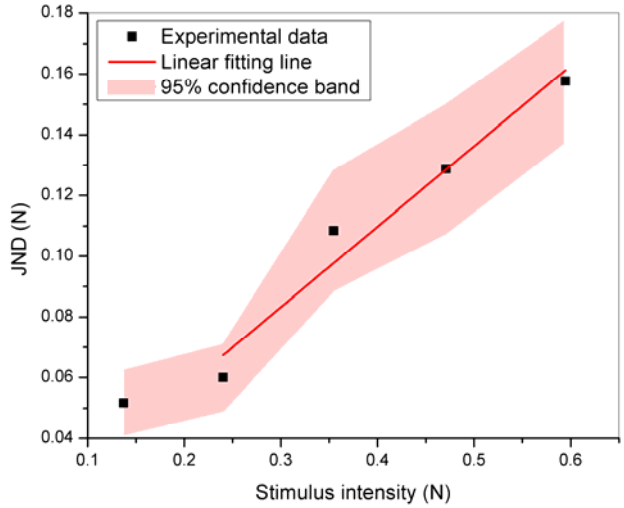

Fig. 9.14. JND as a function of the stimulus intensity (force).The fitting line is used to calculate the Weber constant. The pink shading is 95% confidence band.

The Weber constant was calculated from a linear fitting of the last four data points. It was found to be k=0.27.

A one-way ANOVA was used to evaluate the variability of k values among the different volunteers that tested the system. The analysis showed no statistically significant differences (F=2.46, p=0.290). The larger variance among users (with the respect to that shown by the 'virtual plane' test Fig. 9.12) might be due to the higher complexity of the virtual task, which resulted from the integration of visual and tactile information. However, it is likely that preliminary training could improve the achievable performance (thereby reducing the variance). Indeed, during the test some subject reported difficulties in locating their hand within the virtual environment (only the fingertip was represented). This might have resulted in more scattered psychophysical results.

These drawbacks could be overcome by implementing the representation of the entire hand (instead of the sphere that represented the fingertip) within the virtual environment and the use of a VR headset that might create a more immersive experience.

Second experiment: psychometric curve

The probability that the stimuli provided was perceived as greater than the reference was calculated as the number of positive answers (collected in the second psychophysical experiment) divided by the total number of answers. The

psychometric function was obtained by plotting the probability values as a function of the comparison stimuli (Fig. 9.15).

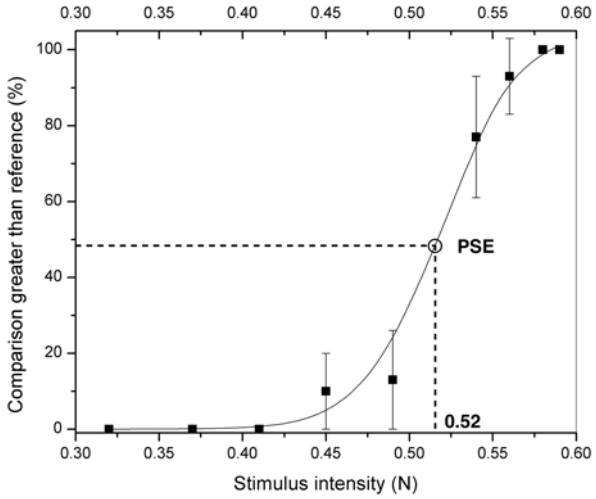

Fig. 9.15. Psychometric function: the experiments data are fitted with a sigmoidal function (solid line). The PSE (0.52 N) is the stimulus that the users would judge equal to the standard with a probability of 50%. Error bars represent the 95% confidence interval.

The maximum probability, corresponding to the value 1, would be obtained if all the users reported the comparison stimulus as "harder" than the standard stimulus.

The experimental data were fitted, with the following sigmoidal function

$$P = \frac{a}{1 + e^{-b(F - F_c)}} \tag{9.14}$$

where F is the force. The fitting returned the following parameters: a=103.69, b=51.40, F_c=0.52.

The function was used to extrapolate the *Point of Subjective Equivalence* (PSE) that is the stimulus that the users would judge equal to the reference stimulus with a probability of 50% (as described in section 3.3.1) as shown in (Fig. 9.15)..

In the ideal case of an infinitely fine resolution in the human tactile channel (where the user is able to discriminate the stimuli with 100% accuracy), the psychometric function would result in a step function as it would present null values before the standard stimulus and values equal to 1 after the standard stimulus.

The average PSE was found to be 0.52 N. It was coincident with the *'point of objective equality'* (POE), which is the stimulus value at which the comparison stimulus is physically equal to the reference stimulus, in this case the P_6, corresponding to 0.52 N.

A one-way ANOVA was used to evaluate the variability of PSE values among the different volunteers that tested the system. The analysis showed no statistically significant differences ($F= 1.58$, $p=0.245$).

9.5.3. Subjective evaluation of the stimulus

Although no specific questions were asked after the psychophysical tests, participants described the sensation provided by the display as "pleasant" and "natural", as if they were really probing a soft object. This was also confirmed by several users that tried the device during the various conferences at which we presented a demonstrator of the tactile display.

However, the intensity of the perceived force was occasionally described as "too low", especially by users at conferences, where they did not have the time to focus on the perception. This suggests that an increase in the force provided is needed.

9.6. Discussion

By comparing the results of the two JND tests it was found that the Weber constant (represented by the slope of the curves) was about 0.38 for the first test and about 0.27 for the second. A smaller Weber constant implies that the system is capable of providing distinguishable stimuli that are closer in intensity.

The better psychophysical performance obtained in the second JND test might be caused by the different experimental setup. Indeed, whereas in the first test the users probed the virtual plane relying only on the haptic sensation (the tactile information provided by the finger and the kinaesthetic feedback provided by the position of the hand and the forearm), in the second test the task was complemented with a visual feedback. These tests allowed us to investigate on the integration of the device with such systems. Despite the larger variance in the results, which is most likely caused by the different practice of the user with 3D

virtual environments, the Weber's constant was smaller. Indeed, the visual feedback, by providing the position of the finger within the virtual environment and with respect to the virtual object in a more intuitive way, allowed the users to foresee the contact with the virtual object, so that they could better focus on the tactile sensation.

Also, the differential sensitivity could be affected by the speed at which the stimulus is varied. Indeed, if the stimulus varies too fast, the user may not respond, or respond with a certain delay so that the value reported might be shifted owing to the human response time (the minimum time required to react to a change). Conversely, very slow variations are difficult to detect as the user's tactile system adapts continuously to the stimulus and does not notice the variations.

However, typical values of Weber's constant for the human capability to discriminate tactile stimuli have been found to be in the range from 0.19 to 0.37 (Bianchi and Serio 2015, Freyberger and Färber 2006), which are comparable with the results of the tests reported here.

Furthermore, the good outcome of the PSE test represents an important result for the wearable tactile display, as it implies that users were able to associate the physical stimulus and the related perceived stimulus with good accuracy.

Nevertheless, the values of stimulus used in the JND tests were extrapolated from the curve used to quantifying the actuator performance (in terms of blocking force) and mainly used to present the psychophysical results in term of force. So, even if they were not able to objectively quantify the tactile perception experienced by the user, they were related to the stimulus provided by the display to the finger pad.

Therefore, despite these uncertainties and the variability in the device's performance (caused by non-optimised materials, components and processes) the psychophysical tests demonstrated the capabilities of the display to convey tactile stimuli that can be distinguished by the users.

9.7. Chapter conclusions

In this chapter the results of the electromechanical and psychophysical test performed to characterise the display were reported. The display was able to

provide forces that appear to be adequate for some applications involving the rendering of soft touch sensation and the exploration of surfaces.

These results can be considered as an effective first attempt at assessing the capabilities of the proposed approach using a new soft actuation technology.

Chapter 10 Actuator miniaturisation: materials and methods

10.1. Introduction

As of today, blind and visually impaired people are largely excluded from today's digital revolution in information and communication technologies. Visually impaired people can mainly access digital information only via text-to-speech readers. Commercially available refreshable Braille displays are based on piezoelectric reeds that actuate the Braille dots. The reeds are mounted as a stair stepped stack of cantilevers, each with a Braille pin resting on its free end (Runyan and Carpi 2011). This solution limits the whole display to a maximum of two lines of Braille characters (Kendrick 2014), which makes backtracking impossible while reading a full page of text. To overcome this limitation, attempts to develop full-page Braille readers based on different types of piezoelectric actuators are in progress, although the only available system so far is non-portable and has an estimated cost of about €60,000 (*HyperBraille* 2016). So, affordable, portable and multiple-line (full-page) Braille displays are needed, as they merely represent technological fiction today.

Aimed at addressing these needs, this section of the thesis focuses on the miniaturisation of the HC-DEA described in section 8.2, with the aim of investigating the applicability of such actuators for refreshable Braille displays or arrays of tactile elements for tactile maps (Fig. 10.1).

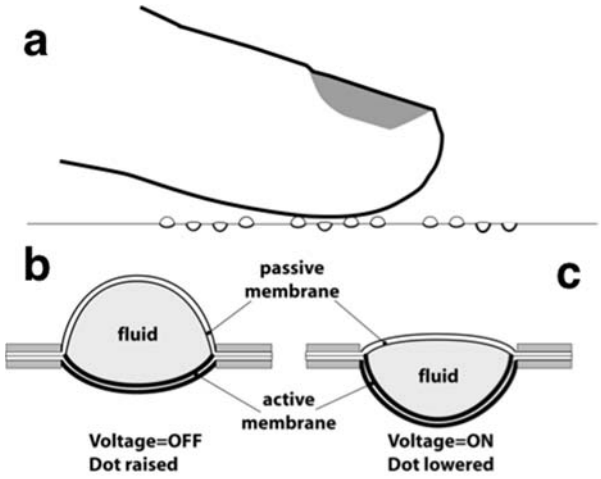

Fig. 10.1. Schematic drawing of the use of the HC-DEA configuration to obtain refreshable Braille dots (a). Lateral section of a HC-DEA-based Braille dot in the rest state (b). Lateral view of an HC-DEA-based Braille dot in an electrically induced state, due to an applied voltage (c).

To this end, the HC-DEA size was reduced, so as to comply with the Braille requirements (Runyan and Carpi 2011). The fabrication process, which was derived from that used for the tactile display and the electromechanical characterisation, which was used to assess the performance and optimise the actuator are described in the next sections.

10.2. A millimetre scale actuator

The actuator dimensions were reduced to those required for a standard Braille dot, as presented in Table 10.1

Table 10.1. Specifications of Braille dot parameters for refreshable Braille displays (Runyan and Carpi 2011).

Dot Parameter	**Typical value**
Base diameter	1.5 mm
Height (assuming no force has been applied by the user)	0.7 mm
Fingertip reading force (dot raised within 0.1 mm of its maximum height)	50 mN
Fingertip reading force (dot raised at least 0.25 mm above the reading surface)	150 mN

According to these requirements, the Braille dot consists of a quasi-hemispherical cap.

Fulfilling these requirements required significant improvements to be made to the fabrication process, the top frame thickness, the electrode pattern creation and the filling fluid deposition. These improvements involved several significant adaptations of the DEA fabrication processes that have been described previously to be made. It is these modifications to the process that are described in details in the following section.

10.3. Actuator fabrication

The fabrication process consisted of several different phases, which are presented in Fig. 10.2 and are described below.

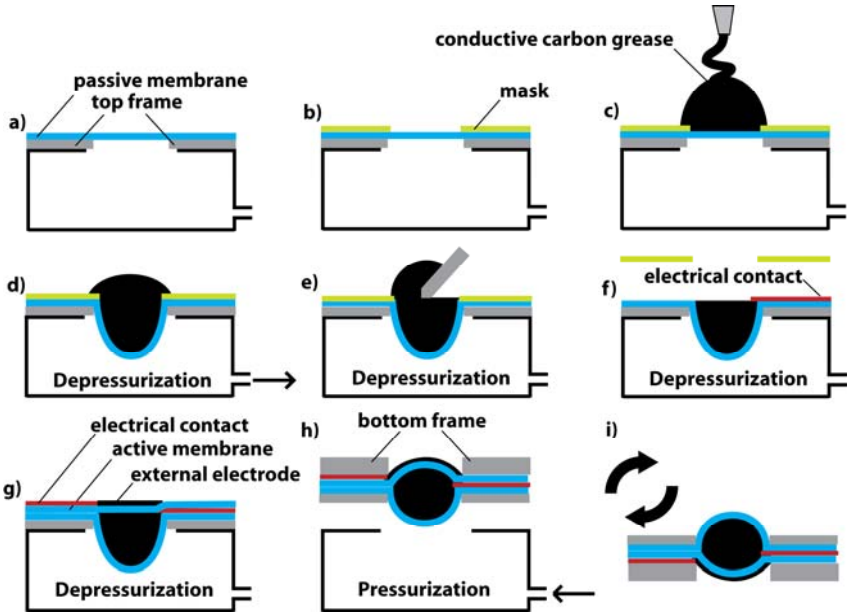

Fig. 10.2. Fabrication steps for a Braille dot. (a) The passive membrane bonded to a PMMA frame is placed over an empty chamber having a circular hole. (b) The membrane is masked. (c) The membrane in coated with conductive carbon grease. (d) A vacuum is applied in order to deform the membrane and create a cavity. (e) The excess grease is removed. (f) The mask is peeled off and an internal electrical contact is applied. (g) The active membrane is coupled to the other membrane; external electrode and electrical contact are applied. (h) The bottom frame is applied and the chamber is pressurised. (i) The Braille dot is removed from the vacuum chamber.

The actuator was assembled using membranes made of commercially available acrylic elastomer films (VHB tape series by 3M). Four combinations of different grades were tested and the outputs from this process are detailed in the next section.

Each membrane was bi-axially pre-stretched to a stretch ratio of 4 (which means that it was subjected to a biaxial pre-strain of 300% pre-strain) using the apparatus shown in Fig. 8.4 of section 8.3.2.

The pre-stretched membrane that had to work as the passive membrane was coupled to a thin steel frame, exploiting the natural adhesion of the VHB films.

In order to maximise the top membrane displacement height, the thickness of the frame was reduced. Indeed, the top frame has to be as thin as possible to ensure that most of the top membrane's cap was above the "touch plane" (i.e.: the top plane, which is touched by the finger). To ensure this a metallic frame was chosen (instead of plastic) to achieve the same stiffness with a significantly reduced thickness. However, the use of a metal in proximity of the high voltage is problematic in terms of safety. So, the selection of a non-conductive material having a comparable stiffness is needed for a real device that can be touched by users.

The membrane coupled to the frame was then placed over a vacuum chamber (Fig. 10.2a). The membrane was masked, using the paper liner that comes with the commercial film (Fig. 10.2b), so as to ensure its removal afterwards. Then, the membrane was coated with a carbon conductive grease (846, M.G. Chemicals, Canada), which was used both as hydrostatic coupling and internal electrode fluid. This simplified the fabrication process. Indeed, given the size of the actuator, the electrodes could not easily be manually deposited as was the case for the tactile display described previously. The deposition of such small quantities of material would have required machinery that was not available.

The volume of deposited grease slightly exceeded the amount that was required for the Braille device (Fig. 10.2c). After this deposition stage, the chamber was depressurised using a vacuum in order to deform the membrane, so as to obtain a grease-filled cavity (Fig. 10.2d), corresponding to a passive cap height of approximately 750 μm. This procedure avoided any air bubbles remaining trapped at the membrane / grease interface, as would likely be the case if the grease was applied after the creation of the cavity. After this step, any excess grease was removed (Fig. 10.2e), the mask was peeled off and a thin aluminium strip was applied to make an effective electrical contact (Fig. 10.2f). The pre-stretched membrane that had to work as the active membrane was then coupled to the other membrane, again taking advantage of the inherent adhesive

properties of the film. The next stage required for the same type of carbon conductive grease being applied to create the external electrode, which was finally connected to an aluminium strip working again as an electrical contact (Fig. 10.2g). A second PMMA frame was finally coupled to the active membrane and the so-obtained actuator was removed from the vacuum chamber by releasing the vacuum (Fig. 10.2h,i).

The resulting shape of the stabilised final structure was asymmetric (Fig. 10.2i), with a difference in the heights of the active and passive caps, owing to two concomitant effects. First, a difference in the stiffness of the two membranes, as a consequence of different thickness of the films (according to the values reported in the next section). Second, the Mullins effect (Mullins 1969), consisting in a stretch-induced softening of the passive membrane, resulting from the overstretch imposed during the depressurisation phase. As the asymmetry of the device was expected to influence its performance, different prototypes with passive and active caps of different heights were assembled and compared. To this end, membranes made of three types of VHB film each of different initial thickness were used, evaluating four combinations, as described in the next section.

10.3.1. Comparison of prototypes made with different thickness membranes

The form factor of the actuator used for the tactile display (same height for active and passive membrane) was not optimized for application where the actuating layer has to be as thin as possible as in portable devices, such tablets and smartphones. The height of the passive membrane, which composes the Braille dot is fixed by the standards, so the parameter that can be tuned is the height of the active membrane. It was tuned by selecting different elastomer stiffness for active and passive membrane as described above.

Four sets of actuators were obtained by using, as active and passive membranes, the following commercially available acrylic films by 3M: VHB 4910, VHB 4905 and VHB 9473PC. The four different tested combinations are presented in Table 10.2.

Table 10.2Combinations of materials used for the active and passive membranes.

Active membrane	Passive membrane
VHB 4910	VHB 4905
VHB 4910	VHB 9473 PC
VHB 4905	VHB 4905
VHB 4905	VHB 9473 PC

The thickness of each of the three films in the non-stretched state was 1000, 500 and 250 μm, respectively. The thickness then was reduced to about 62, 31 and 15 μm respectively that were calculated considering the application of the 300% biaxial pre-strain. The thickness was then further reduced during the manufacture of the device, owing to the hemispherical shaping of the membranes. The final values of the membrane thicknesses were computed, as described in the next section.

For each combination of active and passive membranes, three samples were manufactured and characterised in terms of stress relaxation and voltage-induced displacement (free stroke).

10.3.2. Geometrical estimate of the membrane thickness

The same geometrical assumptions made in section 9.3 for the estimate of the actuator's capacitance can be used to estimate the membrane thickness. Indeed, the Braille dot can be regarded as the union of two ideally spherical caps, as represented in Fig. 10.3.

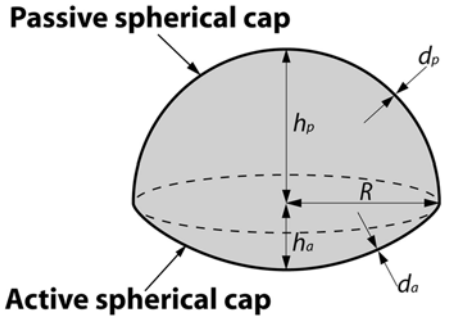

Fig. 10.3. Schematic representation of the proposed Braille dot as the union of two spherical caps, having the same base and different heights.

The two caps are generated by the three-dimensional arrangement of the two membranes that form the structure. The active and passive membranes respectively have a thickness d_a and d_p. A simple geometrical analysis of the

structure allows for estimating d_p and d_p from measured values of the cap heights ha and hp (as defined in Fig. 10.3).

Prior to providing them with a three-dimensional shape (while manufacturing the device), the active and passive membranes initially consisted of flat circular elastomeric layers having a radius R and an initial thickness after pre-stretch $d_{a,0}$ and $d_{p,0}$, respectively. So, their initial surface S_0 and volumes $Vol_{a,0}$ and $Vol_{p,0}$ are:

$$S_0 = \pi R^2 \tag{10.1}$$

$$Vol_{a,0} = S_0 d_{a,0} \qquad Vol_{p,0} = S_0 d_{p,0} \tag{10.2}$$

During the fabrication of the device, the membranes are deformed, such that their final shapes are ideally spherical caps, whose surface areas S_a and S_p are given by the following expressions:

$$S_a = \pi\left(R^2 + {h_a}^2\right) \quad S_p = \pi\left(R^2 + {h_p}^2\right) \tag{10.3}$$

Furthermore, by assuming that the thickness of the two membranes is negligible with respect to the cap height and base radius, the final volumes of the membranes Vol_a and Vol_p can be approximated as follows:

$$Vol_a = S_a d_a \;\; Vol_p = S_p d_p \tag{10.4}$$

Moreover, assuming that during the deformation from flat to spherical each membrane maintains its volume constant, from (10.2) and (10.4) we can write:

$$S_0 d_{a,0} = S_a d_a \qquad S_0 d_{p,0} = S_p d_p \tag{10.5}$$

Therefore, from (10.5) the final thickness of the membranes is obtained as:

$$d_a = d_{a,0}\frac{R^2}{\left(R^2+{h_a}^2\right)} \qquad d_p = d_{p,0}\frac{R^2}{\left(R^2+{h_p}^2\right)} \tag{10.6}$$

10.3.3. Measurement of the blocking force and stress relaxation

The force generated by the Braille dot (without any applied voltage) was assessed for the two applied displacements selected according to the Braille standards (Runyan and Carpi 2011). The force was measured with a double-column dynamometer (Z005, Zwick Roell, Germany), as follows. A cylindrical indenter larger that the dot base diameter, (2 mm), was connected to the machine's load cell (0-10 N, 1mN resolution) mounted on the mobile crossbar of the double-column dynamometer. The indenter was brought in contact with the Braille dot apex and the load cell was displaced and maintained at a given position, so as to displace the apex, for 30 seconds, while the variation of force was recorded with time. Measurements were taken for two values of displacement, 100 and 500 μm, as recommended in (Runyan and Carpi 2011). This procedure allowed the stress relaxation properties of the device to be quantified.

10.3.4. Measurement of the free stroke

Voltage-induced displacements of the Braille dot apex, corresponding to reductions of the passive cap height, were assessed using a laser-based displacement transducer (optoNCDT1800, Micro-Epsilon, Germany), as recommended in (Carpi et al. 2015). The free stroke was measured for step-wise voltages (generated by the high voltage amplifier model 615-10, Trek Inc., USA), whose amplitudes were varied with steps of 250 V, up to the electrical breakdown (which changed according to the thickness of the active membrane).

10.4. Chapter conclusions

This chapter described the Braille dot actuator in terms of its design, actuation technology and fabrication. The methods for its electromechanical characterisation were also described. The results of the tests performed according to those methods are reported in the next chapter.

Chapter 11 Actuator miniaturisation: results and discussion

11.1. Braille dot dimensions at electrical rest

A prototype of the Braille dot is shown in Fig. 11.1.

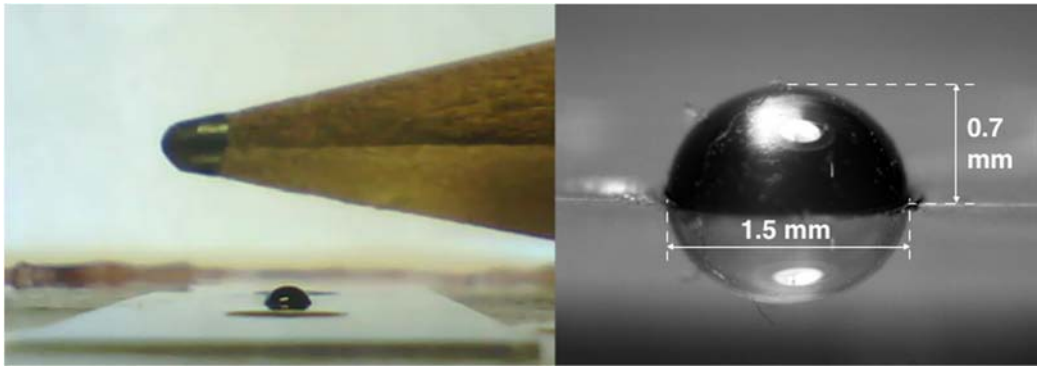

Fig. 11.1. Pictures of the prototype Braille dot at rest (with no voltage applied).

Fig. 11.2 presents the active and passive cap heights h_a and h_p at electrical rest (i.e. without any applied voltage) for each of the four sets of manufactured prototypes.

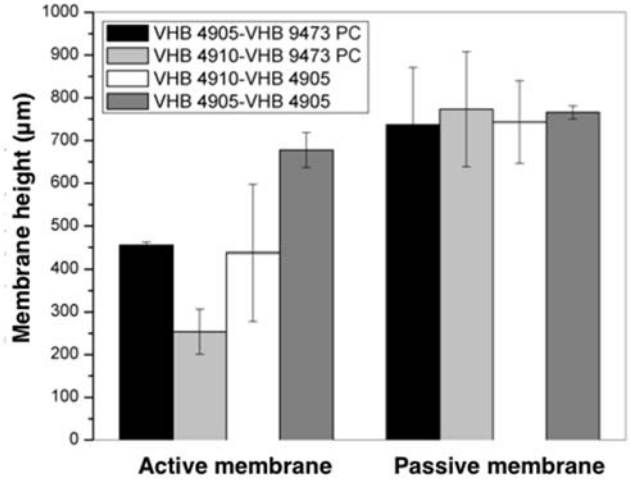

Fig. 11.2. Average active and passive membrane heights h_a and h_p, at electrical rest (with no voltage applied), for three samples of each of the four sets of prototypes. Error bars represent the standard deviation.

Whereas the passive membrane height was reasonably well controlled during the manufacturing process (in order to obtain Braille dots of the same size), the active membrane had a resulting variable height, according to the differences in the stiffness of the membranes (due to the combination of different thickness membranes) as discussed in the manufacturing section.

The average values of the cap heights were used to compute the active and passive membrane thickness, for each combination of materials according to (10.6). The active membrane thickness d_a was also used to calculate the relative actuator's capacitance C as described in section 10.3.2 for the tactile display. The results are presented in Table 11.1.

Table 11.1. Average values of the active and passive cap height h_a and h_p and the estimated active and passive membrane thickness d_a and d_p, and active membrane capacitance C, at electrical rest, for the four different sets of prototypes.

		Active membrane	
		VHB 4910	VHB 4905
Passive membrane	VHB 4905	h_a=438 µm h_p=750 µm d_a=48 µm d_p=18 µm C=1 pF	h_a=736 µm h_p=750 µm d_a=18 µm d_p=16 µm C=4.6 pF
	VHB 9473 PC	h_a=254 µm h_p=750 µm d_a=56 µm d_p=8 µm C=0.75 pF	h_a=455 µm h_p=750 µm d_a=23 µm d_p=8 µm C=2.2 pF

11.2. Braille dot force

The significant viscoelastic properties of the elastomeric material (3M VHB), affected the relaxation behaviour of the actuators. The results of a typical stress relaxation test are shown in Fig. 11.3. This data shows that significant stress relaxation takes place in the actuator after a fixed displacement is applied.

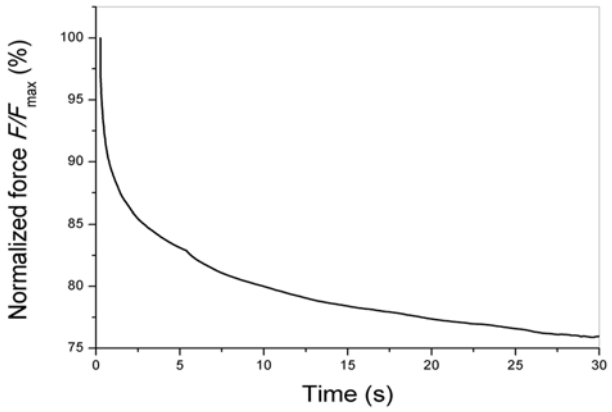

Fig. 11.3. Typical relaxation of the force generated by the Braille dot, for a given applied displacement.

All four sets of prototype Braille dots were found to exhibit a typical decrease in force of about 25% after 30 seconds. The significant viscoelastic behaviour exhibited by the Braille dots was considerably greater than the amount that was exhibited by the tactile display. One potential reason for this might be due to the Braille dots having a much higher stress compared to the tactile display when subjected to these mechanical stress relaxation tests.

Notwithstanding this very significant stress relaxation that was exhibited here, it is proposed that the value measured after 30 seconds is not likely to reflect the realistic force perceived by the user. Indeed, considering a typical Braille reading rate of 100 word per minute (Mousty and Bertelson 1985) and an average of 5.1 letters per word (on average in the English language) (*Web search: "Average word length in the English language"* 2016), the resulting reading speed of 510 letters per minute implies that the user touches a new group of eight Braille dots every 0.1 seconds. So, the value of force measured after just 0.1 seconds in the stress relaxation test is more typical for the dot force, the force perceived by the fingertip while reading. Its value is presented in Fig. 11.4 for each set of actuators. The Braille requirements, as recommended in (Runyan and Carpi 2011), are plotted as well.

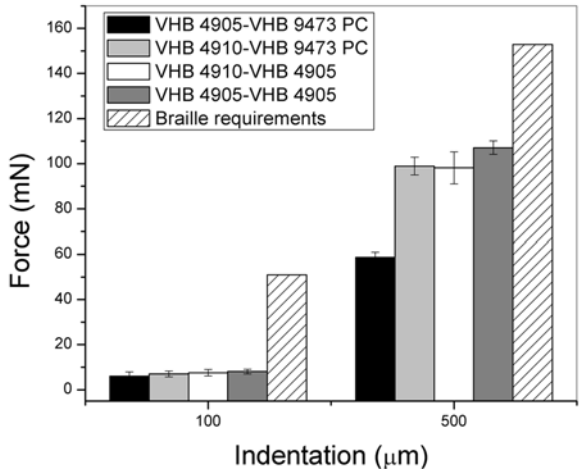

Fig. 11.4. Average Braille dot force at electrical rest for three samples of each of the four sets of prototypes. Error bars represent the standard deviation.

Whereas the dot's performance is close to that foreseen by the Braille requirements in terms of the shape profile of the unactuated dot, it is clear that the dot force is lower than that required under each displacement configuration as is shown in Fig. 11.4. According to Runyan and Carpi, although for some readers with light touch the force shown by this prototype might be sufficient, for others it may result in the so-called tactile noise (Runyan and Carpi 2011). An increased dot force could be achieved by improving the actuator structure by adopting multi-layered structures which result in stiffer membranes or by selecting materials with a higher modulus in the first place to make the dot.

11.3. Voltage-induced Braille dot displacement

A prototype of a single Braille dot is shown in Fig. 11.5.

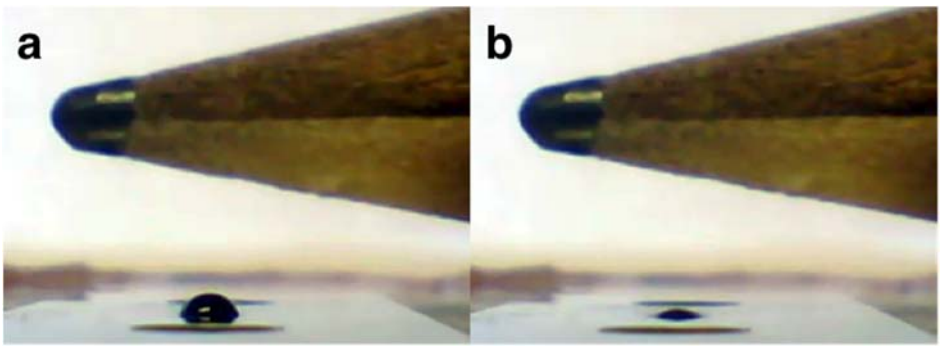

Fig. 11.5. Picture of the prototype Braille dot at rest (a) and when the voltage is applied (b).

Fig. 11.6 presents, for each set of prototypes, the voltage-induced displacement of the Braille dot apex, as a function of the voltage normalised by the active membrane thickness d_a.

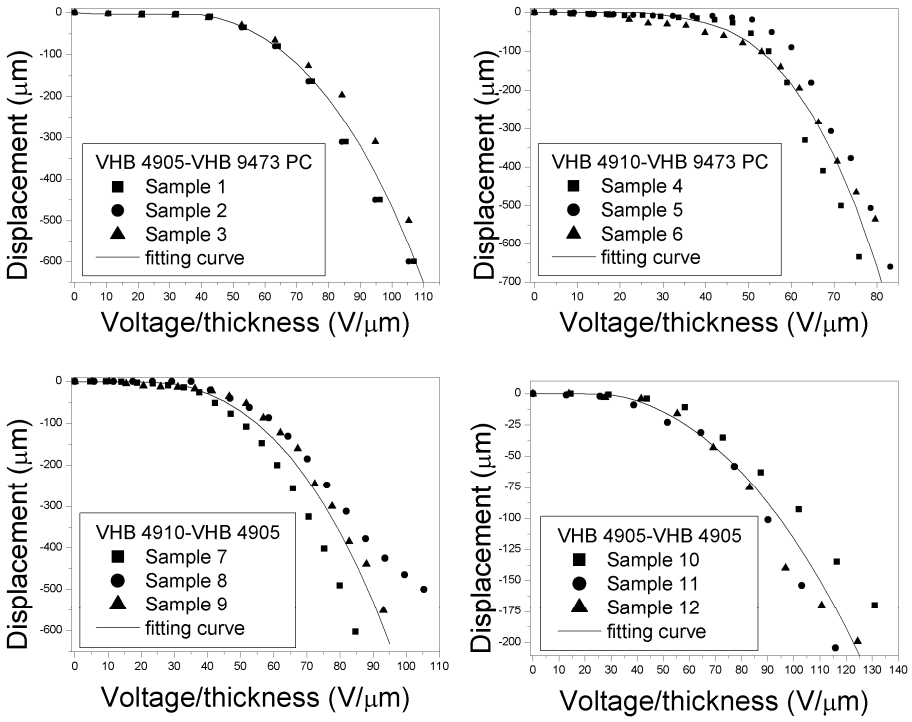

Fig. 11.6. Braille dot apex displacement versus the voltage-to-thickness ratio for the four sets of tested prototypes. A fitting line of the experimental data is used as a guide for the eye.

Fig. 11.7 presents the fitting lines for the four sets of prototypes (as in Fig. 11.6, so as to allow for a visual comparison of the different actuators' performance.

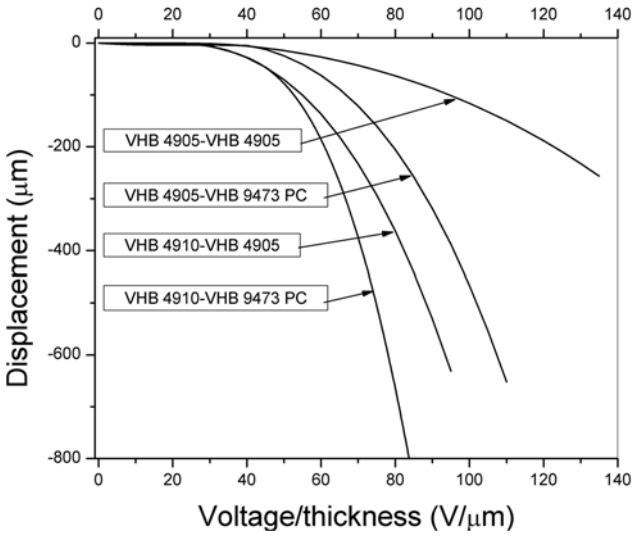

Fig. 11.7. Braille dot apex displacement versus voltage-to-thickness for each set of prototypes. Each curve is the fitting curve of the experimental data shown above (Fig. 11.6).

For each sample tested, Fig. 11.8 shows the displacement at 75 V/µm versus active cap height at rest (h_a).

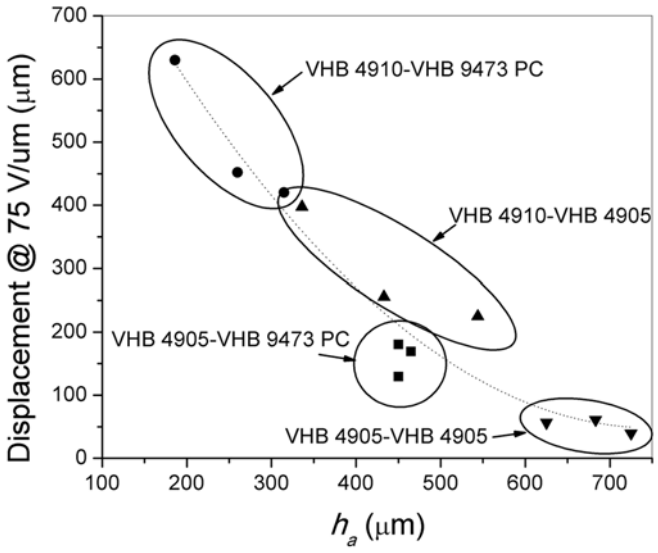

Fig. 11.8. Braille dot apex displacement (at 75 V/µm) versus active cap height at rest for each prototype.

As expected, the asymmetry of passive and active caps influenced the performance of the device in terms of achievable displacement. In particular, the maximum displacement achieved was 660 µm, related to the sample composed of the VHB 4901 and the VHB 9473 PC elastomers.

According to these experimental data, those two elastomers represent the choice to obtain the best trade off in terms of performance. Indeed, as shown in Fig. 11.4 and Fig. 11.8, this combination of materials builds an actuator that maximises the displacement while providing a force that is 10% smaller than the maximum value recorded.

As expected, the asymmetry of the Braille dot influenced its performance in terms of achievable displacement (Fig. 11.8). In particular, the average displacement at 75 V/µm was about 500 µm for the set VHB 4910-VHB 9473PC, which had the lowest height of the active membrane at rest. The dots with increasing values of that height showed decreasing displacement.

This evidence could be interpreted by assuming that the flatter active membranes corresponded to less stretched active membranes, which were therefore less stiff (it is worth noting that during manufacturing each membrane was bi-axially pre-stretched above the flex point of its stress-strain curve). The lower stiffness

determined a higher active deformation in response to any given electrical stimulus.

It is worth noting that the softest set of dots did not show the highest deformation. Indeed, the stiffness inferable from data reported in Fig. 11.4 is not representative of the stiffness of the active membrane only.

11.4. Chapter conclusions

In this chapter the results of the electromechanical characterisation of the Braille dot first prototypes were reported. Different combinations of active and passive membrane have been tested in order to optimise the dimensions and to improve the actuation for application such as portable devices.

The display displacement was demonstrated to be able to meet the braille requirements, while the force has to be improved.

These results can be considered as an effective first attempt at presenting a new technology that could enable thin portable full-page Braille displays.

Chapter 12 Future developments

12.1. Introduction

By enabling the generation of significant forces and displacements with a single membrane of DEA, the smart actuator configuration adopted allowed for the design of a lightweight, silent and wearable tactile display, which was also comfortable for the users.

The "virtual plane" test allowed for a preliminary assessment of the use of the display in a closed loop with a distance sensor.

The "virtual reality" tests provided useful information regarding the integration of the display in a virtual environment in closed loop with a commercial tracking system.

The tests confirmed that the device is capable of providing controllable tactile stimuli to the finger pulp so as to mimic a virtual contact with bodies having different mechanical properties.

However, both the actuator and the control hardware were assembled using off-the-shelf materials and electrical components that were not optimized for the application.

Improved casing design, miniaturised electrical components, custom-made materials and processing, and smart control strategies might lead to reduced encumbrance of the overall system, increased performance and wearability, as well as reduced costs and power consumption. Each of these aspects are discussed in the following sections.

12.2. Display casing: ongoing developments

Notwithstanding the results obtained, the psychophysical tests raised a fundamental issue regarding the integration of the display with hand tracking optical systems. Indeed, as described in section 8.7.3.a, the shape and the dimensions of the display did not allow the Leap motion sensor to define the fingertip position accurately.

This limitation could be overcome by selecting other tracking systems able to detect features other than the finger shape (for example by using markers or infrared LEDs placed on the fingers). However, the most promising approach would require a redesign of the system aimed at reducing the actuator size to a level where it fits within a plastic case that mimics the shape of a finger pulp. Such an approach to build a new design of the device is currently under development and follows the design shown in Fig. 12.1.

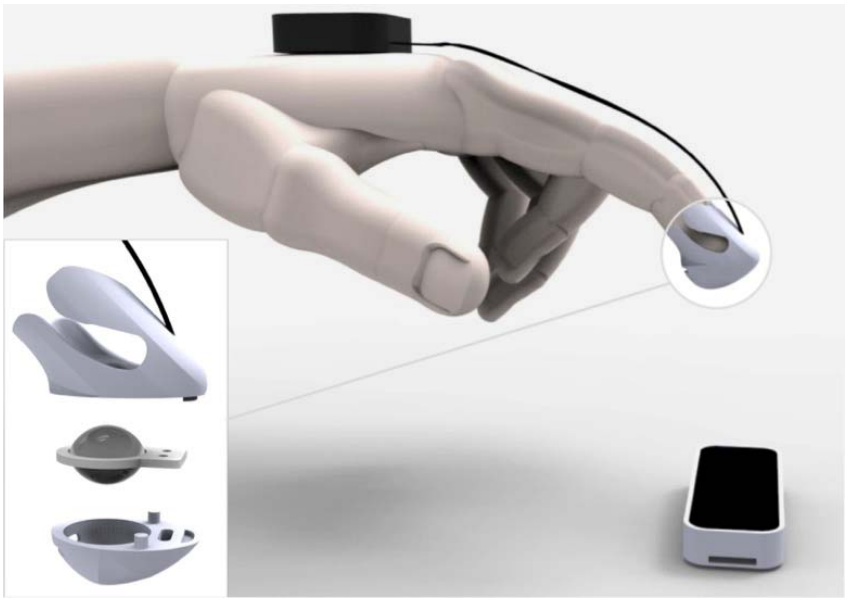

Fig. 12.1. Rendering of the concept for the new design of the tactile display. In the inset on the left-hand side an exploded view is shown.

These modifications would make the haptic device more easily implementable within applications that currently use the Leap Motion sensor and also some other non-marker-based optical motion tracking systems, such as the Xbox Kinect (which is perhaps one of the most widely available 'off the shelf' motion tracking systems).

In the most recent prototype implementation (Fig. 12.2), the high voltage converter has been moved from the top of the fingertip to a separated control box that is intended to be placed on the back of the hand, so as to obtain a further reduction of the size of the display.

Fig. 12.2. Pictures of the new casing for the tactile display.

Furthermore, the reduced encumbrance is expected to allow users to wear one display on each finger, so as to enable a multi-finger interaction.

In a first proof-of-concept testing, the new prototype structure allowed for the tracking of two fingers. Also a new virtual environment is currently under development such that when two spheres representing the fingertip positions (blue spheres in Fig. 12.3) come into contact with the object (green sphere in Fig. 12.3), the latter is deformed and this is represented as a shrinking of the virtual object.

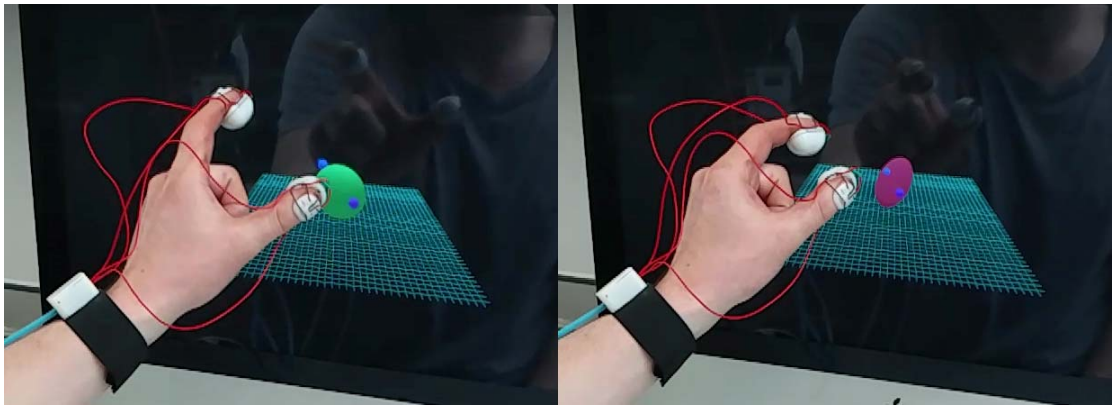

Fig. 12.3. Proof-of-concept demonstration of a two-finger interaction with the latest version of the tactile display. The figure also shows the behaviour of a new virtual environment developed in which the user can pinch a virtual object.

Fig. 12.3 also shows that the object is programmed to change colour (from green to red), so as to create a visual cue that makes the user aware of the contact.

12.3. Tactile experience improvement

The proposed display consisted of one single actuator that stimulated the whole finger pulp at once from a single direction. While it was effective, this kind of approach is not able to simulate the diverse interactions that are experienced during the tactile exploration. To this end, the displays and in particular the actuating parts have to be further redesigned.

One approach might be to use an array of actuators that might be able to provide localised stimuli to the fingertip and which can then stimulate it partially or from several directions that are not necessarily perpendicular (Fig. 12.4).

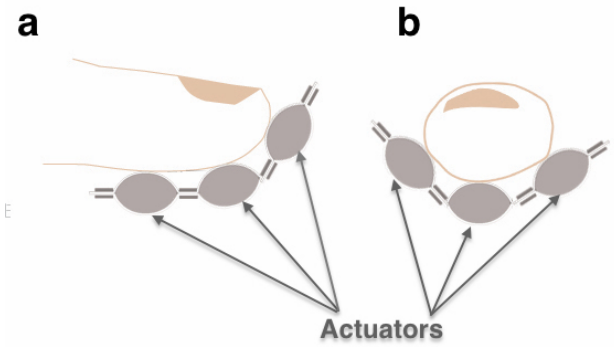

Fig. 12.4 Schematic representation of an array of multiple actuators for the stimulation form different directions of the fingertip (shown in a lateral (a) and a frontal (b) view).

Moreover, extending the tactile displays to multiple fingertips would certainly enrich the overall tactile experience. With respect to this, further activities are ongoing to demonstrate an improved version of the displays located at the same time on the thumb and the index finger, as shown in Fig. 12.5.

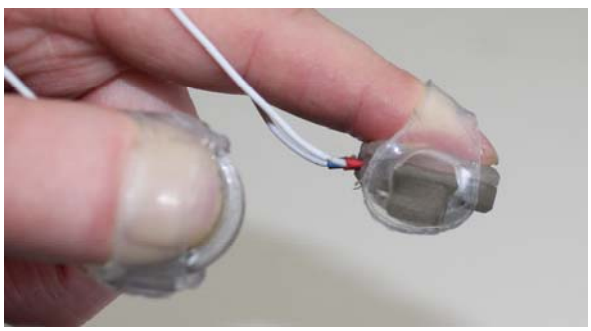

Fig. 12.5. Photograph of two tactile displays mounted on the thumb and index finger. The displays are secured to the fingertips by means of silicone straps.

12.4. Psychophysical validation of the tactile experience realism

The psychophysical tests performed in this work were aimed at assessing the ability of the device to generate tactile stimuli adequately perceivable by the users. This type of test represented the first necessary investigation to qualify the tactile display as a usable interface.

Future psychophysical tests could be aimed at addressing the next logical step, which consists in validating how realistic the tactile experience appears to users. To this end one approach could be to simulate the compliance of physical objects previously tested by the users. For instance, the volunteers could be asked to test the compliance of a given object and, immediately after, make a comparison with the tactile experience offered by the virtual object simulated by the display.

12.5. High voltage driving

One of the major drawbacks of the proposed technology is represented by the need for high voltages. It is a limitation in terms of size, safety and cost of the driving electronics.

In terms of electrical safety, dealing with such high voltages is clearly not desirable. However, the generation of voltages so high is not particularly problematic from a technical standpoint, considering that there is no need for high driving powers (the loads are capacitive) and that all the high-voltage parts are insulated from the user. Indeed, for the presented prototype display the required voltage was generated with a voltage multiplier, which was not only compact, but also allowed for a battery-operated circuitry. This allowed the system to be portable and relatively safe.

A further limitation, when dealing with high voltage components, is represented by the costs, since high-voltage components are more difficult to miniaturise and have a relatively small market, as compared to low-voltage units. To facilitate a wider uptake of DEA devices in general there is a need for a reduction of the applied voltage.

To overcome this problem, future developments should be aimed at lowering the voltages down to 100-200 V, which is the standard for the low-cost and low size

drives of commercial piezoelectric transducers (available in a huge diversity of products today). To address this need, there are currently two strategies: i) synthesis of new elastomers with improved electromechanical transduction properties. This can be expressed simply as having a requirement for a higher dielectric constant (Dünki et al. 2015, Madsen et al. 2016); ii) processing elastomers as very thin films. To this end, the target dielectric elastomer materials that should be more widely evaluated are the family of silicone elastomers, as they represent an existing option which allows for an ease of fabrication, good versatility of design and a high actuation speed (Maffli et al. 2015). Custom manufacturing processes will be necessary to reduce the thickness, so as to obtain any targeted electric field at a lower voltage. The technological aim should be to lower the thickness down to the order of 10 μm. While this is challenging for highly stretchable materials, preliminary investigations have suggested that it might be feasible (Lotz et al. 2011).

These improvements, would both allow for using low-cost components designed for piezoelectric actuators, and also would increase the safety of the device.

The high voltage requirements and the related poorly optimised components are also responsible for most of the power consumption in the overall system. Indeed, as reported in the DC-DC converter datasheet (*EMCO high voltage Q Series datasheet* 2016), at the maximum input voltage of 5 V and in the "full-load" condition (which is required to ensure a proper loading), the input current can reach 400 mA, corresponding to an input power of 2 W. However, as the maximum output power of the converter is 0.5 W (100 μA at 5 kV), the corresponding internal power loss is 1.75 W. Moreover, we can realistically assume that most of the converter's output current is absorbed by the discharge resistor as the actuator's input resistance is greater than that of the external resistor (50 MΩ). So, the greatest part of the overall output power is dissipated by the DC-DC converter and the discharge resistor and only a small amount is actually used to charge the actuator.

Notwithstanding the necessary reduction of the driving voltage, the actuator operating principle ensures the electrical insulation between the high voltage and the fingertip. Indeed, it allows for an electrically safe transmission of force to the finger, as the transmission of actuation is mediated by the dielectric grease, which prevents any contact between the finger and the active membrane.

Furthermore, the dielectric grease, working as an additional insulating layer, guarantees the safety of the user even in the worst case of the rupture of the top membrane.

12.6. Multiple actuator control strategies

The electrical driving of arrays of multiple actuators, as well as the implementation of the multiple finger interaction, imply the control of several high voltage channels, which requires the adoption of control strategies specifically designed for the task.

One straightforward approach would require the use of one high voltage converter for each actuator. Whilst this would result in a relatively simple circuitry, it would adversely increase the size, cost and power consumption of the system.

One potential optimisation would be to multiplex a single high voltage source by means of high voltage MOSFETs (Fig. 12.6).

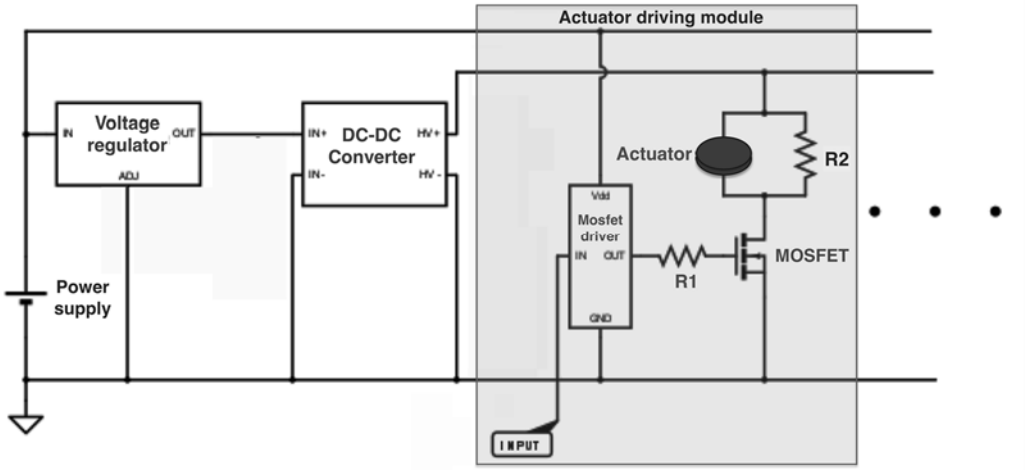

Fig. 12.6. Example of driving circuit for multiple DEA. The power supply is regulated so as to provide the DC-DC converter with the proper low voltage driving. The actuator driving module consists of a MOSFET, which works as a switch for the actuator. The actuator is in parallel to a discharge resistor (R2). The MOSFET requires a driver that provides the control voltage through the resistor R1. The driver is controlled by an input signal that is generated by the control software. The actuator driving module can be repeated so as to have multiple actuators supplied by a single high voltage source but controlled independently.

The adoption of this circuitry would enable the independent control of multiple actuators in on-off mode only, as the MOSFET works as a switch for the high voltage provided to the actuator. However the high speed of switching exhibited

by the MOSFET would allow for a pulse width modulated (PWM) control, so that the driving voltage for each actuator could be set independently.

A more sophisticated control strategy called *Dynamic Scanning Actuation* (DSA) has been proposed by Koo, Jung et al. for arrays of several actuators (Koo et al. 2006). The strategy efficiency increases with the number of actuators to be controlled, as it requires 2n lines to control n^2 actuators, so it is more suited for applications where a large number of actuators are required, such as with a Braille reader. The DSA operating principle adopts the following. One line, called *data line*, delivers the high voltage, while the other line, called *scan line* is connected to the ground (Fig. 12.7).

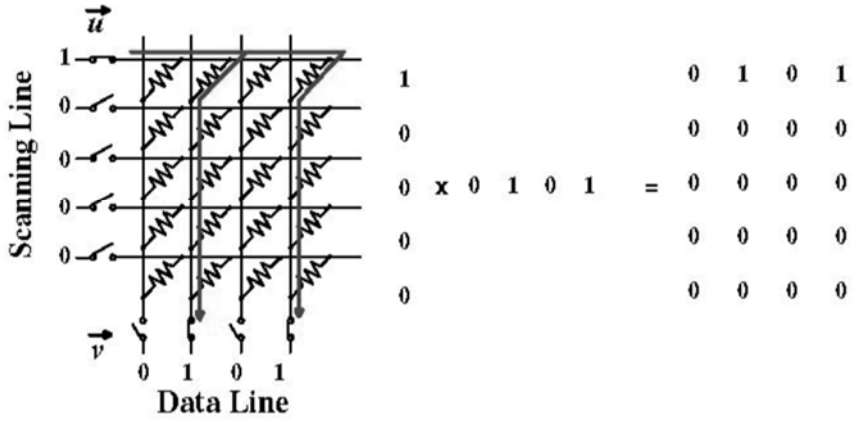

Fig. 12.7. Dynamic scanning actuation (DSA) method. When the first scanning line is on (1), it is possible to refresh the state of the actuators on that line. In the example shown the first and the third actuators are not driven while the second and the fourth are (Koo et al. 2006).

The actuation is triggered only when both the data line and the scan line are active, so that, by sequentially scanning each line, it is possible to continuously refresh each actuator's state and set it to the desired value (on or off).

12.7. Self-sensing capabilities and closed-loop control

The complex dynamic behaviour (characterised by the combination of hyperelasticity and viscoelasticity) exhibited by the DEAs is a significant drawback as it affects the accuracy, stability and speed of the actuators. Like the majority of the real-world applications, even those based on DEAs can benefit from ad-hoc closed-loop control systems, which can help to improve

performance. Closed-loop systems are designed to automatically reach and maintain a desired output condition. They achieve it by comparing the chosen output value with the actual condition. This comparison generates an error signal, which is used to make the necessary corrections. Usually, this kind of systems requires an external sensor, which is used to monitor the output. An interesting feature exhibited by DEAs that can be exploited within such closed-loop control systems is the so-called self-sensing capability. In fact, DEAs can be used to sense their own strain, so as to also work as integrated sensors, using the following idea.

The actuation leads to a change in the elastomer area and thickness, which result in a variation of the electrical resistance of the electrodes and the capacitance of the device. The evaluation of the first parameter is not trivial as it depends on the properties of the electrode materials. The capacitive self-sensing is easily implementable as it only depends on the geometry of the actuator (electrode area and elastomer thickness) (Jung et al. 2008, Rosset et al. 2013).

To exploit the capacitive self-sensing strategy, a self-sensing unit (SSU) capable of driving the actuator and to measure the capacitance is needed. The most common SSUs works by adding a small time-varying signal to the high-voltage signal used to drive the actuator. The capacitance is calculated by using the low voltage and current data that flow through the actuator.

The self-sensing technique offers several advantages in terms of size, costs and efficiency of the systems as it does not require any supplementary connection (other than the two high voltage wires) nor any additional sensors.

A prototype of closed-loop control system that exploits the self-sensing capabilities of DEAs has been developed by Rizzello et al. (Rizzello et al. 2015). The control system was able to improve performance, as it increased the maximum free stroke of the device. Its operation also helped to prevent the instabilities of the actuator, which allowed for a higher actuation speed.

Self-sensing could also be used within the tactile feedback system to precisely determine the stimulus intensity to be provided in order to generate a given desired force, according to the specific size/shape of the finger.

Chapter 13 Conclusions

13.1. Main achievements

In this thesis, a soft tactile display based on dielectric elastomer actuators (DEAs) was demonstrated to be able to provide electrically tuneable tactile stimuli to a user's finger pad.

The tactile element consisted in the so-called hydrostatically coupled dielectric elastomer (HC-DEA), which exploits a fluid coupling between the actuating part and the end effector that stimulates the finger.

The fabrication process specifically conceived for this kind of actuators was described. The casing of the display was designed so as to properly lodge the fingertip and to keep it in contact with the actuator. The electrical driving of the display was achieved by means of a miniaturized high-voltage DC-DC converter and that could be easily controlled via a serial connection to a computer. The overall system resulted to be compact and lightweight for the users.

Notwithstanding the non-optimised materials and electronic components, the actuator's electromechanical performance was found to be adequate to comply to some of the requirements for tactile stimulation, in terms of force provided and displacement achieved.

Indeed, despite the variance in the performance shown by the actuators, which is mainly due to the manual fabrication process, the psychophysical tests confirmed that the display was able to generate tactile stimuli that users could discriminate with good accuracy, comparable to that of state-of-the-art devices.

The psychophysical tests also raised issues regarding the integration of the display in closed loop with distance sensors that are currently leading to the design of a smaller new case, which would also enable a multi-finger interaction.

Furthermore, the final part of this thesis work was focused on the miniaturization of the HC-DEA with the aim of exploiting this kind of actuators for refreshable Braille displays and tactile maps. The fabrication process conceived for the tactile display actuator was modified so as to adapt it to the reduced size of the Braille dot. While force and displacement provided by the miniaturized actuator were found to be

insufficient to comply with the standard Braille requirements, the electromechanical characterisation allowed for the identification of a configuration that maximised the performance.

13.2. Future outlooks

While the tactile display was in a prototype phase, it was proven to be an effective and viable solution for tactile stimulation. However, several aspects have to be improved, as have already been discussed in the previous chapters.

Besides the fundamental developments needed by the constitutive materials and their processing, which were not the object of this thesis, the next step aims at improving the tactile display system to increase the force provided (so as to enable a broader range of tactile experiences), the implementation of the multi-finger interaction (connected with refined design and fabrication process) and the definition of optimised control strategies. This, of course, with the final goal of the integration within already available 3D simulation frameworks.

Appendix A. Non-linear model

Computational models are needed for DEAs, as they can help to improve a given actuating configuration by predicting the electromechanical performance. However due to the large deformation exhibited, the nonlinearities of the materials and the complex geometry of the actuators, modelling is challenging.

Based on the experimental data obtained during the activities of this PhD project, an electromechanical model of the HC-DEA has been developed by the group of Prof. Zhigang Suo (Wang et al. 2012).

The kinematic of the actuator was modelled so as to replicate the free-stroke and blocking force test described in Chapter 8 . Each material particle was defined by its radial coordinate R (Fig. A.1). Fig. A.1a shows the undeformed state (i.e.: the unstretched membrane), which was used as the reference state, while the deformed states are shown in Fig. A.1 c–e.

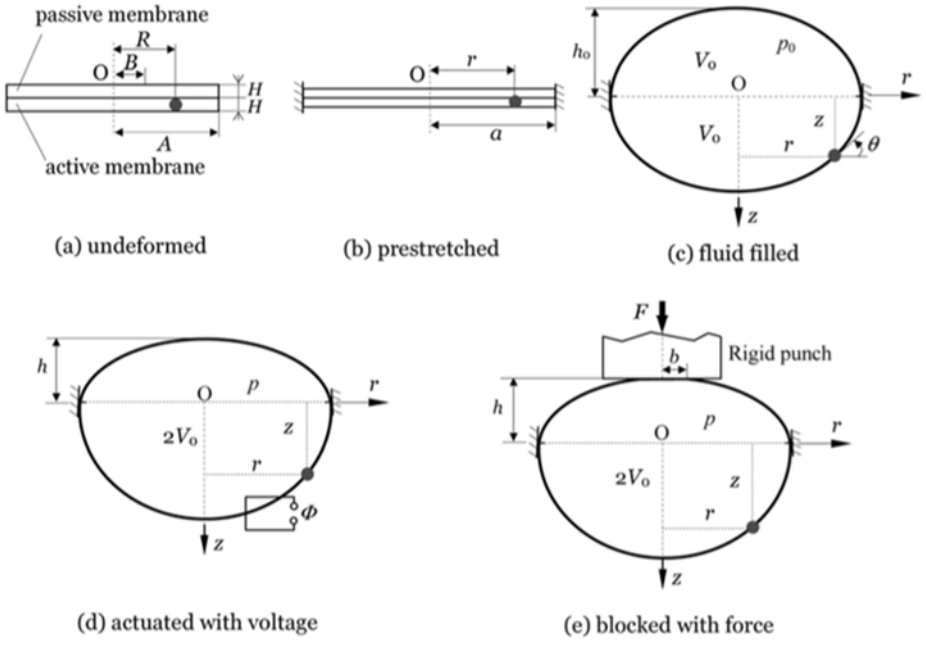

Fig. A.1. Schematics of the states used to describe the computational model. In each state, the position of a particular material particle is identified by a red dot (Wang et al. 2012).

The functions *z(R)* and *r(R)* are the coordinates of the material particle, where the coordinate *z* corresponds to the axis of symmetry and the coordinate *r* corresponds to the radial direction. The coordinates for both membranes in the deformed state are computed as follows.

Let us consider a segment of materials between two particles having coordinates R and $R+dR$, the coordinates of the particles are respectively $z(R)$ and $r(R)$, and $z(R+dR)$ and $r(R+dR)$.

When the membranes are not pre-stretched, the segment is straight and has length dR.

When the pre-stretch is applied, the element length becomes $\lambda_1 dR$, where λ_1 is the longitudinal stretch. In a curved state (i.e.: the two membranes are filled with grease), if the slope of a membrane at the coordinate in R is$\theta(R)$, we can write $dr = r(R + dR) - r(R)$, so that

$$\frac{dr}{dR} = \lambda_1 \cos\theta \tag{A.1}$$

we also can write $dz = z(R + dR) - z(R)$, so that

$$\frac{dz}{dR} = -\lambda_1 \sin\theta \tag{A.2}$$

The pre-stretch causes also the latitudinal stretch λ_2, which is identical to λ_1 and homogeneous as the pre-stretch is radial. However in the curved state those two values become inhomogeneous and must be represented by the functions $\lambda_1(R)$ and $\lambda_2(R)$.

At the mechanical equilibrium, an element of membrane located at position R is subject to tensile stresses in the longitudinal and latitudinal directions, $s_1(R)$ and $s_2(R)$.

According to the stress–stretch relation resulting form the neo-Hookean model used to describe the membranes, the two components of the stress within the region of contact are equal and can be determined as

$$s_1(R) = s_2(R) = \mu\left[\left(\frac{b}{B}\right) - \left(\frac{b}{B}\right)^{-5}\right] \tag{A.3}$$

where μ is the small shear stress, and B and b are the radiuses of contact, in the in the reference state, respectively in the unstretched and stretched state.

By balancing the fluid pressure p and the force F exerted by the rigid punch we can write

$$F = \pi b^2 p$$

(A.4)

The elastomer material is a thermodynamic system (held at a constant temperature) that at the equilibrium is characterized by the independent variables λ_1, λ_2 and $D^{\sim}$, where $D^{\sim}$ is the nominal electric displacement.

The nominal density of the Helmholtz free energy W of an element of the dielectric elastomer can be expressed as a function of the three variables defined above as

$$W = W(\lambda_1, \lambda_2, D^{\sim})$$

(A.5)

so the variation of the free energy associated to the three variables con be written as

$$\delta W = \frac{\partial W(\lambda_1, \lambda_2, D^{\sim})}{\partial \lambda_1}\delta\lambda_1 + \frac{\partial W(\lambda_1, \lambda_2, D^{\sim})}{\partial \lambda_2}\delta\lambda_2 + \frac{\partial W(\lambda_1, \lambda_2, D^{\sim})}{\partial D^{\sim}}\delta D^{\sim}$$

(A.6)

At the equilibrium, the change in the Helmholtz free energy consists in the sum of the work done by the stresses and the work done by the electric field so that we can write

$$\delta W = s_1\delta\lambda_1 + s_2\delta\lambda_2 + E^{\sim}\delta D^{\sim}$$

(A.7)

and, as the three variable are independent, from eq.(A.6) and (A.7) the condition of equilibrium is equivalent to the following three equations of state:

$$s_1 = \frac{\partial W(\lambda_1, \lambda_2, D^{\sim})}{\partial \lambda_1}$$

(A.8)

$$s_2 = \frac{\partial W(\lambda_1, \lambda_2, D^{\sim})}{\partial \lambda_2}$$

(A.9)

$$E^{\sim} = \frac{\partial W(\lambda_1, \lambda_{2,} D^{\sim})}{\partial D^{\sim}}$$

(A.10)

For Eq.(A.10) to take an explicit form, the function $W(\lambda_1, \lambda_{2,} D^{\sim})$ has to be defined. The function $W(\lambda_1, \lambda_{2,} D^{\sim})$ can be separated in two components: the free energy associated to the electric field W_{el} and the free energy associated with the stretching of the elastomer $W_{stretch}$.

By adopting the model of ideal dielectric elastomers, which assumes a liquid-like of elastomer unaffected by the deformation, W_{el} can be written as

$$W_{el}(D^{\sim}) = \frac{D^{\sim 2}}{2\varepsilon} \lambda_1^{-2} \lambda_2^{-2}$$

(A.11)

where ε is the permittivity of the elastomer.

For simplicity, a neo-Hookean model for the material was adopted so that $W_{stretch}$ can be written as

$$W_{stretch}(\lambda_1, \lambda_2) = \frac{\mu}{2}(\lambda_1^2 + \lambda_2^2 + \lambda_1^{-2}\lambda_2^{-2} - 3)$$

(A.12)

By inserting eq.(A.11) and (A.12) into eq. (A.8) and (A.9) we obtain

$$s_1 = \mu(\lambda_1 - \lambda_1^{-3}\lambda_2^{-2}) - \frac{D^{\sim 2}}{\varepsilon} \lambda_1^{-3} \lambda_2^{-2}$$

(A.13)

$$s_2 = \mu(\lambda_2 - \lambda_1^{-2}\lambda_2^{-3}) - \frac{D^{\sim 2}}{\varepsilon} \lambda_1^{-2} \lambda_2^{-3}$$

(A.14)

The governing equations, along with the material model, resulted in four first-order differential equations, which were solved and used to compute the blocking force and the membrane displacements (Fig. A.2).

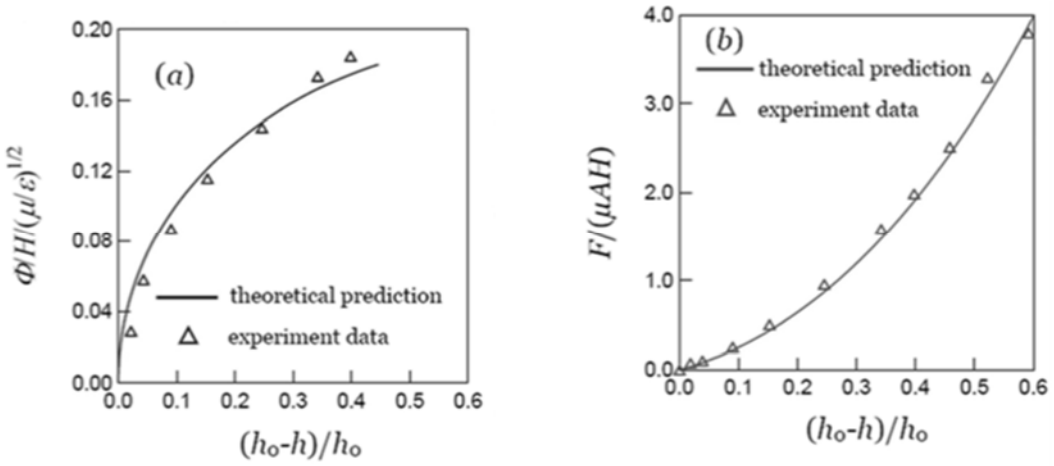

Fig. A.2. Voltage and force as a function of the membrane apical displacement. The experimental data are the results of the electromechanical test presented in Chapter 9 (Wang et al. 2012).

The displacement was normalized as $(h_0\text{-}h)/h_0$ where h_0 and h are respectively the membrane height at rest (no voltage applied) and actuated with voltage, as in Fig. A.1. The voltage Φ was normalized as $\Phi/\left(H\sqrt{\mu/\varepsilon}\right)$ where H is the unstretched thickness (as in Fig. A.1). The force F was normalized as $F/(\mu A\mathrm{H})$ where A is the unstretched membrane radius.

Fig. A.2 shows the excellent agreement between the computational results and experimental data. The only adjustable parameter in the model was the small strain shear modulus $\mu.$, which was set to 12.5 kPa for the computational results to best fit the voltage versus displacement experimental data and to 15 kPa to best fit the voltage versus displacement data.

Given the uncertainty caused by the elastomer model, and by the well-known viscoelasticity of the material, the agreement of the two values of the shear modulus can be considered satisfactory. Thus the computational model can be considered as an effective means to predict strokes and blocking forces of HC-DEAs.

Appendix B. Ethical approval

B.1. Introduction

The involvement of human participants in the psychophysical tests described in Chapter 8 might give rise to an ethical risk. Thus, according to the QMUL College policy, an ethical approval from the Ethics of Research Committee was required so as to ensure an effective management of those risks. As we believed that the research was extremely low-risk, as it involved adult subjects and it wasn't related to issue of sensitive nature, we opted for the QMUL "Expedited (fast-track) review" (*Research ethics committee web page* 2015).

In order to obtain the ethical approval an online questionnaire must be filled in and, as a good practice, an informed consent form for the participants had to be prepared. The two documents are reported in the next sections.

B.2. Research ethics questionnaire

Along with a description of the research topics and the tasks performed, the questionnaire included detailed questions aimed at understanding the ethical risks related to the research. The receipt of the questionnaire online filling is reported below.

Research ethics questionnaire receipt (reference number: 1336)

Dear Gabriele Frediani,
Thank you for filling in our online form. The information you supplied has been sent to our team. This email has been copied to you and your supervisor as confirmation.

Please send any further enquiries to research-ethics@qmul.ac.uk, quoting the reference number at the top of this email in the subject line.

Yours Sincerely,

The QM Research Ethics Team

Name: Gabriele Frediani
Student number: 130207241

Email address: g.frediani@qmul.ac.uk
Programme of study: PhD Student
Department: SEMS
Title of study: Psychophysical characterization of a wearable tactile display
Supervisor or PI: Federico Carpi (f.carpi@qmul.ac.uk)

I confirm that QMUL is responsible for this study and that I am not receiving any funding for this project (other than that provided by myself or through my course):
Yes
Funding body: None specified
Level of funding: None specified

Summary of the research:

The aim of our research is to perform psychophysical test in order to assess the performance of a wearable tactile display we developed. The device is able to mechanically stimulate the fingertip of users, so as to stimulate contact with soft bodies. It is based on dielectric elastomer actuators (DEAs) which are one of the most recent and most promising technologies for polymer-based electromechanical transduction. DEAs are a class of 'smart' materials for soft actuators capable of high strains, high energy density, high efficiency, fast response, noise-and heat-free operation, high resilience and light weight. The device consists of a DEA based actuator arranged at the fingertip. The actuator can provide a variable force to the finger pulp so as to simulate contact with a surface. In order to assess the ability of the system to generate different levels of force, which can be perceived by users, the following psychophysical tests will be performed.

The first test is aimed at assessing an important parameter in the psychophysics of perception, which is the differential threshold. It quantifies the minimum intensity difference that allows the subject to distinguish between two stimuli. The differential threshold of a perceptual stimulus, or, as it is often called, the "just noticeable difference" (JND), is a figure reflecting the fact that people are usually more sensitive to changes in weak stimuli than they are to similar changes in stronger or more intense stimuli. The methodology will consist in providing the subject with a reference force. After the subject will have familiarized with the stimulus, the force will be slowly decreased (or increased) until the subject will detect a difference with respect to the initial reference stimulus. This difference will be then recorded as the

JND.
In the second test, we will focus our attention on another parameter widely used in psychophysical studies: the psychometric function. The experiment will consists in asking volunteers to compare the force applied by the tactile display in two successive trials. In the first the volunteer will be provided with the middle value of the range of forces that the display can generate. This will be the reference stimulus. In the latter a force, chosen randomly, will be provided. The volunteer will be asked to tell whether the force perceived is "harder" than the reference stimulus. The second stimulus will be varied, within the working range of the display, in order to obtain the psychometric function which is a measure of sensorial resolution.

These tests will allow us to investigate the relationship between the physical stimuli provided by the tactile display and the sensations and perceptions they effect.

Relevant paper:
Frediani, G., Mazzei, D., De Rossi, D., Carpi, F., Wearable wireless tactile display for virtual interactions with soft bodies. Frontiers in Bioengineering and Biotechnology, 2014.

Responses to detailed questions:

- Are the participants under 16?
No
No comments supplied

- Could the participants be classified as vulnerable adults?
No
No comments supplied

- Do the participants have learning difficulties?
No
No comments supplied

- Does the research involve using or collecting human tissue?
No
No comments supplied

- Could this research uncover illegal activities (drug use, immigration etc.)?

No

No comments supplied

- Could this research cause stress or anxiety in the participant?

No

No comments supplied

- Will you be asking questions relating to issues of a personal sensitive nature?

No

No comments supplied

- Could this research bring the University into disrepute?

No

No comments supplied

- Does the research involve the person taking a drug of any description (even over the counter medicines)?

No

No comments supplied

- Does the research involve an intervention e.g. exercise, hypnotherapy?

No

No comments supplied

- Does the research rely on covert observation of the participants?

No

No comments supplied

- Will this research be conducted in the participants' homes?

No

No comments supplied

- Will the participant be paid (not just expenses)?

No

No comments supplied

- Will the data collected be sent or used overseas?

No

The collected data (related to the perceptual tests) might be published in scientific journals

B.3. Informed consent form

The informed consent form consisted of two parts: the information sheet and the consent form. The information sheet is required when recruiting participants, as it ensures that they have the sufficient information to decide whether to take part in the research or not. After reading the information sheet, each participant had to sign the consent form before the test in order to confirm that the decision to participate was based on a complete understanding of the risks and benefits of participation. The two documents are reported in the next sections.

B.3.1 Information sheet

Queen Mary
University of London

Psychophysical characterization of a wearable tactile display

Information sheet for participants

We would like to invite you to be part of this research project, if you would like to. You should only agree to take part if you want to, it is entirely up to you. If you choose not to take part there won't be any disadvantages for you and you will hear no more about it.

Please read the following information carefully before you decide to take part; this will tell you why the research is being done and what you will be asked to do if you take part. It is up to you to decide whether or not to take part. If you do decide to take part you will be given this information sheet to keep and be asked to sign the attached consent form to confirm that you agree.

You are still free to withdraw at any time and without giving a reason.

DESCRIPTION

The aim of this research is to perform psychophysical test in order to assess the performance of a wearable fingertip tactile display we developed. During the study you will be asked to wear the tactile display on your dominant's hand index finger. The display consists of a soft actuator able to provide a variable force to the finger pulp, so as to simulate contact with a surface. The stimulus that the device is able to generate will not exceed 1 N (100 grams), so it will not reach any discomfort level.

The tests will consist in a series of trials in which you will be asked to compare two or more stimuli that will be provided to your finger pulp.

The data recorded will be only related to the perceptual trials described above. Your name will never appear and your data will be handled as completely anonymous.

FURTHER INFORMATION

Please ask if there is anything that is not clear or if you would like more information.

If you have any questions or concerns, please contact, in the first instance, the researcher responsible for the study.

If this is unsuccessful, or not appropriate, please contact the Secretary at the Queen Mary Ethics of Research Committee, Room W117, Queen's Building, Mile End

Campus, Mile End Road, London or research-ethics@qmul.ac.uk.

B.3.2. Consent form

Queen Mary
University of London

Psychophysical characterization of a wearable tactile display

Consent form

Please complete this form after you have read the Information Sheet and listened to an explanation about the research.

Title of Study: "Psychophysical characterization of a wearable tactile display "Queen Mary Ethics of Research Committee Ref: _____

Thank you for considering taking part in this research. The person organizing the research must explain the project to you before you agree to take part. If you have any questions arising from the Information Sheet or explanation already given to you, please ask the researcher before you decide whether to join in. You will be given a copy of this Consent Form to keep and refer to at any time.

Participant's statements:

I agree that the research project named above has been explained to me to my satisfaction and I agree to take part in the study. I have read the Information Sheet about the project, and understand what the research study involves.

I understand that if I decide at any other time during the research that I no longer wish to participate in this project, I can withdraw from it immediately.

I am aware that the device that I will test is driven at a high voltage in the range 4-5 kV although at a maximum DC current of 100mA, which is not harmful. I am also

aware that in the worst case of failure of the device, I might be exposed to an electrostatic shock similar to those that can be experienced, for instance, from a car door in dry days.

I state that I don't have any implanted (or I don't wear any) electrical device, such as pace-maker, defibrillator, electrical stimulator, etc.

I consent to the processing of my personal information for the purposes of this research study. I understand that such information will be treated as strictly confidential and handled in accordance with the provisions of the Data Protection Act 1998.

Participant's name _____

Participant's signature: _____

Date: _____

Investigator's statement:

I confirm that I have carefully explained the nature and demands of the proposed research to the volunteer.

Investigator'sname _____

Investigator's signature: _____

Date: _____

B.5. Ethics of Research Committee approval

The research was approved by the Ethics of Research Committee through the "Expedited review" process, as stated in the following document.

Queen Mary
University of London

Queen Mary, University of London
Room W117
Queen's Building
Queen Mary University of London
Mile End Road
London E1 4NS

Queen Mary Ethics of Research Committee
Hazel Covill
Research Ethics Administrator

Tel: +44 (0) 20 7882 7915
Email: h.covill@qmul.ac.uk

c/o Dr Federico Carpi
Eng 317
Department of Engineering and Materials
Queen Mary University of London
Mile End Road
London 3rd
November 2014

To Whom It May Concern:

Re: QMERC1336 – Psychophysical characterization of a wearable tactile display.

I can confirm that Mr Gabriele Frediani has completed a Research Ethics Questionnaire with regard to the above research.
The result of which was the conclusion that his proposed work does not present any ethical concerns: is extremely low risk; and thus does not require the scrutiny of the full Research Ethics Committee.

Yours faithfully

Ms Hazel Covill – QMERC Administrator

List of publications and conference presentations

Journal papers

1. Cei, D., J. Costa, G. Gori, **G. Frediani**, C. Domenici, F. Carpi and A. Ahluwalia (2016). "A bioreactor with an electro-responsive elastomeric membrane for mimicking intestinal peristalsis." Bioinspiration & biomimetics**12**(1): 016001.
2. Carpi, F., I. Anderson, S. Bauer, **G. Frediani**, G. Gallone, M. Gei, C. Graaf, C. Jean-Mistral, W. Kaal and G. Kofod (2015). "Standards for dielectric elastomer transducers." Smart Materials and Structures**24**(10): 105025.
3. Carpi, F., **G. Frediani**, C. Gerboni, J. Gemignani and D. De Rossi (2014). "Enabling variable-stiffness hand rehabilitation orthoses with dielectric elastomer transducers." Med Eng Phys**36**(2): 205-211.
4. **Frediani, G.**, D. Mazzei, D. De Rossi and F. Carpi (2014). "Wearable wireless tactile display for virtual interactions with soft bodies." Frontiers in Bioengineering and Biotechnology**2**: 1-7.
5. Raiteri, R., N. Becerra, M. Tedesco, C. Ward, F. Carpi, **G. Frediani** and P. Vena (2014). "A Novel Platform for Simultanoues Mechanical Stimulation and Characterization of Single Cells Based on Dielectric Elastomers and Atomic Force Microscopy." Biophysical Journal**106**(2): 798a.
6. Hanley, C. A., Y. K. Gun'ko, **G. Frediani** and F. Carpi (2013). "Stretchable optical device with electrically tunable absorbance and fluorescence." Smart Materials and Structures**23**(1): 015009.

Conference proceedings

1. **Frediani, G.**, H. Boys, S. Poslad and F. Carpi (2016). Enabling wearable soft tactile displays with dielectric elastomer actuators. EuroEAP 2016 Third international conference on Electrocmehcnicaly Active Polymer (EAP) transducers & articficial muscles, Helsingør (Copenhagen), Denmark.
2. **Frediani, G.**, H. Boys, S. Poslad and F. Carpi (2016). Enabling Wearable Soft Tactile Displays with Electroactive Smart Elastomers. International Conference on Human Haptic Sensing and Touch Enabled Computer Applications, Springer.
3. Calabrese, L., **G. Frediani**, M. Gei, D. De Rossi and F. Carpi (2015). Limb compression band made of dielectric elastomer actuators. EuroEAP 2015 Fifth international conference on Electrocmehcnicaly Active Polymer (EAP) transducers & articficial muscles, Tallinn, Estonia.
4. **Frediani, G.**, H. Boys, S. Poslad and F. Carpi (2015). Wearable system for multi-finger tactile interactions with virtual soft bodies based on dielectric elastomer actuators. EuroEAP 2015 Fifth international

conference on Electrocmehcnicaly Active Polymer (EAP) transducers & articficial muscles, Tallinn, Estonia.

5. Gori, G., D. Cei, C. Curreli, **G. Frediani**, J. Costa, C. Domenici, A. Ahluwalia and F. Carpi (2015). EAP actuator as a dynamic in vitro model of the intestinal barrier. EuroEAP 2015 Fifth international conference on Electrocmehcnicaly Active Polymer (EAP) transducers & articficial muscles, Tallinn, Estonia.
6. **Frediani, G**., D. De Rossi and F. Carpi (2014). Wearable fingertip tactile display for virtual interactions with soft bodies: preliminary psychophysical test. EuroEAP 2014 Fourth international conference on Electrocmehcnicaly Active Polymer (EAP) transducers & articficial muscles, Linköping, Sweden.
7. Hanley, C. A., Y. K. Gun'ko, **G. Frediani** and F. Carpi (2014). Electrically tuneable fluorescence device based on transparent dielectric elastomer actuators. EuroEAP 2014 Fourth international conference on Electrocmehcnicaly Active Polymer (EAP) transducers & articficial muscles, Linköping, Sweden.
8. **Frediani, G**. and F. Carpi (2013). Electromechanical characterization of fingertip tactile display based on hydrostatically coupled dielectric elastomer actuators. EuroEAP 2013 Third international conference on Electrocmehcnicaly Active Polymer (EAP) transducers & articficial muscles, Dübendorf (Zürich), Switzerland.

Conference presentations

1. Invited speaker at: Mediplas 2013, Birmingham (UK), 25th -26th September 2013.
2. Invited speaker at: RubberCon 2014, Manchester (UK), 14th-15th May

Poster presentations

1. **Frediani, G.**, H. Boys, S. Poslad and F. Carpi (2016). Enabling wearable soft tactile displays with dielectric elastomer actuators. EuroEAP 2016 Third international conference on Electrocmehcnicaly Active Polymer (EAP) transducers & articficial muscles, Helsingør (Copenhagen), Denmark.
2. **Frediani, G.**, H. Boys, S. Poslad and F. Carpi (2016). Enabling Wearable Soft Tactile Displays with Electroactive Smart Elastomers. International Conference on Human Haptic Sensing and Touch Enabled Computer Applications, Springer.
3. **Frediani, G**., H. Boys, S. Poslad and F. Carpi (2015). Wearable system for multi-finger tactile interactions with virtual soft bodies based on dielectric elastomer actuators. EuroEAP 2015 Fifth international conference on Electrocmehcnicaly Active Polymer (EAP) transducers & articficial muscles, Tallinn, Estonia.
4. **Frediani, G.**, D. De Rossi and F. Carpi (2014). Wearable fingertip tactile display for virtual interactions with soft bodies: preliminary psychophysical test. EuroEAP 2014 Fourth international conference on

Electrocmehcnicaly Active Polymer (EAP) transducers & articficial muscles, Linköping, Sweden.

5. Hanley, C. A., Y. K. Gun'ko, **G. Frediani** and F. Carpi (2014). Electrically tuneable fluorescence device based on transparent dielectric elastomer actuators. EuroEAP 2014 Fourth international conference on Electrocmehcnicaly Active Polymer (EAP) transducers & articficial muscles, Linköping, Sweden.
6. **Frediani, G.** and F. Carpi (2013). Electromechanical characterization of fingertip tactile display based on hydrostatically coupled dielectric elastomer actuators. EuroEAP 2013 Third international conference on Electrocmehcnicaly Active Polymer (EAP) transducers & articficial muscles, Dübendorf (Zürich), Switzerland.

References

Aiple, M. and A. Schiele. *Pushing the limits of the CyberGrasp™ for haptic rendering*. in *IEEE International Conference on Robotics and Automation (ICRA)*. 2013.

Altinsoy, M.E. and S. Merchel, *Electrotactile feedback for handheld devices with touch screen and simulation of roughness.* IEEE Transactions on Haptics, 2012. **5**(1): p. 6-13.

Anderson, I.A., et al., *A thin membrane artificial muscle rotary motor.* Applied Physics A, 2010. **98**(1): p. 75-83.

Anderson, I.A., *Soft muscle motors with improved freedom of movement.* SPIE Newsroom, 2011. **28**.

Anderson, I.A., et al., *Multi-functional dielectric elastomer artificial muscles for soft and smart machines.* Journal of Applied Physics, 2012. **112**(4): p. 041101.

Arduino UNO overview. 2016; Available from: https://http://www.arduino.cc/en/Main/ArduinoBoardUno - overview.

Asaka, K., et al., *Bending of polyelectrolyte membrane-platinum composites by electric stimuli I. Response characteristics to various waveforms.* Polymer Journal, 1995. **27**(4): p. 436-440.

Aschwanden, M., D. Niederer, and A. Stemmer. *Tunable transmission grating based on dielectric elastomer actuators*. in *Proc. SPIE*. 2008.

Ayers, J. and J. Witting, *Biomimetic approaches to the control of underwater walking machines.* Philosophical Transactions of the Royal Society of London A: Mathematical, Physical and Engineering Sciences, 2007. **365**(1850): p. 273-295.

Bach-y-Rita, P. and S.W. Kercel, *Sensory substitution and the human–machine interface.* Trends in cognitive sciences, 2003. **7**(12): p. 541-546.

Bar-Cohen, Y., *Electroactive polymer (EAP) actuators as artificial muscles: reality, potential, and challenges*. Vol. 5. 2004: SPIE press Bellingham, WA.

Baughman, R.H., *Conducting polymer artificial muscles.* Synthetic metals, 1996. **78**(3): p. 339-353.

Baughman, R.H., et al., *Carbon nanotube actuators.* Science, 1999. **284**(5418): p. 1340-1344.

Bell, J., S. Bolanowski, and M.H. Holmes, *The structure and function of Pacinian corpuscles: A review.* Progress in neurobiology, 1994. **42**(1): p. 79-128.

Bianchi, M. and A. Serio, *Design and characterization of a fabric-based softness display.* IEEE transactions on haptics, 2015. **8**(2): p. 152-163.

Blake, D.T., K.O. Johnson, and S.S. Hsiao, *Monkey cutaneous SAI and RA responses to raised and depressed scanned patterns: effects of width, height, orientation, and a raised surround.* Journal of neurophysiology, 1997. **78**(5): p. 2503-2517.

Blum, M., et al. *Optotune focus tunable lenses and laser speckle reduction based on electroactive polymers*. in *Spie moems-mems*. 2012. International Society for Optics and Photonics.

Bogacz, R., et al., *The physics of optimal decision making: a formal analysis of models of performance in two-alternative forced-choice tasks.* Psychological review, 2006. **113**(4): p. 700.

Bozlar, M., et al., *Dielectric elastomer actuators with elastomeric electrodes.* Applied Physics Letters, 2012. **101**(9): p. 091907.

Brisben, A.J., S.S. Hsiao, and K.O. Johnson, *Detection of vibration transmitted through an object grasped in the hand.* Journal of Neurophysiology, 1999. **81**(4): p. 1548-1558.

Brochu, P. and Q. Pei, *Advances in dielectric elastomers for actuators and artificial muscles.* Macromolecular Rapid Communications, 2010. **31**(1): p. 10-36.

Brochu, P., et al., *All-silicone prestrain-locked interpenetrating polymer network elastomers: free-standing silicone artificial muscles with improved performance and robustness.* Smart Materials and Structures, 2013. **22**(5): p. 055022.

Brodal, A. and E. Rinvik, *The somatic afferent pathways.* Neurological anatomy, 3rd edn. Oxford University Press, New York, 1981: p. 56-57.

Bruckheimer, E., et al., *Computer-generated real-time digital holography: first time use in clinical medical imaging.* Eur Heart J Cardiovasc Imaging, 2016: p. jew087.

Carpi, F., C. Salaris, and D. De Rossi, *Folded dielectric elastomer actuators.* Smart Materials and Structures, 2007. **16**(2): p. S300.

Carpi, F., et al., *Dielectric Elastomers as Electromechanical Eransducers: Fundamentals, Materials, Devices, Models and Applications of an Emerging Electroactive Polymer Technology*. 2008, Oxford: Elsevier.

Carpi, F., et al., *Millimetre-scale bubble-like dielectric elastomer actuators.* Polymer International, 2009. **59**(3): p. 407-414.

Carpi, F. and E. Smela, *Biomedical applications of electroactive polymer actuators.* 2009.

Carpi, F., *Electromechanically Active Polymers.* Polymer International, 2010. **59**(3): p. 277-278.

Carpi, F., S. Bauer, and D. De Rossi, *Stretching dielectric elastomer performance.* Science, 2010a. **330**(6012): p. 1759-1761.

Carpi, F., G. Frediani, and D. De-Rossi, *Hydrostatically coupled dielectric elastomer actuators.* IEEE/ASME Transactions on Mechatronics, 2010b. **15**(2): p. 308-315.

Carpi, F., et al., *Dielectric elastomers as electromechanical transducers: Fundamentals, materials, devices, models and applications of an emerging electroactive polymer technology*. 2011a: Elsevier.

Carpi, F., et al., *Bioinspired Tunable Lens with Muscle-Like Electroactive Elastomers.* Advanced Functional Materials, 2011b. **21**(21): p. 4152-4158.

Carpi, F., et al., *Electroactive polymer actuators as artificial muscles: are they ready for bioinspired applications?* Bioinspiration & biomimetics, 2011c. **6**(4): p. 045006.

Carpi, F., G. Frediani, and D. Rossi, *Contractile Hydrostatically Coupled Dielectric Elastomer Actuators.* Mechatronics, IEEE/ASME Transactions on, 2012. **17**(5): p. 987-994.

Carpi, F., et al., *Standards for dielectric elastomer transducers.* Smart Materials and Structures, 2015. **24**(10): p. 105025.

Carter, T., et al. *UltraHaptics: multi-point mid-air haptic feedback for touch surfaces*. in *Proceedings of the 26th annual ACM symposium on User interface software and technology*. 2013. ACM.

Chen, Z., S. Shatara, and X. Tan, *Modeling of biomimetic robotic fish propelled by an ionic polymer–metal composite caudal fin.* IEEE/ASME transactions on mechatronics, 2010. **15**(3): p. 448-459.

Cho, K.-J., et al. *Design, fabrication and analysis of a body-caudal fin propulsion system for a microrobotic fish*. in *Robotics and Automation, 2008. ICRA 2008. IEEE International Conference on*. 2008. IEEE.

Clark, F.J. and K.W. Horch, *Kinesthesia: In: Boff KR, Kaufman L, Thomas JP (eds) Sensory processes and perception (Handbook of perception and human performance, vol 1)*. 1986, Wiley, New York.

Collins, D.F. and A. Prochazka, *Movement illusions evoked by ensemble cutaneous input from the dorsum of the human hand.* The Journal of physiology, 1996. **496**(3): p. 857-871.

Colorado, J., et al., *Biomechanics of smart wings in a bat robot: morphing wings using SMA actuators.* Bioinspiration & biomimetics, 2012. **7**(3): p. 036006.

CyberGlove Systems LLC. *CyberGrasp system overview*. 2016a [cited 2016; Available from: http://www.cyberglovesystems.com/cybergrasp/.

CyberGlove Systems LLC. *CyberTouch system overview*. 2016b [cited 2016; Available from: http://www.cyberglovesystems.com/cybertouch/.

D.E.Hodgson, M.H.Wu, and R.J.Biermann, *Shape memory alloys*, in *ASM Handbook*. 1990. p. 897-902.

Daerden, F. and D. Lefeber, *Pneumatic artificial muscles: actuators for robotics and automation.* European journal of mechanical and environmental engineering, 2002. **47**(1): p. 11-21.

Darian–Smith, I., *Thermal sensibility*, in *Handbook of Physiology. Vol. III. Sensory Processes.*, M.V. Darian–Smith I, Brookhart JM, Editor. 1984, American Physiological Society

: Bethesda, MD. p. 879 –914.

Dehaene, S., *The neural basis of the Weber–Fechner law: a logarithmic mental number line.* Trends in cognitive sciences, 2003. **7**(4): p. 145-147.

Dorkenoo, K.D.H., et al., *Monitoring the Contractile Properties of Optically Patterned Liquid Crystal Based Elastomers.* Advanced Elastomers-Technology, Properties and Applications, 2012: p. 37-60.

Dünki, S.J., et al., *Self□Repairable, High Permittivity Dielectric Elastomers with Large Actuation Strains at Low Electric Fields.* Advanced Functional Materials, 2015. **25**(16): p. 2467-2475.

Duo MLX embeddable stereo imagining for high performance 3D sensing. 2015; Available from: https://duo3d.com/public/pdf/CL_DUO_MINILX_PB_1.1.pdf.

Edin, B.B., *Quantitative analysis of static strain sensitivity in human mechanoreceptors from hairy skin.* Journal of neurophysiology, 1992. **67**(5): p. 1105-1113.

Edin, B.B. and N. Johansson, *Skin strain patterns provide kinaesthetic information to the human central nervous system.* The Journal of physiology, 1995. **487**(1): p. 243-251.

EMCO high voltage Q Series datasheet. 2016; Available from: http://www.emcohighvoltage.com/datasheets/qseries.pdf.

Fechner, G., *Elemente der Psychophysik*. 1860, Leipzig: Breitkopf und Härtel.

Feil, H., et al., *Mutual influence of pH and temperature on the swelling of ionizable and thermosensitive hydrogels.* Macromolecules, 1992. **25**(20): p. 5528-5530.

Frediani, G., et al., *Wearable wireless tactile display for virtual interactions with soft bodies.* Frontiers in Bioengineering and Biotechnology, 2014. **2**: p. 1-7.

Freyberger, F.K. and B. Färber. *Compliance discrimination of deformable objects by squeezing with one and two fingers*. in *EuroHaptics 2006*. 2006.

Friedl, R. *Virtual reality and 3D visualizations in heart surgery education*. in *The Heart surgery forum*. 2002.

Fujita, K. and Y. Oyama. *Control strategies in human pinch motion to detect the hardness of an object*. in *Systems, Man, and Cybernetics, 1999. IEEE SMC'99 Conference Proceedings. 1999 IEEE International Conference on*. 1999. IEEE.

Fujita, K. and H. Ohmori. *A new softness display interface by dynamic fingertip contact area control*. in *5th World Multiconference on Systemics, Cybernetics and Informatics*. 2001.

Geomagic Inc. *Geomagic Touch Overview*. 2016 [cited 2016 February]; Available from: http://geomagic.com/en/products/phantom-omni/overview.

Gescheider, G., *Psychophysics: the fundamentals Lawrence Erlbaum.* Mahwah, NJ, 1997a.

Gescheider, G., *Chapter 3. The Classical Psychophysical Methods.* Psychophysics: the fundamentals. 3rd ed. Mahwah: Lawrence Erlbaum Associates, 1997b.

Goodwin, A.W., K.T. John, and A.H. Marceglia, *Tactile discrimination of curvature by humans using only cutaneous information from the fingerpads.* Experimental brain research, 1991. **86**(3): p. 663-672.

Goodwin, A.W. and H.E. Wheat, *Human tactile discrimination of curvature when contact area with the skin remains constant.* Experimental brain research, 1992. **88**(2): p. 447-450.

Goodwin, A.W., A.S. Browning, and H.E. Wheat, *Representation of curved surfaces in responses of mechanoreceptive afferent fibers innervating the monkey's fingerpad.* Journal of Neuroscience, 1995. **15**(1): p. 798-810.

Guna, J., et al., *An analysis of the precision and reliability of the leap motion sensor and its suitability for static and dynamic tracking.* Sensors, 2014. **14**(2): p. 3702-3720.

Harvey, L.O., *Efficient estimation of sensory thresholds.* Behavior Research Methods, Instruments, & Computers, 1986. **18**(6): p. 623-632.

Hayward, V. and M. Cruz-Hernandez. *Tactile display device using distributed lateral skin stretch*. in *Proceedings of the haptic interfaces for virtual environment and teleoperator systems symposium*. 2000. ASME.

Hentschke, R., *Thermodynamics: for physicists, chemists and materials scientists*. 2013: Springer Science & Business Media.

Hoshi, T. and H. Shinoda, *Airborne Ultrasound Tactile Display*, in *Pervasive Haptics*. 2016, Springer. p. 121-138.

How Does the Leap Motion Controller Work? 2016 [cited 2016; Available from: http://blog.leapmotion.com/hardware-to-software-how-does-the-leap-motion-controller-work/.

Huang, J., et al., *Giant, voltage-actuated deformation of a dielectric elastomer under dead load.* Applied Physics Letters, 2012. **100**(4): p. 041911.

Hunter, I.W., et al. *Fast reversible NiTi fibers for use in microrobotics*. in *Micro Electro Mechanical Systems, 1991, MEMS'91, Proceedings. An Investigation of Micro Structures, Sensors, Actuators, Machines and Robots. IEEE*. 1991. IEEE.

HyperBraille. 2016; Available from: http://web.metec-ag.de/graphik display.html.

Ilievski, F., et al., *Soft robotics for chemists.* Angewandte Chemie, 2011. **123**(8): p. 1930-1935.

Iwamoto, T., et al. *Airborne ultrasound tactile display*. in *ACM SIGGRAPH 2008 new tech demos*. 2008. ACM.

Jager, E.W.H., E. Smela, and O. Inganäs, *Microfabricating conjugated polymer actuators.* Science, 2000. **290**(5496): p. 1540-1545.

Jani, J.M., et al., *A review of shape memory alloy research, applications and opportunities.* Materials & Design, 2014. **56**: p. 1078-1113.

Jo, C., et al., *Recent advances in ionic polymer–metal composite actuators and their modeling and applications.* Progress in Polymer Science, 2013. **38**(7): p. 1037-1066.

Johansson, R.S. and Å.B. Vallbo, *Tactile sensibility in the human hand: relative and absolute densities of four types of mechanoreceptive units in glabrous skin.* The Journal of physiology, 1979. **286**(1): p. 283-300.

Johansson, R.S. and G. Westling, *Roles of glabrous skin receptors and sensorimotor memory in automatic control of precision grip when lifting rougher or more slippery objects.* Experimental brain research, 1984. **56**(3): p. 550-564.

Johnson, K.O. and G.D. Lamb, *Neural mechanisms of spatial tactile discrimination: neural patterns evoked by braille□like dot patterns in the monkey.* The Journal of physiology, 1981. **310**(1): p. 117-144.

Johnson, K.O., T. Yoshioka, and F. Vega–Bermudez, *Tactile functions of mechanoreceptive afferents innervating the hand.* Journal of Clinical Neurophysiology, 2000. **17**(6): p. 539-558.

Johnson, K.O., *The roles and functions of cutaneous mechanoreceptors.* Current opinion in neurobiology, 2001. **11**(4): p. 455-461.

Jung, K., K.J. Kim, and H.R. Choi, *A self-sensing dielectric elastomer actuator.* Sensors and Actuators A: Physical, 2008. **143**(2): p. 343-351.

Kajimoto, H., et al. *Tactile feeling display using functional electrical stimulation*. in *Proc. 1999 ICAT*. 1999.

Kajimoto, H., et al. *Electro-tactile display with force feedback*. in *Proc. World Multiconference on Systemics, Cybernetics and Informatics (SCI2001)*. 2001.

Kang, B.-S., et al. *Dynamic modeling of Mckibben pneumatic artificial muscles for antagonistic actuation*. in *Robotics and Automation, 2009. ICRA'09. IEEE International Conference on*. 2009. IEEE.

Katz, D., *The world of touch. Translated by LE Krueger*. 1925, Erlbaum.[RLK].

Kendrick, D., *Freedom Scientific Focusing On Braille Part 2: A Review of the Focus Blue 40 Braille Display.* American Foundation for the Blind Magazine, 2014. **15**(9): p. 2-3.

Kim, H.-J., S.-H. Song, and S.-H. Ahn, *A turtle-like swimming robot using a smart soft composite (SSC) structure.* Smart Materials and Structures, 2012. **22**(1): p. 014007.

Kim, S., et al. *Micro artificial muscle fiber using NiTi spring for soft robotics*. in *2009 IEEE/RSJ International Conference on Intelligent Robots and Systems*. 2009. IEEE.

Kim, S.-C., et al. *SaLT: Small and lightweight tactile display using ultrasonic actuators*. in *RO-MAN 2008-The 17th IEEE International Symposium on Robot and Human Interactive Communication*. 2008. IEEE.

Kinect for Windows. 2010; Available from: https://http://www.microsoft.com/enus/kinectforwindows/meetkinect/default.aspx.

Kitamura, N., J. Chim, and N. Miki, *Electrotactile display using microfabricated micro-needle array.* Journal of micromechanics and Microengineering, 2015. **25**(2): p. 025016.

Klatzky, R.L., S.J. Lederman, and C. Reed, *Haptic integration of object properties: texture, hardness, and planar contour.* Journal of Experimental Psychology: Human Perception and Performance, 1989. **15**(1): p. 45.

Klein, S.A., *Measuring, estimating, and understanding the psychometric function: A commentary.* Perception & Psychophysics, 2001. **63**(8): p. 1421-1455.

Knoop, E. and J. Rossiter. *The tickler: a compliant wearable tactile display for stroking and tickling*. in *Proceedings of the 33rd Annual ACM Conference Extended Abstracts on Human Factors in Computing Systems*. 2015a. ACM.

Knoop, E. and J. Rossiter, *A compliant soft-actuator laterotactile display.* Smart Materials and Structures, 2015b. **24**(4): p. 045034.

Knoop, E., M. Bächer, and P. Beardsley, *Contact Pressure Distribution as an Evaluation Metric for Human-Robot Hand Interactions*. 2017.

Kofod, G., et al., *Actuation response of polyacrylate dielectric elastomers.* Journal of intelligent material systems and structures, 2003. **14**(12): p. 787-793.

Koh, S.J.A., et al., *Mechanisms of large actuation strain in dielectric elastomers.* Journal of Polymer Science Part B: Polymer Physics, 2011. **49**(7): p. 504-515.

Koo, I., et al., *Wearable fingertip tactile display*, in *2006 Sice-Icase International Joint Conference*. 2006: Busan. p. 1911-1916.

Kordonsky, W., *Elements and devices based on magnetorheological effect.* Journal of Intelligent Material Systems and Structures, 1993. **4**(1): p. 65-69.

Kornbluh, R.D., et al. *Ultrahigh strain response of field-actuated elastomeric polymers*. in *SPIE's 7th Annual International Symposium on Smart Structures and Materials*. 2000. International Society for Optics and Photonics.

Kornbluh, R.D., et al. *Electroelastomers: applications of dielectric elastomer transducers for actuation, generation, and smart structures*. in *SPIE's 9th Annual International Symposium on Smart Structures and Materials*. 2002. International Society for Optics and Photonics.

Kovac, M., et al. *A 1.5 g sma-actuated microglider looking for the light*. in *Proceedings 2007 IEEE International Conference on Robotics and Automation*. 2007. IEEE.

Kovacs, G. and L. During. *Contractive tension force stack actuator based on soft dielectric EAP*. in *Proc. SPIE*. 2009.

Kovacs, G., et al., *Stacked dielectric elastomer actuator for tensile force transmission.* Sensors and Actuators A: Physical, 2009. **155**(2): p. 299-307.

Krantz, J., *Experiencing sensation and perception*. 2012: Pearson Education (Us).

Krueger, L.E., *David Katz's Der Aufbau der Tastwelt (The world of touch): A synopsis.* Perception & Psychophysics, 1970. **7**(6): p. 337-341.

Lawrence, D.A., *Stability and transparency in bilateral teleoperation.* IEEE transactions on robotics and automation, 1993. **9**(5): p. 624-637.

Lederman, S.J., *The perception of surface roughness by active and passive touch.* Bulletin of the Psychonomic Society, 1981. **18**(5): p. 253-255.

Lee, C.-H. and M.-G. Jang, *Virtual surface characteristics of a tactile display using magneto-rheological fluids.* Sensors, 2011. **11**(3): p. 2845-2856.

Lee, H.S., et al., *Design analysis and fabrication of arrayed tactile display based on dielectric elastomer actuator.* Sensors and Actuators A: Physical, 2014. **205**: p. 191-198.

Leek, M.R., *Adaptive procedures in psychophysical research.* Perception & psychophysics, 2001. **63**(8): p. 1279-1292.

Lehmann, W., et al., *Giant lateral electrostriction in ferroelectric liquid-crystalline elastomers.* Nature, 2001. **410**(6827): p. 447-450.

Lenay, C., et al., *Sensory substitution: limits and perspectives.* Touching for knowing, 2003: p. 275-292.

Lin, H.-T., G.G. Leisk, and B. Trimmer, *GoQBot: a caterpillar-inspired soft-bodied rolling robot.* Bioinspiration & biomimetics, 2011. **6**(2): p. 026007.

Liu, L., et al., *Experimental study on the dynamic response of in-plane deformation of dielectric elastomer under alternating electric load.* Smart Materials and Structures, 2014. **23**(2): p. 025037.

Loewenstein, W.R. and R. Skalak, *Mechanical transmission in a Pacinian corpuscle. An analysis and a theory.* The Journal of physiology, 1966. **182**(2): p. 346-378.

Lotz, P., M. Matysek, and H.F. Schlaak, *Fabrication and application of miniaturized dielectric elastomer stack actuators.* IEEE/ASME Transactions on Mechatronics, 2011. **16**(1): p. 58-66.

Macefield, V.G., C. Häger-Ross, and R.S. Johansson, *Control of grip force during restraint of an object held between finger and thumb: responses of cutaneous afferents from the digits.* Experimental Brain Research, 1996. **108**(1): p. 155-171.

Madsen, F.B., et al., *The Current State of Silicone□Based Dielectric Elastomer Transducers.* Macromolecular rapid communications, 2016. **37**(5): p. 378-413.

Maffli, L., et al., *Ultrafast All□Polymer Electrically Tunable Silicone Lenses.* Advanced Functional Materials, 2015. **25**(11): p. 1656-1665.

Massat, M.B., *True 3D: Unlocking the full potential of medical imaging.* Applied Radiology, 2014.

Matsunaga, T., et al. *Tactile display for 2-D and 3-D shape expression using SMA micro actuators*. in *2005 3rd IEEE/EMBS Special Topic Conference on Microtechnology in Medicine and Biology*. 2005. IEEE.

Michel, S., et al., *A comparison between silicone and acrylic elastomers as dielectric materials in electroactive polymer actuators.* Polymer international, 2010. **59**(3): p. 391-399.

Minamizawa, K., et al. *Gravity grabber: wearable haptic display to present virtual mass sensation*. in *ACM SIGGRAPH 2007 emerging technologies*. 2007. San Diego, California: ACM.

Mousty, P. and P. Bertelson, *A study of braille reading: 1. Reading speed as a function of hand usage and context.* The Quarterly Journal of Experimental Psychology, 1985. **37**(2): p. 217-233.

Mullins, L., *Softening of rubber by deformation.* Rubber chemistry and technology, 1969. **42**(1): p. 339-362.

Nalwa, H.S., *Ferroelectric polymers: chemistry: physics, and applications*. 1995: CRC Press.

Nam, D.N.C. and A.K. Kwan, *Ionic Polymer Metal Composite Transducer and Self-Sensing Ability.* Smart Actuation and Sensing Systems-Recent Advances and Future Challenges, Berselli, G., Vertechy, R., and Vassura, G.,(Eds.), InTech, 2012.

Nemat-Nasser, S. and Y. Wu, *Comparative experimental study of ionic polymer–metal composites with different backbone ionomers and in various cation forms.* Journal of Applied Physics, 2003. **93**(9): p. 5255-5267.

Niklaus, M., S. Rosset, and H. Shea. *Array of lenses with individually tunable focal-length based on transparent ion-implanted EAPs*. in *SPIE Smart Structures and Materials+ Nondestructive Evaluation and Health Monitoring*. 2010. International Society for Optics and Photonics.

Niu, X., et al., *Synthesizing a new dielectric elastomer exhibiting large actuation strain and suppressed electromechanical instability without prestretching.* Journal of Polymer Science Part B: Polymer Physics, 2013. **51**(3): p. 197-206.

Olausson, H., J. Wessberg, and N. Kakuda, *Tactile directional sensibility: peripheral neural mechanisms in man.* Brain research, 2000. **866**(1): p. 178-187.

Optotune website. [cited 2016; Available from: http://www.optotune.com/.

Osada, Y., *Conversion of chemical into mechanical energy by synthetic polymers (chemomechanical systems)*, in *Polymer Physics*. 1987, Springer. p. 1-46.

Pasquero, J. and V. Hayward. *STReSS: A practical tactile display system with one millimeter spatial resolution and 700 Hz refresh rate*. in *Proc. Eurohaptics*. 2003.

Pei, Q., et al. *Multifunctional electroelastomer roll actuators and their application for biomimetic walking robots*. in *Smart Structures and Materials*. 2003. International Society for Optics and Photonics.

Pei, Q., et al., *Multiple-degrees-of-freedom electroelastomer roll actuators.* Smart Materials and Structures, 2004. **13**(5): p. N86.

Pelrine, R., et al., *High-field deformation of elastomeric dielectrics for actuators.* Materials Science and Engineering: C, 2000a. **11**(2): p. 89-100.

Pelrine, R., et al., *High-speed electrically actuated elastomers with strain greater than 100%.* Science, 2000b. **287**(5454): p. 836-839.

Pelrine, R.E., R.D. Kornbluh, and J.P. Joseph, *Electrostriction of polymer dielectrics with compliant electrodes as a means of actuation.* Sensors and Actuators A: Physical, 1998. **64**(1): p. 77-85.

Poulin, A., S. Rosset, and H.R. Shea, *Printing low-voltage dielectric elastomer actuators.* Applied Physics Letters, 2015. **107**(24): p. 244104.

Prattichizzo, D., et al. *Using a fingertip tactile device to substitute kinesthetic feedback in haptic interaction*. in *International Conference on Human Haptic Sensing and Touch Enabled Computer Applications*. 2010. Springer.

Prattichizzo, D., C. Pacchierotti, and G. Rosati, *Cutaneous force feedback as a sensory subtraction technique in haptics.* IEEE Transactions on Haptics, 2012. **5**(4): p. 289-300.

Prattichizzo, D., et al., *Towards wearability in fingertip haptics - a 3-dof wearable device for cutaneous force feedback.* IEEE Transactions on Haptics, 2013. **6**(4): p. 506-516.

Raja, S.N., R.A. Meyer, and J.N. Campbell, *Peripheral mechanisms of somatic pain.* Anesthesiology, 1988. **68**(4): p. 571-590.

RealView medical holography. 2016; Available from: http://www.realviewimaging.com/.

Research ethics committee web page. 2015; Available from: http://www.arcs.qmul.ac.uk/research-degrees/research-degree-students/ethics/94438.html.

Rizzello, G., et al., *Modeling of the effects of the electrical dynamics on the electromechanical response of a DEAP circular actuator with a mass–spring load.* Smart Materials and Structures, 2015. **24**(9): p. 094003.

Roentgen, W., *About the changes in shape and volume of dielectrics caused by electricity.* Section III in G. Wiedemann (Ed.), Annual Physics and Chemistry Series, 1880. **11**: p. 771-786.

Rosset, S., et al., *Self-sensing dielectric elastomer actuators in closed-loop operation.* Smart Materials and Structures, 2013. **22**(10): p. 104018.

Rosset, S. and H.R. Shea, *Flexible and stretchable electrodes for dielectric elastomer actuators.* Applied Physics A, 2013. **110**(2): p. 281-307.

Runyan, N.H. and F. Carpi, *Seeking the 'holy Braille' display: might electromechanically active polymers be the solution?* Expert review of medical devices, 2011. **8**(5): p. 529-532.

Sakas, G., *Trends in medical imaging: from 2D to 3D.* Computers & Graphics, 2002. **26**(4): p. 577-587.

Sarakoglou, I., et al., *A high performance tactile feedback display and its integration in teleoperation.* IEEE Transactions on Haptics, 2012. **5**(3): p. 252-263.

Schacter, D.L., D.T. Gilbert, and D.M. Wegner, *Psychology (2nd Edition)*. 2011, New York: Worth.

Schorr, S.B., et al. *Sensory substitution via cutaneous skin stretch feedback*. in *Robotics and Automation (ICRA), 2013 IEEE International Conference on*. 2013. IEEE.

Scilingo, E.P., et al. *Haptic displays based on magnetorheological fluids: design, realization and psychophysical validation*. in *Haptic Interfaces for Virtual Environment and Teleoperator Systems, 2003. HAPTICS 2003. Proceedings. 11th Symposium on*. 2003a. IEEE.

Scilingo, E.P., et al., *Magnetorehological devices*. 2003b.

Scilingo, E.P., et al., *Rendering softness: integration of kinesthetic and cutaneous information in a haptic device.* Ieee Transactions on Haptics, 2010. **3**(2): p. 109-118.

Seok, S., et al., *Meshworm: a peristaltic soft robot with antagonistic nickel titanium coil actuators.* IEEE/ASME Transactions on mechatronics, 2013. **18**(5): p. 1485-1497.

Serina, E.R., C.D. Mote, and D. Rempel, *Force response of the fingertip pulp to repeated compression—effects of loading rate, loading angle and anthropometry.* Journal of biomechanics, 1997. **30**(10): p. 1035-1040.

Seth, A., J. Vance, and J. Oliver, *Virtual reality for assembly methods prototyping: a review.* Virtual Reality, 2011. **15**(1): p. 5-20.

Seymour, N.E., et al., *Virtual reality training improves operating room performance: results of a randomized, double-blinded study.* Annals of surgery, 2002. **236**(4): p. 458.

Shepard, R.N., D.W. Kilpatric, and J.P. Cunningham, *The internal representation of numbers.* Cognitive psychology, 1975. **7**(1): p. 82-138.

Shepherd, R.F., et al., *Multigait soft robot.* Proceedings of the National Academy of Sciences, 2011. **108**(51): p. 20400-20403.

Smela, E., *Conjugated polymer actuators for biomedical applications.* Advanced materials, 2003. **15**(6): p. 481-494.

Smith, A.M., G. Gosselin, and B. Houde, *Deployment of fingertip forces in tactile exploration.* Experimental brain research, 2002. **147**(2): p. 209-218.

Snodgrass, J.G. and B.S. Psychophysics, *Experimental sensory psychology.* Scott, Foresman & Co., Glenview, Illinois, 1975.

Srinivasan, M.A., J.M. Whitehouse, and R.H. LaMotte, *Tactile detection of slip: surface microgeometry and peripheral neural codes.* Journal of Neurophysiology, 1990. **63**(6): p. 1323-1332.

Srinivasan, M.A. and R.H. LaMotte, *Tactual discrimination of softness.* Journal of Neurophysiology, 1995. **73**(1): p. 88-101.

Suo, Z., *Theory of dielectric elastomers.* Acta Mechanica Solida Sinica, 2010. **23**(6): p. 549-578.

Tanaka, T., et al., *Collapse of gels in an electric field.* Science, 1982. **218**(4571): p. 467-469.

Taylor, M. and C.D. Creelman, *PEST: Efficient estimates on probability functions.* The Journal of the Acoustical Society of America, 1967. **41**(4A): p. 782-787.

Tezuka, M., et al., *Presentation of various tactile sensations using micro-needle electrotactile display.* PloS one, 2016. **11**(2): p. e0148410.

Treutwein, B., *Adaptive psychophysical procedures.* Vision research, 1995. **35**(17): p. 2503-2522.

Ultrahaptics, UK. [cited 2017; Available from: https://http://www.ultrahaptics.com/.

Vallbo, Å.B. and R.S. Johansson, *Properties of cutaneous mechanoreceptors in the human hand related to touch sensation.* Hum Neurobiol, 1984. **3**(1): p. 3-14.

Vega-Bermudez, F. and K.O. Johnson, *SA1 and RA receptive fields, response variability, and population responses mapped with a probe array.* Journal of neurophysiology, 1999. **81**(6): p. 2701-2710.

Velazquez, R., et al. *A low-cost highly-portable tactile display based on shape memory alloy micro-actuators*. in *IEEE Symposium on Virtual Environments, Human-Computer Interfaces and Measurement Systems, 2005.* 2005. IEEE.

Wang, H., et al., *Computational Model of Hydrostatically Coupled Dielectric Elastomer Actuators.* Journal of Applied Mechanics, 2012. **79**(3): p. 031008.

Wang, Q. and V. Hayward, *Biomechanically optimized distributed tactile transducer based on lateral skin deformation.* The International Journal of Robotics Research, 2010. **29**(4): p. 323-335.

Watson, A.B. and D.G. Pelli, *Quest: A Bayesian adaptive psychometric method.* Perception & Psychophysics, 1983. **33**(2): p. 113-120.

Web search: "Average word length in the English language". 2016; Available from: http://www.wolframalpha.com/input/?i=average+word+length+English+language.

Weber, E.H., *De tactu.* Koehler, Leipzig, 1834.

Weichert, F., et al., *Analysis of the accuracy and robustness of the leap motion controller.* Sensors, 2013. **13**(5): p. 6380-6393.

Yoo, J., et al., *Position controlled pneumatic tactile display for tangential stimulation of a finger pad.* Sensors and Actuators A: Physical, 2015. **229**: p. 15-22.

Yun, S., et al., *Three-axis pneumatic tactile display with integrated capacitive sensors for feedback control.* Microsystem Technologies, 2016. **22**(2): p. 275-282.

Yurekli, K., et al., *Structure and dynamics of carbon black□filled elastomers.* Journal of Polymer Science Part B: Polymer Physics, 2001. **39**(2): p. 256-275.

Zhang, Q.M., V. Bharti, and X. Zhao, *Giant electrostriction and relaxor ferroelectric behavior in electron-irradiated poly (vinylidene fluoride-trifluoroethylene) copolymer.* Science, 1998. **280**(5372): p. 2101-2104.

Zhao, X. and Z. Suo, *Theory of dielectric elastomers capable of giant deformation of actuation.* Physical Review Letters, 2010. **104**(17): p. 178302.